ILLINOIS CENTER FOR TRANSPORTATION

Report No. FHWA-ICT-25-011

Using Advanced Binder Rheological Parameters to Predict Cracking Potential of Hot-Mix Asphalt Mixtures with Modified Binders

Imad L. Al-Qadi
Abdulgafar O. Sulaiman
Uthman Mohamed Ali
Hong Lang
Javier J. García Mainieri

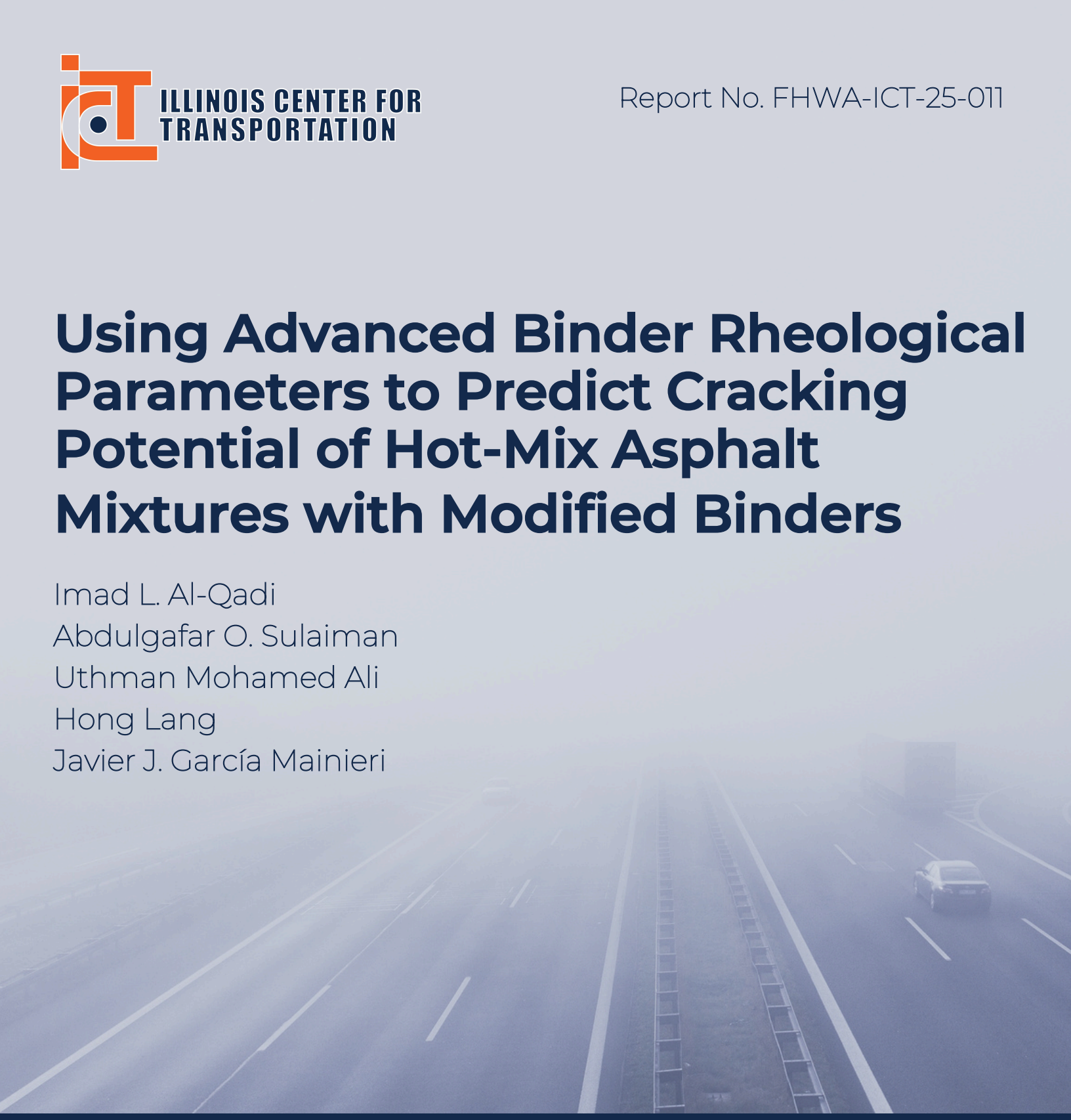

ICT Project R27-250

October 2025

ISSN: 0197-9191
ICT Series Report No. 25-011
https://doi.org/10.36501/0197-9191/25-011

TECHNICAL REPORT DOCUMENTATION PAGE

1. Report No.	2. Government Accession No.	3. Recipient's Catalog No.
FHWA-ICT-25-011	N/A	N/A

4. Title and Subtitle	5. Report Date
Using Advanced Binder Rheological Parameters to Predict Cracking Potential of Hot-Mix Asphalt Mixtures with Modified Binders	October 2025
	6. Performing Organization Code N/A

7. Authors	8. Performing Organization Report No.
Imad L. Al-Qadi, https://orcid.org/0000-0002-5824-103X Abdulgafar Sulaiman, https://orcid.org/0000-0002-7455-5039 Uthman Mohamed Ali, https://orcid.org/0009-0004-1070-0374 Hong Lang, https://orcid.org/0000-0003-1015-5797 Javier J. García Mainieri, https://orcid.org/0000-0002-8302-474X	ICT-25-011 UILU-2025-2011

9. Performing Organization Name and Address	10. Work Unit No.
Illinois Center for Transportation Department of Civil and Environmental Engineering University of Illinois Urbana-Champaign 205 North Mathews Avenue, MC-250 Urbana, IL 61801	N/A
	11. Contract or Grant No. R27-250

12. Sponsoring Agency Name and Address	13. Type of Report and Period Covered
Illinois Department of Transportation (SPR) Bureau of Research 126 East Ash Street Springfield, IL 62704	Final Report 8/16/22–10/31/25
	14. Sponsoring Agency Code

15. Supplementary Notes

Conducted in cooperation with the U.S. Department of Transportation, Federal Highway Administration.
https://doi.org/10.36501/0197-9191/25-011

16. Abstract

This study provides insights into the complexities of asphalt binder modifications and their impact on hot-mix asphalt (HMA) cracking potential. An experimental program was developed to assess the cracking potential of HMA from binder characteristics. Various binder types, including polymer-softener-modified binders, were considered. Rheological tests were performed on binders at short- and long-term aging conditions. A multiple stress creep recovery test was conducted to evaluate the stress-dependent rutting potential of binder blends, while Fourier-transform infrared spectroscopy was used to evaluate oxidative aging and polymer degradation of the binder. Rheological parameters of binders were used to predict HMA cracking potential utilizing test results of the Illinois Flexibility Index Test. Statistical analyses, primarily based on multi-linear regression, were used to develop predictive models linking binder rheological properties to HMA cracking potential. The HMA flexibility index (FI) was predicted using the following binder rheological parameters: creep stiffness at 60 s (S-value), rate of stress relaxation at 60 s (m-value), asphalt binder content (BC), asphalt binder replacement (ABR), number of design gyrations (Ngyr), and $\Delta|G^*|_{peak\ \tau}$. For simplicity, short- and long-term aged HMA FI prediction models are based on S-value, m-value, and ABR. Three uncertainty categories of predicting FI from binder rheological parameters are introduced. The categories are associated with binder acceptance based on potential cracking risk.

17. Key Words	18. Distribution Statement
Binder Modification, Polymer-Modified Binder, Softener-Modified Binder, Polymer-Softener-Modified Binder, Binder Rheology, Delta Tc, Delta G Star	No restrictions. This document is available through the National Technical Information Service, Springfield, VA 22161.

19. Security Classif. (of this report)	20. Security Classif. (of this page)	21. No. of Pages	22. Price
Unclassified	Unclassified	96	N/A

ACKNOWLEDGMENT, DISCLAIMER, MANUFACTURERS' NAMES

This publication is based on the results of **ICT-R27-250: Using Advanced Binder Rheological Parameters to Predict Cracking Potential of Hot-Mix Asphalt Mixtures with Modified Binders**. ICT-R27-250 was conducted in cooperation with the Illinois Center for Transportation; the Illinois Department of Transportation; and the U.S. Department of Transportation Federal Highway Administration.

Members of the Technical Review Panel (TRP) were the following:

- Kelly Senger, TRP Chair, Illinois Department of Transportation
- Brian Hill, TRP Co-Chair, Illinois Department of Transportation
- David Adedokun, Federal Highway Administration
- Dennis Bachman, Federal Highway Administration
- Rick Beyers, Emulsicoat, Inc.
- Kevin Burke, Illinois Asphalt Pavement Association
- Kevin Finn, Illinois Department of Transportation
- Justin Grant, Illinois Department of Transportation
- Apurva Patel, R. W. Dunteman
- Brian Pfeifer, Illinois Department of Transportation
- Ronald Price, Illinois Department of Transportation
- Stephanie Smith, Flint Hills Resources
- William Snyder, Illinois Department of Transportation
- Trey Summers, Illinois Department of Transportation
- Jason Wielinski, Asphalt Institute
- Thomas Zehr, Illinois Department of Transportation

The authors acknowledge the technical support of ICT research engineers Uthman Mohamed Ali, Greg Renshaw, and Mohsen Motlagh.

policies of the Illinois Center for Transportation, the Illinois Department of Transportation, or the Federal Highway Administration. This report does not constitute a standard, specification, or regulation.

Trademark or manufacturers' names appear in this report only because they are considered essential to the objectives of this document and do not constitute an endorsement of any product by the Federal Highway Administration, the Illinois Department of Transportation, or the Illinois Center for Transportation.

EXECUTIVE SUMMARY

The performance of hot-mix asphalt (HMA) plays a critical role in the durability and service life of flexible pavements. With increasing traffic loads, severe environmental conditions, and the growing use of recycled asphalt pavement (RAP), the need for better-performing HMA has become more pressing. A major component of HMA is asphalt binder (AB), which is responsible for binding the aggregates and providing the necessary flexibility to resist stresses from traffic loading and environmental conditions. Modified binders have been developed to improve the rheological and mechanical properties of asphalt binder, addressing the limitations of conventional binders. This study provided valuable insights into the complexities of AB modifications and their impact on the cracking potential of HMA. It explored the use of binder rheological parameters to predict HMA cracking potential.

To achieve the study's objectives, an experimental program was developed to assess the cracking potential of HMA from binder rheological parameters. Various binder types, including base binders, softener-modified binders, and polymer-softener-modified binders, were considered in HMA. Rheological tests were performed on the binders after they were aged under simulated short- and long-term aging (STA and LTA) conditions, like those experienced during mixing and paving as well as field service, respectively. The performance of HMA designs was also evaluated using the Illinois Flexibility Index Test (I-FIT), which measures cracking potential. In addition, the Hamburg Wheel-Tracking Test (HWTT), which indicates potential rutting, was performed.

Two base binders were selected, classified as "good" and "borderline," and were modified with a range of softeners and styrene-butadiene-styrene (SBS) polymers, either independently or in combination. The binder blends underwent STA and LTA simulations using a rolling thin-film oven (RTFO) and two levels in a pressure aging vessel (PAV), respectively. In addition, the study examined the influence of modifiers and RAP on HMA cracking potential. The combination of polymers and softeners showed a synergistic effect in reducing cracking potential. Polymer-softener modification led to a greater increase in binder potential performance than a simple summation of each modifier. However, the sequence of adding both modifiers to the binder is critical to the modified binder's performance.

The inherent quality of base binder significantly influenced HMA performance. In addition to typical rheological tests, a multiple stress creep recovery (MSCR) test was conducted to evaluate the stress-dependent rutting potential of binder blends, while Fourier-transform infrared (FTIR) spectroscopy analysis identified characteristic peaks and functional groups of softeners and polymers and was used to evaluate oxidative aging and polymer degradation of the binder. Rheological parameters such as ΔT_c (an indicator of low-temperature cracking risk), S-value (creep stiffness at 60 s), m-value (rate of stress relaxation at 60 s), and $\Delta|G^*|_{peak\,\tau}$ (a measure of fatigue tolerance and stiffness degradation) were evaluated and correlated to HMA cracking potential for both aging conditions. It is recommended that a −5°C ΔT_c threshold for PAV-aged binders should be maintained for polymer-softener-modified binders as well as $\Delta|G^*|_{peak\,\tau}$ values of 60%.

The MSCR test revealed that polymer-modified and polymer-softener-modified binders exhibited markedly improved elasticity, as reflected by higher percent recovery (R) and lower nonrecoverable creep compliance (J_{nr}) values compared to neat and softened binders. The "borderline" binders showed less rutting potential than the "good" binders. This highlights the importance of the balanced design approach for HMA. From FTIR, no remarkable differences were observed in the aging trend between the various types of polymer-softener-modified binders.

Statistical analyses, primarily based on multi-linear regression, were used to develop predictive models linking binder rheological properties to HMA cracking potential. For STA FI prediction, a multi-linear regression model that included ABR content, $\Delta|G^*|_{peak\,\tau}$, binder content, design number of gyrations, S-value, and m-value achieved a good explanation ($R^2 = 0.770$). On the other hand, for LTA FI, the model using the same parameters resulted in $R^2 = 0.835$. Leave-one-out cross-validation confirmed reasonable generalization performance, supporting the robustness of the model.

Residual analyses confirmed normality assumptions, enabling the estimation of prediction uncertainty using first-order error propagation. A risk-based framework is proposed to compute the probability of FI falling below a critical threshold (e.g., FI < 8 for STA), supporting more informed decisions regarding binder acceptance or further testing. Overall, this study demonstrates that binder rheological parameters can predict HMA cracking potential reliably and inform performance-based specifications.

The study proposed the following practical equation for implementation by contractors utilizing binder rheological parameters available in the binder's certificate of analysis for a specific mix design of known RAP and number of design gyrations:

$$FI\ (STA) = -9.65 + 77.02 \times m + 4.52 \times BC - 0.254 \times Ngyr - 0.678 \times \mathrm{A}BR + 0.89 \times \log S$$

Other equations, including $\Delta|G^*|_{peak\,\tau}$ for STA and for LTA, are presented and found to be robust.

Finally, three uncertainty categories of predicting FI from binder rheological parameters are introduced. The categories are associated with binder acceptance based on potential cracking risk. The use of the developed model may offer significant benefits for the paving industry, particularly in the context of binder selection to achieve cost-effective and resilient HMA that meets set requirements.

TABLE OF CONTENTS

CHAPTER 1: INTRODUCTION 1

BACKGROUND 1

RESEARCH OBJECTIVES AND SCOPE 2

POTENTIAL IMPLEMENTATION 3

CHAPTER 2: CURRENT STATE OF KNOWLEDGE 4

ASPHALT BINDER MATERIALS AND MODIFICATIONS 4

Superpave Performance Grading System 4

Binder Modification 5

Binder Characterization 7

Binder Potential Performance Parameters 9

HOT-MIX ASPHALT AND CRACKING POTENTIAL 10

Relationship between Binder and HMA Cracking Potential 11

CHAPTER 3: EXPERIMENTAL PROGRAM 13

BINDER MATERIALS AND MODIFICATION 13

Modification Protocol 14

BINDER STABILITY AND RHEOLOGY 17

Binder Thermal and Storage Stability 17

Binder Rheology 17

Binder Chemistry 18

HMA DESIGNS 19

Binder Selection Protocol for HMA 19

MIXTURE POTENTIAL PERFORMANCE 20

Illinois Flexibility Index Test 20

Hamburg Wheel-Tracking Test 21

STATISTICAL ANALYSIS 22

CHAPTER 4: CHARACTERIZATION OF MODIFIED BINDERS 24

MODIFIED BINDER STABILITY AND MASS LOSS 24

THERMOGRAVIMETRIC ANALYSIS OF MODIFIED BINDER 25

MODIFIED BINDER RHEOLOGICAL PARAMETERS **28**
DELTA-TC (ΔT_C) **30**
DELTA-G-STAR ($\Delta|G^*|_{PEAKT}$) **33**
MULTIPLE STRESS CREEP RECOVERY **38**
Effect of Modifiers on MSCR 40
Summary 47
FOURIER-TRANSFORM INFRARED SPECTROSCOPY **47**
Effect of Modification 47
Aging Evaluation 49
Polymer Degradation Evaluation 52
CHAPTER 5: MIXTURE POTENTIAL PERFORMANCE **54**
ILLINOIS FLEXIBILITY INDEX TEST **54**
Effect of Binder Modifiers on HMA Flexibility Index 58
Effect of ABR on HMA Flexibility Index 61
Statistical Analysis of the Binder Modification Effect 63
HAMBURG WHEEL-TRACKING TEST **63**
CHAPTER 6: CRACKING POTENTIAL OF HOT-MIX ASPHALT FROM BINDER RHEOLOGICAL PARAMETERS **67**
DATA SOURCE AND PREPROCESSING **67**
STATISTICAL EVALUATION OF BINDER-MIXTURE RELATIONSHIPS **70**
Correlation Analysis 70
Initial Multi-Linear Statistical Analysis of I-FIT Parameters 73
Variable Screening and FI Model Development 74
FI Prediction Results 76
FI Prediction Uncertainty and Risk Estimation 78
SUMMARY **81**
SUGGESTED PERFORMANCE TESTING RECOMMENDATIONS **81**
CHAPTER 7: CONCLUSIONS AND RECOMMENDATIONS **82**
SUMMARY **82**
CONCLUSIONS **82**

RECOMMENDATIONS **83**

REFERENCES **85**

LIST OF FIGURES

Figure 1. Equation. Delta T_c determination. 9
Figure 2. Equation. Glover-Rowe equation. 12
Figure 3. Flowchart. Binder modification sequence. 14
Figure 4. Photo. Cafarmo BDC1850 shear mixer. 15
Figure 5. Photo. Silverson L5M-A high shear mixer 16
Figure 6. Equation. Homogeneity index. 17
Figure 7. Graph. Typical asphalt binder response to repeated loading. 18
Figure 8. Equation. Calculation of FI. 20
Figure 9. Photo. Specimen in the I-FIT fixture. 21
Figure 10. Graph. Typical I-FIT test result. 21
Figure 11. Photo. Specimen in the SmarTracker machine. 22
Figure 12. Graph. Typical HWTT test result. 22
Figure 13. Graph. Thermograms of ramp TGA. 26
Figure 14. Graph. Thermograms of heat-and-hold TGA. 27
Figure 15. Bar plot. ΔT_c values for 1PAV- and 2PAV-aged base binders. 30
Figure 16. Bar plot. 1PAV and 2PAV ΔT_c values for softened binders. 31
Figure 17. Bar plot. 1PAV ΔT_c values for polymer-modified binders 32
Figure 18. Bar plots. 1PAV and 2PAV ΔT_c values for polymer-softener-modified binders (PG 70-28). . 32
Figure 19. Bar plot. 1PAV and 2PAV ΔT_c values for polymer-softener-modified binders (PG 76-28). ... 33
Figure 20. Bar plot. 2PAV $|\Delta G^*|_{peak\,\tau}$ values for softened binders. 34
Figure 21. Bar plot. 2PAV $\Delta|G^*|_{peak\,\tau}$ values for polymer-modified binders (experimental base). 35
Figure 22. Bar plot. 2PAV $\Delta|G^*|_{peak\,\tau}$ values for polymer-modified binders (comparison base) 36
Figure 23. Graph. Binder behavior during the LAS. 36
Figure 24. Bar plot. 2PAV $\Delta|G^*|_{peak\,\tau}$ values for polymer-softener-modified binders. 38
Figure 25. Bar plot. $R_{3.2}$ values for base and softened binders. 40
Figure 26. Bar plot. $J_{nr\,3.2}$ values for base and softened binders. 41
Figure 27. Bar plot. $R_{3.2}$ values for base and binder blends containing polymer. 41
Figure 28. Bar plot. $J_{nr\,3.2}$ values for base and binder blends containing polymer. 42

Figure 29. Graph. $R_{3.2}$ vs $J_{nr\ 3.2}$ for binder blends. 43
Figure 30. Equation. Percent difference between average recovery, R_{diff}. 44
Figure 31. Equation. Percent difference between nonrecoverable creep compliance, $J_{nr\ diff}$. 44
Figure 32. Graph. R_{diff} values for binder blends. 45
Figure 33. Graph. $J_{nr\ diff}$ values for binder blends. 46
Figure 34. Graph. Typical FTIR spectra for softened binders. 48
Figure 35. Graph. Typical FTIR spectra for polymer-modified binders. 49
Figure 36. Equation. Carbonyl-based FTIR oxidation index. 49
Figure 37. Equation. Carbonyl- and sulfoxide-based FTIR oxidation index. 49
Figure 38. Graph. Aging evolution for binder blends using $\boldsymbol{IC = O}$. 50
Figure 39. Graph. Aging evolution for binder blends using $\boldsymbol{IC = O + S = O}$. 51
Figure 40. Equation. Butadiene- and styrene-based FTIR degradation index. 52
Figure 41. Graph. Polymer degradation for binder blends using $\boldsymbol{IB/S}$. 53
Figure 42. Bar plot. FI values for selected mixes. 56
Figure 43. Bar plot. Fracture energy values for selected mixes. 57
Figure 44. Bar plot. Post-peak slope values for selected mixes. 58
Figure 45. Bar plot. FI values for mixes with relatively high ABR. 59
Figure 46. Bar plot. FI values for mixes with moderate ABR. 59
Figure 47. Bar plot. FI values for no ABR mixes (SBS 76-28, SBS 76-28 w/C, and SBS 76-28 w/M). 60
Figure 48. Bar plot. FI values for no ABR mixes (58-28, SBS 70-28, and SBS 76-28). 60
Figure 49. Bar plot. FI for no ABR mixes (neat 64-22, SBS 76-28 w/C, and SBS 76-28 w/M). 61
Figure 50. Bar plot. FI values for neat 58-28 (no and high ABR). 62
Figure 51. Bar plot. FI values for SBS PG 70-28 (no and medium ABR). 62
Figure 52. Graph. HWTT results for mixes with no ABR (limestone mix). 65
Figure 53. Graph. HWTT results for mixes with no ABR (traprock mix). 66
Figure 54. Graph. Distribution of binder and HMA parameters. 69
Figure 55. Graph. Distribution of normalized binder and HMA parameters. 70
Figure 56. Graph. Shapiro-Wilk normality test results. 72
Figure 57. Equation. Regression equation for STA FI. 76
Figure 58. Equation. Regression equation for LTA FI. 76

Figure 59. Equation. Regression equation for STA FI without $\Delta|G^*|_{peak\ \tau}$. 76
Figure 60. Equation. Regression equation for LTA FI without $\Delta|G^*|_{peak\ \tau}$..... 76
Figure 61. Graph. Prediction results vs. residual plots. 77
Figure 62. Graph. FI residual distribution with Shapiro-Wilk test. 78
Figure 63. Equation. Total prediction uncertainty. 78
Figure 64. Equation. FI risk evaluation. 79
Figure 65. Graph. STA/LTA FI uncertainty quantification. 80

LIST OF TABLES

Table 1. Characteristics of Tested Binders 13
Table 2. Softener Type and Designation 14
Table 3. Mix Design Volumetrics 19
Table 4. Selected Binders and Mixes 20
Table 5. Cigar Tube Test Results 24
Table 6. Binder Mass Loss Results 25
Table 7. Ramp TGA Results 25
Table 8. Heat-and-Hold TGA Results 26
Table 9. Low-Temperature PG of Softener N in Polymer-Softener-Modified Binders 27
Table 10. Low-Temperature PG of Softener N in Polymer-Softener-Modified Binders (Alternate Protocol) 28
Table 11. True PG of Base and Modified Binders 29
Table 12. MSCR Values for Binder Blends 39
Table 13. Percentage Difference in R and J_{nr} 44
Table 14. FI Values for Selected Mixes (Limestone Mix) 55
Table 15. FI Values for Selected Mixes (Traprock Mix) 55
Table 16. T-test p-values for FI Values 63
Table 17. HWTT Results for Mixes with No ABR (Limestone Mix) 64
Table 18. HWTT Results for Mixes with No ABR (Traprock Mix) 64
Table 19. Mix Design Characteristics of Hot-Mix Asphalt 67
Table 20. Correlation Matrix for I-FIT and Binder Parameters 71
Table 21. Multiple Linear Regression Results for STA G_f and LTA G_f 73
Table 22. Multiple Linear Regression Results for FI and Slope 74
Table 23. Model Input Definitions for STA and LTA FI Prediction 75
Table 24. Variable Combinations Selected for STA FI and LTA FI Prediction 75
Table 25. Performance Metrics of STA and LTA FI Models (Full Sample vs. LOOCV) 76
Table 26. Risk-Based Decision Framework for FI Prediction 79

CHAPTER 1: INTRODUCTION

BACKGROUND

Hot-mix asphalt (HMA) is used in the construction of flexible pavements, offering a balance of durability, cost-effectiveness, and adaptability to varying environmental and traffic conditions. The performance and longevity of flexible pavements are influenced primarily by the properties of asphalt binder (AB) (Bahia & Anderson, 1995), which serves as the glue that holds the aggregate together and provides the necessary flexibility and resilience to withstand repeated traffic loads and environmental stresses. The viscoelastic properties of HMA primarily stem from AB, as aggregates are considered elastic materials.

The desire to improve flexible pavement performance, resiliency, and cost-effectiveness, particularly with the advent of heavier traffic loads and more extreme weather conditions, has spurred interest in the use of modified binders (Liu et al., 2018; Chen et al., 2002). Two categories of modifiers have been used commonly: polymers and softeners. Polymers improve the mechanical properties, durability, and performance of flexible pavements (Behnood & Modiri Gharehveran, 2019) by increasing the elastic recovery of asphalt binder and reducing the potential for rutting (DuBois et al., 2014; D'Angelo & Dongré, 2009). Softeners, on the other hand, enhance flexibility and reduce the cracking potential of AB, particularly at low temperatures. They counteract the stiffening effect of recycled binder from recycled asphalt pavement (RAP), making the binder less brittle and more pliable (Singhvi et al., 2020; Bennert et al., 2014).

Consequently, the combination of frequent heavy traffic loads, extreme weather conditions, and increased RAP usage has led to the consideration of polymer-softener-modified binders to meet performance expectations as well as cost and sustainability goals. These modifications could complicate the prediction of HMA cracking potential from AB. This complexity primarily arises from the fact that modification alters a binder's rheological and viscoelastic properties in ways that traditional testing methods, such as those prescribed by the Superpave system, may not fully capture (Kriz et al., 2019; Hintz et al., 2011). Modified binder properties are affected by the rheological and chemical properties of its components as well as the binder source, modifier/softener dosage and type, and blending procedure. In addition, softeners may degrade polymer-modified binders or affect established crosslinking. Hence, a polymer-softener AB blend must remain stable.

Another important aspect of predicting the cracking potential of HMA with modified binders is understanding the effects of aging on AB properties. Asphalt binder undergoes both short-term aging, which occurs during the production and construction phases, and long-term aging, which occurs over the service life of the flexible pavement. These aging processes lead to an increase in binder stiffness and a corresponding increase in susceptibility to cracking. The current laboratory aging protocols, using a rolling thin-film oven (RTFO) for short-term aging and a single pressure aging vessel (PAV) cycle for long-term aging, are not sufficient to represent the realistic long-term aging of binders (Elwardany et al., 2018; Glover et al., 2005). The use of polymer-softener-modified binders may warrant testing AB beyond the Superpave recommended linear viscoelastic range and a single PAV

cycle. Using advanced binder rheological parameters may better predict the cracking potential of HMA with modified binders.

Recent research has highlighted the potential of using advanced rheological parameters, such as delta T_c (ΔT_c) (Asphalt Institute, 2019; Anderson et al., 2011) and $\Delta|G^*|_{peak\tau}$ (García Mainieri et al., 2021). ΔT_c represents the difference between critical temperatures for cracking, determined by stiffness and relaxation properties. A negative ΔT_c indicates that the binder's relaxation properties degrade more rapidly than its stiffness properties, signaling an increased risk of cracking. $\Delta|G^*|_{peak\tau}$ is the reduction in complex shear modulus, $|G^*|$, from the start of the linear amplitude sweep (LAS) test until the peak shear-stress condition is reached. Higher $\Delta|G^*|_{peak\tau}$ indicates higher fatigue tolerance.

In addition to evaluating binders using advanced rheological testing and aging simulations, the stiffness and flexibility of the HMA itself must be considered when predicting its cracking potential. A previous Illinois Center for Transportation study (Al-Qadi et al., 2017) led to the development of the Illinois Flexibility Index Test (I-FIT), which became AASHTO standard T 393. The test can distinguish between various mixes and predict HMA cracking potential. A correlation between field cracking progression and laboratory-measured flexibility index (FI) was established. Given that cracking is highly dependent on binder characteristics, a relationship between binder properties and FI should exist.

While traditional binder testing methods provide valuable baseline information, the complexities introduced by binder modifications necessitate the use of advanced testing techniques and parameters. By incorporating proper parameters into the evaluation process, pavement engineers can better predict HMA cracking potential and design more resilient flexible pavements.

RESEARCH OBJECTIVES AND SCOPE

The objectives of this study are twofold:

- Evaluate the potential of advanced binder rheological parameters in predicting HMA cracking potential.
- Evaluate the impact of blending softener-modified binders with styrene-butadiene-styrene (SBS) polymer on AB and HMA.

The scope of this study includes the following:

- Base binders, softener-modified binders, and polymer-softener-modified binders were tested at different binder and mixture levels. The relationship between binder rheology and mixture potential cracking was investigated.
- Rheological parameters were obtained for modified and straight-run binders after being conditioned for up to 40 hours in a PAV.

- Multiple stress creep recovery testing was used to evaluate the elastic recovery of polymer-modified binders.

- Laboratory-designed HMA, in accordance with IDOT's volumetric and performance-related requirements, was prepared and tested using selected base and modified AB.

POTENTIAL IMPLEMENTATION

This study presents a data-driven approach to guide modified binder selection for mitigating potential HMA cracking. The cracking potential of HMA, represented by the cracking index (FI), is predicted using binder rheological parameters. The accuracy of this prediction model is expected to improve as more data become available. It is recommended that IDOT validate the use of softener-modified binders in field projects over the next two years to allow for an inclusive evaluation and potential adoption. The study provides guidelines for blending and thresholds for softener-modified binders, along with a model that supports informed material selection. This approach aims to enhance proactive pavement management, reduce the risk of premature failure, and contribute to more cost-effective pavement strategies. This aligns with IDOT's long-term performance and sustainability goals.

CHAPTER 2: CURRENT STATE OF KNOWLEDGE

ASPHALT BINDER MATERIALS AND MODIFICATIONS

Asphalt binder, a residual fraction obtained from the fractional distillation of crude oil, is a complex chemical composite of several molecules and compounds interacting together to give asphalt binder its properties (Allen et al., 2014; Masson, 2008). It behaves between two extremes: as a purely elastic material with rapid loading at low temperature and as a purely viscous liquid with slow loading at high temperature. This complex behavior is governed by the chemical composition and microstructure of asphalt binder (Mazumder et al., 2018a).

The characterization of asphalt binder using different technologies and tests has been central to many scholarly and engineering studies. This characterization can be based on physical properties such as stiffness, elasticity, and plasticity (Allen et al., 2014; Kim et al., 2017); chemical properties such as its fractionalization (Guo et al., 2017; Han et al., 2018; Wang et al., 2019); or microstructure, using techniques such as scanning electron microscopy or atomic force microscopy (Jahangir et al., 2015; Mikhailenko et al., 2017). Because AB plays a significant role in the resistance/susceptibility of HMA to pavement distresses, binder characterization is needed.

Superpave Performance Grading System

The Superpave performance grading (PG) system, developed in the U.S. as part of the Strategic Highway Research Program (SHRP) in the early 1990s (Harrigan et al., 1994), is used to evaluate performance and to select AB. An improvement over the previous two systems, penetration grading and viscosity grading, the Superpave system offers several advantages (Hajj & Bhasin, 2018). The Superpave system tests the asphalt binder considering long-term aging and pavement conditions such as temperature, speed, and traffic volume (Bahia et al., 2001; McGennis et al., 1995).

These advantages were made possible through novel tests and specifications developed to address performance requirements such as rutting and cracking potential. Tests included dynamic shear rheometer (DSR), bending beam rheometer (BBR), and direct tension (DT). The system consists of two temperature limits, in which the upper and lower temperature are determined by the average seven-day maximum and the one-day minimum pavement design temperature, respectively (Zeiada et al., 2022).

In summary, the primary philosophy for the PG system is to relate the physical properties of AB to field performance (Harrigan et al., 1994). The potential for each pavement distress, including rutting, fatigue, and thermal cracking, is evaluated at the most critical temperature and aging conditions (e.g., short-term aged and high temperature for rutting, long-term aged and intermediate temperature for fatigue cracking, and long-term aged and low temperature for low-temperature cracking) (Liu et al., 2021). A grade is then assigned to the binder based on the highest and lowest temperatures at which the AB meets performance criteria related to these distresses.

For rutting, a DSR is used to perform a reversed cyclic loading test at a frequency of 10 rad/s on original and RTFO-aged AB samples to determine the dynamic shear modulus (G*) and phase angle

(δ). G* indicates the stiffness, while δ describes the lag between shear stresses and strains. Rutting is governed by |G*|/sinδ, where AB needs to be stiff enough to resist rutting. Therefore, the rutting parameter is limited to a minimum of 1 kPa for original binder and 2.2 kPa for RTFO-aged binder.

Fatigue cracking is governed by the DSR's parameter, |G*|sinδ. The test is conducted on PAV-aged samples. The PAV exposes binder samples to heat and pressure to simulate years of in-service aging of a pavement. Asphalt binder needs to be soft enough to resist fatigue cracking. Therefore, the fatigue cracking parameter is limited to a maximum of 5,000 kPa for PAV-aged AB.

For thermal cracking, the BBR test is used to perform a creep test on AB beams after being RTFO- and PAV-aged. The creep stiffness (S) and the slope of log creep stiffness versus log time (m) are determined. AB needs to be soft enough and relax stresses fast enough to resist thermal cracking. Therefore, thermal cracking parameters, creep stiffness and m-value, are limited to a maximum of 300 MPa and a minimum of 0.3, respectively.

Binder Modification

With increasing traffic loading and volume and/or harsher climate conditions, premature pavement deterioration has become more prevalent. To address this challenge, researchers have attempted to modify AB properties using polymers, fibers, softeners, plastics, anti-strip agents, and antioxidants. This section discusses binder modification using polymers and softeners.

Polymer Modification

Polymers are the most widely used AB modifiers and can be classified into three main types: thermoplastic elastomers, plastomers, and reactive. Thermoplastic elastomers mainly enhance the elastic properties of binder, improving cracking resistance. Plastomers and reactive polymers mainly enhance AB's stiffness, improving rutting resistance (García-Travé et al., 2016). Several studies have reported that adding polymers to AB improves performance by enhancing resistance to rutting, fatigue cracking, thermal cracking, and stripping potential (Behnood & Modiri Gharehveran, 2019; Brasileiro et al., 2019; Habbouche et al., 2020). As a result, polymer-modified binders are commonly used in high-stress locations, such as high-volume roads, intersections of busy streets, airports, and vehicle weigh stations.

Adding SBS to asphalt binder causes a physical combination in which the lighter AB fractions are absorbed by the elastomeric phase of the copolymer. This combination then swells to about five to nine times its initial volume (Sengoz et al., 2009). SBS is usually added as a percentage of the total binder weight, and optimizing this percentage is required to achieve the best performance. In addition to dosage of SBS, several other factors, including temperature, shear rate, and duration of blending, affect the interaction, and ultimately the performance, of SBS polymer-modified binders (Kumar et al., 2020; Xu et al., 2016). At low concentrations (4%), the polymer is dispersed in the bituminous matrix. At intermediate dosages (~5%), an unstable co-continuous matrix is observed, and at higher dosages (7%), the polymer volume increases substantially such that the binder is dispersed in the polymer matrix (Brule, 1996). The morphology wherein binder is dispersed in the polymer matrix is said to provide maximum performance benefits in polymer-modified systems (Chen et al., 2021; Nivitha et al., 2022).

Binder Softening

Binder softening refers to modification efforts aimed at rejuvenating aged binders, particularly those obtained from RAP. Softeners help ensure acceptable HMA performance when higher RAP percentages are incorporated. Common softeners used to adjust AB grade and enhance compatibility with RAP include waste vegetable oil and grease, organic oil, plasticizers, anti-aging agents, and aromatic extracts (Miliutenko et al., 2013; Zaumanis et al., 2014; García Mainieri et al., 2021; Xie, Tran, et al., 2017; Zhang et al., 2018). Other advantages offered by softeners include lower costs and ease of use (Zaumanis et al., 2015).

As with other types of modifiers used in asphalt binder, the performance of softened binders depends on factors such as dosage, composition, and blending approach. Thus, optimizing these factors is necessary to balance cracking resistance and rutting control (Mogawer et al., 2013; Silva et al., 2012). The most common and easiest blending approach is shear mixing. In the laboratory, this involves blending AB and softener at high temperatures between 120°C and 160°C and high shear rates, greater than 1,000 revolutions per minute (rpm). Other approaches are adding softeners to AB by spraying and encapsulation (Lin et al., 2014; Zhao et al., 2016; Aguirre et al., 2016; Xu et al., 2018). Spraying involves the application on an already placed HMA pavement, while encapsulation is used prior to compaction.

The most common methods for selecting the optimum softener dosage are based on linear blending charts relating softener dosage with a basic binder property such as penetration grade, PG, ductility, softening point, and viscosity (Chen et al., 2014a; Chen et al., 2014b; Tran et al., 2012). A maximum and minimum softener dosage could be obtained from blending charts. Using the PG system, the maximum dosage is obtained from the rutting parameter at high PG temperature, while the minimum dosage is obtained from the fatigue parameter at intermediate PG temperature. Stiffness and m-value are obtained at low PG temperature (Behnood, 2019). Other methods include using a space diagram of rutting and fatigue cracking potential as well as performance tests such as I-FIT and HWTT (Zhou et al., 2019; Espinoza-Luque et al., 2018; Im et al., 2016). Generally, the softener dosage used is less than 10% by the weight of AB. Organic softeners usually require smaller doses compared to petroleum softeners to cause a similar softening effect on aged RAP binder (Zaumanis et al., 2014).

Interaction of Polymer Modification and Softeners

Because polymer modification and softeners each offer distinct benefits, combining them has been explored as an AB modification strategy. Polymer modification has been used to control potential rutting due to the use of softeners. Sun et al. (2017) used linear SBS polymer (L-SBS) and recycled low-density polyethylene (R-LDPE) to modify waste cooking oil residue (WCOR) due to its low viscosity and poor adhesion. In the study, a bio-asphalt containing 31.8% hard asphalt binder, 33.3% WCOR, 30.3% hydrocarbon resin, 4.6% recycled low-density polyethylene, and 4% external linear SBS polymer was developed as the optimum blending proportion, showing similar high-temperature performance and better low-temperature performance than the SBS-modified binder. HMA using this bio-binder had similar rutting potential and moisture susceptibility and better low-temperature cracking control compared to HMA containing SBS-modified binder. Bonicelli et al. (2017) also concluded that a proper calibration of softeners and polymer can enhance overall HMA durability in mixtures with high RAP content (e.g., 40%).

Binder Characterization

Fourier-Transform Infrared Spectroscopy

Homogeneity is an important consideration when using modified AB. Hence, it is important to study the blending process between the modifier and asphalt. Fourier-transform infrared spectroscopy (FTIR) can be used to measure blending efficiency by testing different parts of the asphalt-modifier blend and mapping the modifier's distribution in asphalt.

FTIR is used to obtain the infrared spectrum of absorption, emission, and photoconductivity of materials. It detects different functional groups in a mixture, recording spectrums between 4,000 cm^{-1} and 400 cm^{-1} (Sindhu et al., 2015). The primary applications of FTIR on AB include studying polymer modification mechanisms and evaluating the aging effects on AB at the molecular level (Hou et al., 2018).

Functional groups such as carbonyl and sulfoxide are commonly used (Araujo et al., 2012; Yao et al., 2015). The level of aging in AB can be identified through a relationship between aging and changes in some functional groups. Several researchers have used the FTIR test (Abdelrahman et al., 2014; Bowers et al., 2014; Xu et al., 2017; Xu & Huang, 2010; Yang et al., 2014). However, data analysis methods can vary, requiring standardization for inter-laboratory comparisons (Marsac et al., 2014).

Singhvi et al. (2021) investigated the chemical and aging characteristics of binders using the FTIR spectrum (800–1,800 cm^{-1}). Carbonyl and sulfoxide functional groups were analyzed as markers of oxidative aging. Laboratory aging processes such as RTFO, PAV, 2PAV, and 3PAV induced measurable changes in these chemical groups, particularly increasing sulfoxide and certain carbonyl peaks. Softener-modified binders showed a decrease in the carbonyl region near 1,750 cm^{-1} with aging, suggesting chemical stabilization effects. Regions associated with aromatic and aliphatic hydrocarbons exhibited little variation, indicating their lower sensitivity to oxidative conditions. Two oxidation indices, carbonyl-based and carbonyl-sulfoxide-based, were developed and normalized against stable aromatic peaks to quantify aging severity. The evolution of oxidation indices under progressive aging conditions indicates long-term performance in pavements.

The study extended the FTIR-based aging evaluation to field-aged samples, illustrating a gradient in oxidation products (especially carbonyl and sulfoxide groups) with depth, which is consistent with exposure-related aging. Carbonyl groups centered at ~1,696 cm^{-1} increased near the pavement surface, while others (~1,727 cm^{-1}) diminished with depth, indicating the need for selective use of carbonyl metrics in aging studies. Overall, these findings support the use of FTIR chemical characterization in both laboratory and field settings to assess binder durability as part of a tool for material selection strategies.

Linear Amplitude Sweep Test

The linear amplitude sweep (LAS) test represents the third development in the search for the best test of binder fatigue potential. The first, the $|G|^*\sin\delta$ fatigue index developed by the SHRP, was insufficient because it does not account for traffic loads or pavement structure (Bahia et al., 2001; Zhou et al., 2013). The second, the time sweep test, developed during the NCHRP 9–10 project, was time-consuming and unsuitable for characterizing fatigue behavior because of unstable flow and edge fracture effects in some cases (Anderson et al., 2001; Bonnetti et al., 2002). The LAS test presents a time-saving and more effective binder fatigue test method that has been correlated well with long-term pavement performance fatigue cracking field data (Hintz et al., 2011).

In the LAS test, systematically increasing load amplitudes are applied under cyclic loading using a DSR (AASHTO, 2019). First, the binder is subjected to a frequency sweep to determine a damage analysis parameter (α). Second, a strain-controlled, oscillatory shear test is conducted at a frequency of 10 Hz. The strain is increased linearly from 0.1% to 30% over the course of 3,100 cycles, for a total test time of 310 s. Peak shear stress and strain, phase angle, and complex shear modulus are recorded every 10 load cycles (1 s). Test results are analyzed using principles from the viscoelastic continuum damage model. Several researchers have used the LAS test to assess binder fatigue behavior (Cao & Wang, 2018; Hintz & Bahia, 2013; Notani et al., 2019; Sabouri et al., 2018; Xie, Castorena, et al., 2017).

Multiple Stress Creep Recovery Test

The multiple stress creep recovery (MSCR) test was developed to overcome the deficiencies of the Superpave PG system, specifically the rutting parameter $|G^*|/\sin\delta$. This parameter does not simulate real-world HMA rutting mechanisms. One limitation of this parameter is that it is derived based on the total strain energy dissipated within a loading cycle and assumes a fully reversible load, which does not reflect actual field conditions (Bahia et al., 1997; Chen & Tsai, 1999). The MSCR test applies several creep and recovery cycles at different stress levels. The viscoelastic strain induced in the creep portion can be recovered after the removal of shear stress, providing a means to separate permanent strain from the total strain, which is better correlated with field rutting (Liu et al., 2021). Other advantages include its application of different stress levels and its testing temperature, which is done at a PG high-temperature grade (D'Angelo, 2009; Zhang et al., 2015).

The MSCR test evaluates two primary parameters: nonrecoverable creep compliance and percent recovery. Nonrecoverable creep compliance, measured at 3.2 kPa, indicates the potential of AB for permanent deformation under repeated loading conditions, while percent recovery identifies the presence of elastic response and stress dependence of tested AB (D'Angelo, 2009; Zhang et al., 2015). Several studies have shown that nonrecoverable creep compliance relates better with rutting when compared with $G^*/\sin\delta$, and rutting potential of both unmodified and modified AB can be predicted (Domingos & Faxina, 2016; Wasage et al., 2011; Zhang et al., 2015; Zhang et al., 2016a).

Bending Beam Rheometer Test

The bending beam rheometer (BBR) test, introduced as part of the Superpave PG system, is used to evaluate low-temperature properties of AB (AASHTO, 2019). It applies static stress to a PAV-aged binder beam and measures the strain rate to derive the stiffness of the beam. The low-temperature PG is determined using both the stiffness and m-value at a 60 s load time. The m-value, the slope of

the creep curve at a 60 s load time, indicates the AB's ability to dissipate stresses. As with other parameters developed from the SHRP, the BBR test has some shortcomings, including insufficient conditioning in the BBR and absence of fracture/failure tests for brittle and ductile states (Hesp et al., 2009; Walubita et al., 2021). From field data, Hu and Walubita (2015) have found differences between binder performances of the same grade. The correlation between BBR test data and field pavement cracking has been reported (Hesp et al., 2009; Tabib et al., 2018).

Binder Potential Performance Parameters

In addition to the parameters (G*, δ, m-value, S-value) used to grade AB using the Superpave PG system, other parameters were introduced to better understand the behavior of AB.

Delta T_c (ΔT_c)

ΔT_c, as presented in Figure 1, is the difference in the two critical low PG temperatures: the critical temperature from stiffness, $\Delta T_{c,s}$, and the critical temperature from m-value, $\Delta T_{c.m}$. This parameter was originally conceptualized during SHRP and later suggested by the Airfield Asphalt Pavement Technology Program, Project 06-01 (Baumgardner, 2021). It gives an insight into the relaxation properties of AB, which can contribute to non-load-related cracking or other age-related distresses in HMA pavement (Asphalt Institute, 2019).

$$\Delta T_c = \Delta T_{c,s} - \Delta T_{c.m}$$

Figure 1. Equation. Delta T_c determination.

Source: Christensen et al. (2019)

It is normally used on AB that has been exposed to long-term aging in a pressure aging vessel (PAV). The proposed 40-hour PAV conditioning and ΔT_c parameter have been gaining momentum. A ΔT_c value of less than −5°C after 40-hour PAV conditioning suggests a high potential for cracking (Reinke et al., 2015).

Delta G Peak ($\Delta|G^*|_{peak\,\tau}$)*

The reduction in complex shear modulus, |G*|, as measured from the start of the LAS test until the peak shear-stress condition is reached, $\Delta|G^*|_{peak\,\tau}$, was proposed by García Mainieri et al. (2021) as a parameter to describe the effect of aging and modification on binder performance. In this study, the LAS test was used to study the damage characteristics of modified and unmodified binders in short- and long-term aging conditions. The higher the $\Delta|G^*|_{peak\,\tau}$, the better the binder's performance as it tolerates a higher loss of material integrity before its capacity decreases (in terms of shear resistance). An advantage of using the $\Delta|G^*|_{peak\,\tau}$ parameter is its simplicity to calculate. The limitation of |G*| is that it does not account for stress nonuniformity or potential crack formation (García Mainieri et al., 2021). The applicability of $\Delta|G^*|_{peak\,\tau}$ to polymer-modified binders was not investigated prior to this study. Singhvi et al. (2021) proposed a 53.5% threshold for $\Delta|G^*|_{peak\,\tau}$ as an intermediate temperature measure of damage tolerance, while the IDOT *Bureau of Design and Environment Manual* special provision uses 54% as a threshold.

HOT-MIX ASPHALT AND CRACKING POTENTIAL

Hot-mix asphalt, the most widely used pavement construction material, is a multiphase heterogeneous mixture consisting of viscoelastic AB, angular rigid aggregate particles, and air voids (Nega et al., 2013; Uzun & Terzi, 2012; Yilmaz et al., 2011). It may also contain various additives, such as fibers to enhance durability and ductility, mineral fillers to extend the binder and improve HMA density, and hydrated lime to reduce moisture sensitivity and prevent stripping (Salari et al., 2018; Xiong et al., 2015; Al-Hdabi, 2016; Kütük-Sert & Kütük, 2013; Hicks, 1991; Mohammad et al., 2000). The diverse properties of HMA's materials result in its complex physical, chemical, and mechanical behavior. Its performance depends on conditions such as temperature, loading rate, and age. Hence, HMA performance prediction must consider the properties of its components and the interaction of its constituent materials.

Asphalt pavement can experience several forms of distress, including rutting, fatigue cracking, and thermal cracking. The combined effect of traffic loading and environmental conditions impact pavement service life. Cracking, one of the major distresses in asphalt pavements, can be caused by a variety of reasons such as traffic-related bottom-up cracking and thermal cracking (Marasteanu et al., 2004). Cracks usually result from repeated horizontal strains at the bottom of the HMA layer or due to thermally induced stresses (repeated or single event), causing top-down cracking in cold temperatures, or by horizontal movements of lower overlaid cracked (or jointed) layers, developing reflection cracks that propagate to the surface (Newcomb, 2021).

Various cracking potential tests are used as part of balanced mix design to predict HMA field performance. Zhou et al. (2016) categorized these tests into two groups: (1) methods that produce engineering indices and apply failing and passing criteria to assess cracking potential of HMA, and (2) methods that provide results or properties used as inputs in cracking models. Criteria to evaluate these tests include variability, applicability, simplicity, sensitivity of measured parameters to mixture design, correlation to field performance, engineering intuition, and availability and cost of the device (Al-Qadi et al., 2015; Newcomb, 2021).

Al-Qadi et al. (2015) developed the Illinois Flexibility Index Test (I-FIT) to quantify HMA cracking potential. The test demonstrated consistent and repeatable trends in response to changes in HMA design. The flexibility index (FI) parameter was introduced and shown to capture HMA cracking potential. I-FIT was validated using two sets of field data from FHWA's accelerated loading facility sections and random field cores provided by IDOT districts. A short- and long-term aging protocol was later developed by Al-Qadi et al. (2019) as part of the implementation of this test. I-FIT does not impose limits on HMA designs, such as RAP and RAS content, or other alternative materials or technologies, but focuses on potential performance (Barry, 2016; Batioja-Alvarez et al., 2019; Jeong et al., 2022; Ling et al., 2017; Rivera-Perez et al., 2018). I-FIT was selected to test HMA cracking potential in this study.

Polymers such as SBS improve elasticity and rut resistance, while softeners restore flexibility and mitigate brittleness in high-RAP mixtures. While beneficial individually, their combined use affects binder rheology in a complex way that may compromise the long-term stability and performance consistency of HMA. The modifiers may influence the aging rate and interact unpredictably under

heat and oxidative conditions, potentially altering FI outcomes. Hence, advanced rheological parameters may offer deeper insights into aging and fatigue behavior and, hence, a quantitative impact of I-FIT results.

Relationship between Binder and HMA Cracking Potential

Several research efforts have aimed to use binder parameters to predict HMA cracking potential. This section summarizes some of these parameters.

Delta Tc (ΔT_c)

Anderson et al. (2011) investigated the use of a binder's ΔT_c parameter as an indicator of non-load-related cracking. In their study, ΔT_c was measured after 20, 40, and 80 hours of aging in a PAV. ΔT_c became more negative with increased aging. In addition, with increased oxidative aging, ΔT_c became more negative, suggesting asphalt binder became more m-controlled (failing the 0.3 m value threshold at a warmer temperature than the S-value temperature). This finding indicates the asphalt binder could not relax from stresses and was losing flexibility and gaining brittleness, becoming susceptible to cracking (Asphalt Institute, 2019).

The ΔT_c parameter has also been used to detect the effect of using recycled engine oil bottoms (REOB) in asphalt binder (Lesueur et al., 2021). Li et al. (2017) conducted a performance evaluation of REOB-modified asphalt binders and mixtures, concluding that ΔT_c was the most practical indicator of substantial REOB content, reflecting significant changes in rheological and performance characteristics. They suggested it was related to a physical disruption occurring at the microstructural level of the binder. ΔT_c has been used to examine the influence of RAP, RAS, and rejuvenators on binder performance (Oldham et al., 2019; Sharma et al., 2017; Xie, Tran, et al., 2017).

R-value

The R-value is a binder parameter derived from the complex modulus master curve, representing the difference between the log G* at crossover frequency and the log elastic asymptote of the master curve (Anderson et al., 1994). Aging of binders flattens the master curve, consequentially increasing the R-value. In their study comparing asphalt binder and HMA cracking parameters, Rahbar-Rastegar et al. (2017) found a strong correlation between R-value and ΔT_c (Pearson correlation factor > 0.98).

G'/(η'/G')

G'/(η'/G') was developed at Texas A&M University by Glover et al. (2005) from a study aimed at developing an improved method of screening asphalt binder for long-term pavement performance. The function correlated well with ductility (at 15°C, 1 cm/min) below 10 cm for unmodified asphalt binder. G'/(η'/G') was computed using an original procedure that measures G' and η' by DSR testing at 44.7°C and 10 rad/s for easy accessibility to standard laboratory rheological equipment and methods. In AAPTP project 06-01, the parameter was selected because of its correlation to ductility (R^2 = 85%), to identify binders with different block cracking potential (Asphalt Institute, 2019). However, a concern with the G'/(η'/G') parameter was the potential variability due to temperature-frequency sweep and master curve plotting (Anderson et al., 2011).

Glover-Rowe Parameter

This parameter, developed by Glover et al. (2005) and simplified by Rowe (2011), presents another parameter to evaluate low-temperature cracking potential of HMA. The Glover-Rowe (G-R) parameter, as presented in Figure 2, uses a complex shear modulus (G*) and binder phase angle (δ) at a temperature-frequency combination of 15°C–0.005 rad/s. At a frequency of 0.005 rad/s, the G-R parameter has a threshold of 0.18 MPa as the onset of cracking and a threshold of 0.60 MPa as an indicator of significant cracking (Blankenship et al., 2010).

$$\frac{G^*(cos\delta)^2}{sin\delta}$$

Figure 2. Equation. Glover-Rowe equation.

Source: Rahbar-Rastegar et al. (2017)

Elastic Recovery

Elastic recovery refers to the ability of an asphalt binder to return to its original shape after the removal of a load (Mogawer et al., 2011). This property is measured using a ductilometer following the AASHTO T 301 standard test method (AASHTO, 2022a), which evaluates elastic recovery by stretching a binder specimen to a specified elongation and then allowing it to retract. Elastic recovery is often cited as a critical indicator of HMA cracking resistance (Yan et al., 2022; Zhang et al., 2016b). Zhang et al. (2016b) concluded that HMA with asphalt binder that had elastic recovery of over 59% had longer fatigue lives. This is similar to findings by Yan et al. (2022), who reported a good correlation between elastic recovery and fatigue life of the LAS test. The correlation increased with increasing strain levels. However, Mogawer et al. (2011), in a study using continuum damage and overlay test-based analyses, observed inconsistent trends between elastic recovery and HMA fatigue cracking resistance. Although elastic recovery rankings among different binders were similar, the parameter itself was not consistently predictive of fatigue cracking performance.

Delta m (Δm)

In a study by Zhu et al. (2020), the parameter Δm—defined as the m-value of 20-hour PAV-aged (1PAV) binder minus the m-value of a 40-hour PAV-aged (2PAV) binder—was proposed as a parameter for HMA aging rate. In their study, seven laboratory mixes were designed and produced at three asphalt binder replacement (ABR) levels using binders of the same PG from different sources. The HMA designs were tested using I-FIT under unaged and long-term aged conditions. Binder testing included the standard Superpave and temperature-frequency sweep tests on virgin binders under various aging conditions. Mixes with the same design, but different binder sources, can show significantly different flexibility under unaged and long-term aged conditions, and the ranking of FI for long-term aged specimens did not necessarily align with that of unaged specimens. Therefore, they recommended avoiding binders with high Δm to control the excessive drop in HMA flexibility after aging.

CHAPTER 3: EXPERIMENTAL PROGRAM

The main objectives of this study were to evaluate the feasibility of modifying asphalt binder with both polymer and softener as well as the feasibility of predicting HMA cracking potential using measured binder rheological parameters. Therefore, an experimental program was developed that encompassed the following:

1. Diverse range of binders: Base binders of various sources and properties were selected and then modified with different softeners and SBS to obtain softened binders, polymer-modified binders, and polymer-softener-modified binders.

2. Binder stability and rheology: Stability of modified binders was examined, and the rheology of the binders was evaluated.

3. HMA design: Various mixes were designed with selected binders, including different RAP contents and, ultimately, different asphalt binder replacements.

4. HMA potential performance: HMA designs were tested for cracking and rutting potential using the I-FIT and HWTT, respectively.

5. Correlation development: Statistical analysis has been used to predict cracking potential from binder properties.

Details of these steps are presented in the following sections.

BINDER MATERIALS AND MODIFICATION

Two PG 64-22 binders were used as the primary experimental binders. The two binders are designated as good (G) and borderline (B), based on generally adopted ΔT_c thresholds: −2.0 at PAV-aged condition and −5.0 at double-PAV-aged condition. They were either softened to PG 58-28 or polymer-softener-modified to PGs 70-28 and 76-28. Table 1 presents the asphalt binder used in this study.

Table 1. Characteristics of Tested Binders

Designation	True PG	PAV ΔT_c	2PAV ΔT_c	1PAV $\Delta\lvert G^*\rvert_{peak\,\tau}$ (%)	2PAV $\Delta\lvert G^*\rvert_{peak\,\tau}$ (%)
64-22G	66.9-23.5	0.8	−1.4	59.1	57.8
64-22B	66.3-24.0	−2.2	−7.6	62.0	56.5
58-28G	58.0-30.1	0.7	−3.2	61.8	58.2
58-28B	60.1-29.7	−0.3	−4.8	62.7	58.3

Figure 3 presents the binder modification process, which involves softening the binder prior to polymer modification.

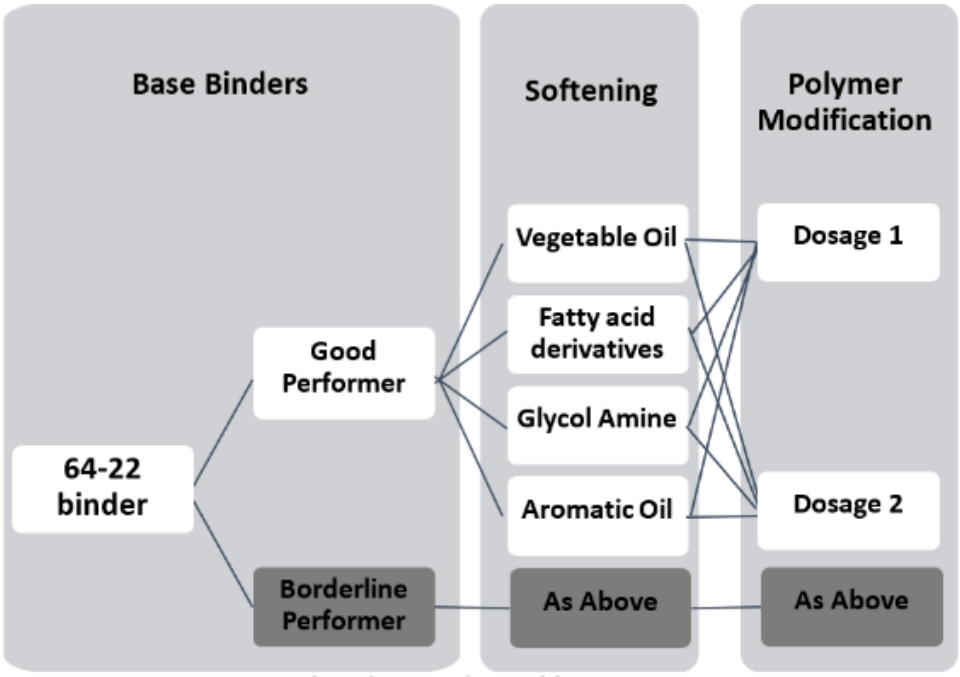

Figure 3. Flowchart. Binder modification sequence.

Four softeners were used on both base binders to attain PG 58-28. Hence, two unmodified PG 58-28 binders were included in the study for comparative analyses. These unmodified PG 58-28 binders are designated as 58-28G and 58-28B, as presented in Table 1.

Softeners: Four bio-based softeners were used in this study, primarily to achieve the low-temperature PG of −28°C. Table 2 presents details of the softeners used in this study. The type of softener indicates its most predominant functional group.

Table 2. Softener Type and Designation

Designation	Modifier	Type
F	Softener	Vegetable Oil
C	Softener	Fatty Acid Derivative
M	Softener	Aromatic Oil
N	Softener	Glycol Amine
S	Polymer	SBS

Polymer: The polymer used in the study is styrene-butadiene-styrene (SBS), a family of synthetic rubber derived from styrene and butadiene. SBS was used to achieve high-temperature PGs of 70°C and 76°C. Sulfur was used as a crosslinking agent.

Modification Protocol

A shear mixer (Cafarmo BDC1850) equipped with a Heidolph PR31 ringed propeller (33 mm diameter fan) was used to blend softeners and binders (Figure 4). Blending was performed at a constant

temperature of 130 ± 10°C, maintained using a Glas-Col LLC heating mantle. The following steps were taken to soften binders:

1. Binders were sampled from the refinery terminal in 1 gal cans. The cans were heated at 135°C and then split into quart-cans to get binders weighing between 500 g–600 g.

2. Quart-can-sized binders were heated in the heating mantle at 80% power for 10 min and then at 10% power for 15 min to reach 130 ± 10°C, ensuring the binder is fluid enough prior to blending.

3. A softener was added (weight measured with a 0.01 g readability scale). The propeller was inserted halfway into the can, and set to 1,000 revolutions per minute (rpm) for 20 min. During blending, the temperature was maintained at 130 ± 10°C, and vortices were prevented to avoid air bubbles in the blends.

Figure 4. Photo. Cafarmo BDC1850 shear mixer.

A high shear mixer (Figure 5) with an "emulsor screen" work head was used for all blending involving SBS due to the higher rpm required. Blending was performed at a constant temperature of 185 ± 10°C, maintained using a Glas-Col LLC heating mantle. The following steps were taken for polymer modification of binders:

1. Quart-can-sized binders, weighing between 500 g–600 g, were heated in the mantle at 80% power for 10 min and then at 10% power for 15 min to reach 130 ± 10°C, ensuring the binder was fluid enough prior to blending.

2. The propeller was inserted halfway into the depth of the material and was set to 4,500 rpm, while the heating mantle was set at 100% power for about 6–8 min to reach about 165°C.

3. The heating mantle was set to 0% power, and the temperature was allowed to rise to 185 ± 10°C (about 3–4 min).

4. SBS pellets were added, and shearing continued for 30 min. Sulfur pellets were then added, and shearing continued for another 30 min. Vortices were prevented to avoid air bubbles in the blends.

5. The blend was placed in an oven for 18 hours of curing at 163°C.

6. The modified blend was split into 8 oz cans for subsequent binder testing.

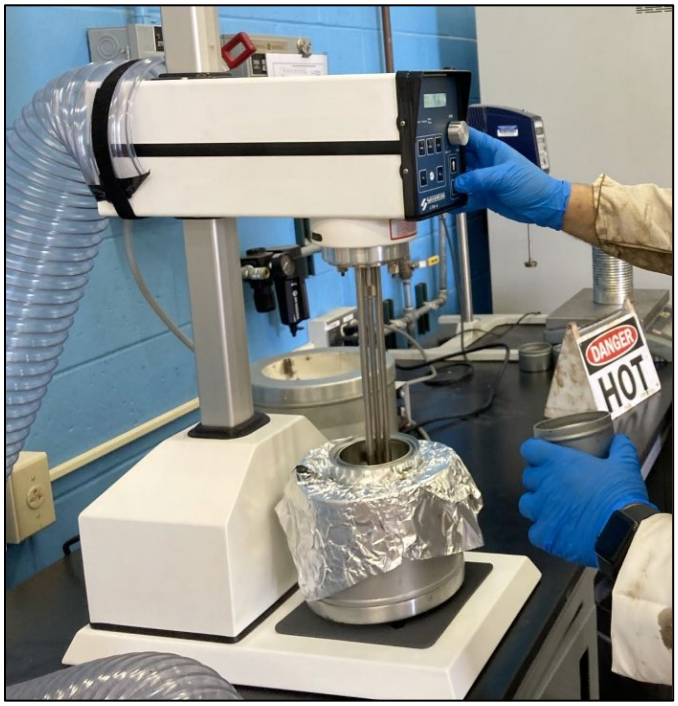

Figure 5. Photo. Silverson L5M-A high shear mixer.

Polymer-softener-modified binders: The modification sequence determines the steps taken. For polymer modification after softening, step 2 of the polymer-modified binder process begins immediately after completing step 3 of the softened-binders process. For softening after polymer modification, after the polymer-modified binder is cooled to room temperature at the end of step 5, the softened-binders process commences with the first step.

The adopted polymer-softener modification protocol in this study involved polymer modification of an already softened binder. A softened binder, having already met the required low-PG temperature, was then modified with SBS and placed in the curing oven for 18 hours at 163°C to get a polymer-softener-modified binder.

Binders were named based on their composition. Binary blends (polymer-modified binders or softener-modified binders) were identified with the base binder's designation, followed by a plus sign, the dosage (% by weight), and the designation of the modifier. For example, G+4C is a blend obtained from base binder G blended with 4% of softener "C." Ternary blends (polymer-softener-modified binders) were identified with the base binder's designation, a plus sign, and the sequence of

modification. For example, B+4C+4.5S represents a blend obtained from base binder B, softened with 4% softener "C," and then polymer modified with 4.5% SBS. G+5S+3.5F represents a blend obtained from base binder G, polymer modified with 5% SBS, and then softened with 3.5% softener "F."

BINDER STABILITY AND RHEOLOGY

Binder Thermal and Storage Stability

Thermal Stability

The thermal stability of blends was evaluated using the Superpave binder mass loss protocol and thermogravimetric analysis (TGA). Binder mass loss was conducted in accordance with AASHTO T 240. TGA was performed on softeners at the University of Illinois Urbana-Champaign's Materials Research Laboratory. Q50 TGA equipment was used to conduct two heating protocols at a constant heating rate of 20°C/min in a nitrogen environment: a ramp protocol from 0°–600°C and a heat-and-hold protocol (ramp from 0°–163°C and hold for one hour). A thermogram is plotted to visualize the change in mass with temperature or time. A 10–20 mg sample weight was used with two replicates tested for each sample.

Storage Stability

Storage stability was evaluated using the cigar tube separation test per ASTM D7173 (2020). Two conditioned replicates were tested for each sample. After the heating period, the tube is removed from the oven and cooled to room temperature. The top and bottom sections were tested in the DSR for complex modulus (G*) and phase angle (δ). The homogeneity index is calculated as presented in Figure 6.

$$Homogeneity\ index = \frac{G^*/sin\delta_{top}}{G^*/sin\delta_{bottom}}$$

Figure 6. Equation. Homogeneity index.

Binder Rheology

Performance Grading

The PG of binders was evaluated following the Superpave method per AASHTO M 320. This suite of tests involves using the DSR to get high and intermediate PG temperatures and the BBR to get the low-PG temperature and ΔT_c parameter.

Linear Amplitude Sweep

The fatigue cracking potential of binders was evaluated using the LAS test performed in the DSR, in accordance with AASHTO T 391 (2024). All samples were tested at their respective intermediate temperature: 19°C for PG 58-28, 25°C for PG 70-28, and 28°C for PG 76-28. Shear stress was applied at a frequency of 10 Hz, while progressively increasing the strain from a low to a high amplitude until

failure. The fatigue tolerance parameter, $\Delta|G^*|_{peak\tau}$, was reported. Two replicates were tested for each sample.

Multiple Stress Creep Recovery

The high-temperature performance of binders, particularly their potential for permanent deformation, was evaluated using the MSCR test in accordance with AASHTO T 350 (2025). In the DSR, the binder is subjected to a series of short-duration (1 s) shear stresses, followed by a recovery period (9 s) where no load is applied. Two key parameters are reported: percent recovery (R), which indicates a binder's ability to recover its original shape after a load is removed, and nonrecoverable creep compliance (J_{nr}), which measures a binder's susceptibility to permanent deformation. Tests were carried out at PG RTFO temperature. Two replicates were tested for each sample. Figure 7 presents a typical MSCR curve, showing the creep and recovery cycles.

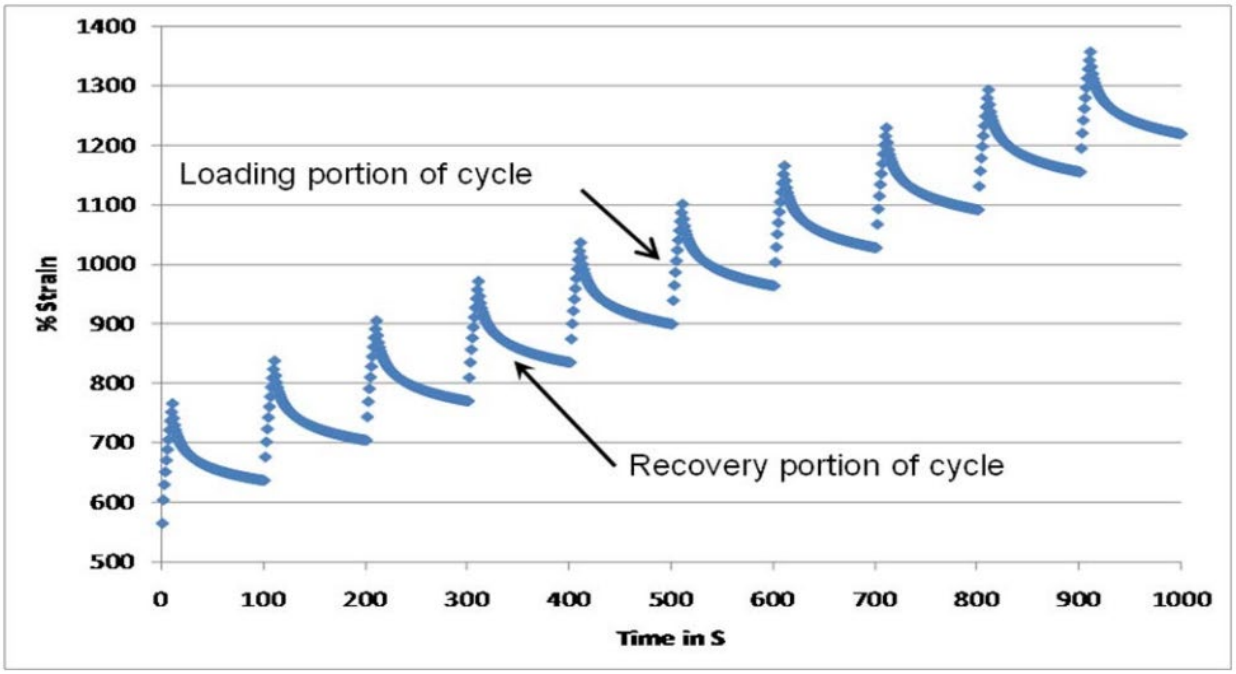

Figure 7. Graph. Typical asphalt binder response to repeated loading.

Source: Harman et al. (2011)

Binder Chemistry

Fourier-Transform Infrared Spectroscopy

The Jasco FT/IR-4X spectrometer was used to identify the chemical functional groups present in the modified binders within the spectral range of 400 to 4,000 cm^{-1}. Molecules vibrate in characteristic ways (stretching, bending, twisting), and each type of bond absorbs infrared radiation at specific frequencies (measured in wavenumbers, cm^{-1}). By recording the absorption spectrum, FTIR produces a unique fingerprint that reflects the chemical composition of the blend. The measurements were conducted using a spectral resolution of 4 cm^{-1} and averaged over 50 scans per sample. The analysis

was carried out using the attenuated total reflectance (ATR) technique. Functional groups related to carbonyl, sulfoxide, polybutadiene, and polystyrene were examined to assess the oxidative aging of asphalt binders and degradation of polymer. Oxidation and degradation indices based on these functional groups were used for the assessments. Five replicates were tested for each sample.

HMA DESIGNS

Two coarse materials (CM-16s), limestone and trap rock, were used in three mix designs of varying ABRs: high (23.7%), medium (14.8%), and no (0%) ABR. Table 3 presents the six HMA designs. The HMA design process, through optimizing voids in mineral aggregate (VMA) and asphalt content (AC), ensured all mixes had 4.0 ± 0.1% air void (AV) content. The VMA was maintained above the IDOT minimum requirement of 15.0%.

Table 3. Mix Design Volumetrics

Parameter	Limestone Mix			Trap Rock Mix		
	No ABR	Moderate ABR	High ABR	No ABR	Moderate ABR	High ABR
Mix Bulk Specific Gravity (G_{mb})	2.348	2.341	2.352	2.353	2.351	2.352
Theoretical Maximum Specific Gravity (G_{mm})	2.446	2.439	2.450	2.450	2.449	2.453
AV	4.0	4.0	4.0	3.9	4.0	4.1
VMA	15.5	15.9	15.4	15.3	15.2	15.3
ABR	0.0	14.8	23.7	0.0	14.9	23.7
Binder PG	64-22	64-22	58-28	64-22	64-22	58-28
AC	6.1	6.2	6.0	5.7	5.8	5.9
Aggregate Bulk Specific Gravity (G_{sb})	2.609	2.611	2.612	2.621	2.610	2.612

Binder Selection Protocol for HMA

The protocols that guided binder selection are listed as follows:

1. All selected binders were paired (good vs borderline).
2. Selection would favor extreme performing softeners (1st [best] and 4th [worst]).
3. Mixes with 0% ABR were prioritized to serve as a control.
4. All softeners were represented.
5. For practical purposes, mixes with relatively high ABR would use softer binders.

Table 4 presents the selected binders and mixes using the selection protocol. A total of 48 mixes using 20 different binders were tested.

Table 4. Selected Binders and Mixes

	Limestone Mix		Traprock Mix	
Mix Design / Binder*	**Experimental (PG 64-22)**	**Comparison (PG 58-28)**	**Experimental (PG 64-22)**	**Comparison (PG 58-28)**
High ABR (6)	PG 58-28 w/C		PG 58-28 w/C	
	PG 58-28 w/N		PG 58-28 w/N	
		Neat PG 58-28		Neat PG 58-28
Moderate ABR (6)	SBS PG 70-28 w/N		SBS PG 70-28 w/N	
	SBS PG 70-28 w/F		SBS PG 70-28 w/F	
		SBS PG 70-28		SBS PG 70-28
No ABR (12)	Neat PG 64-22		Neat PG 64-22	
	SBS PG 76-28 w/C		SBS PG 76-28 w/C	
	SBS PG 76-28 w/M		SBS PG 76-28 w/M	
		Neat PG 58-28		Neat PG 58-28
		SBS PG 70-28		SBS PG 70-28
		SBS PG 76-28		SBS PG 76-28

* Selected binders are paired (good and borderline), doubling the total number of mixes to 48.

MIXTURE POTENTIAL PERFORMANCE

Illinois Flexibility Index Test

The flexibility and cracking potential of mixes were evaluated using I-FIT in accordance with AASHTO T 393 (2022b). The test was conducted at 25°C. I-FIT parameters such as the FI, fracture energy (G_f), post-peak slope (m), and strength (in psi) were reported for aged and unaged specimens. The FI is calculated using a load-displacement curve (Figure 8):

$$FI = \frac{G_f}{|m|} \times A$$

Figure 8. Equation. Calculation of FI.

where *A* is a correction coefficient set to 0.01.

Each mixture was tested with three to four replicates per aging condition. Figure 9 presents an I-FIT specimen in the test fixture, while Figure 10 displays a typical test result.

Figure 9. Photo. Specimen in the I-FIT fixture.

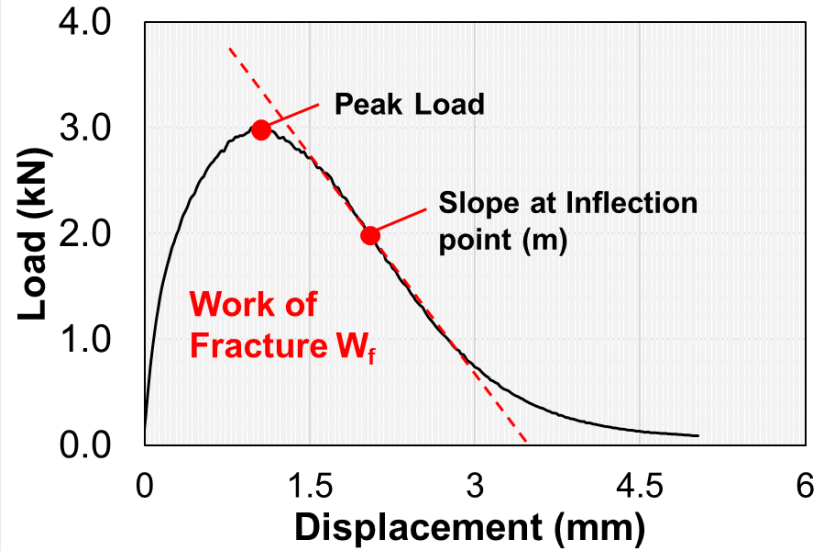

Figure 10. Graph. Typical I-FIT test result.

Hamburg Wheel-Tracking Test

The rutting potential and moisture susceptibility of mixes were evaluated using the HWTT in accordance with AASHTO T 324 (2014a). Specimens were compacted to a height of 130 mm and then cut in half to obtain Hamburg specimens with a target air void content of 7 ± 0.5%. The depth of the rut formed on the specimen is monitored and recorded continuously, providing a measure of the mixture's potential for permanent deformation. Two replicates were tested for each sample. Figure 11 illustrates a specimen placed in the HWTT SmarTracker test machine, while Figure 12 presents a typical HWTT test result.

Figure 11. Photo. Specimen in the SmarTracker machine.

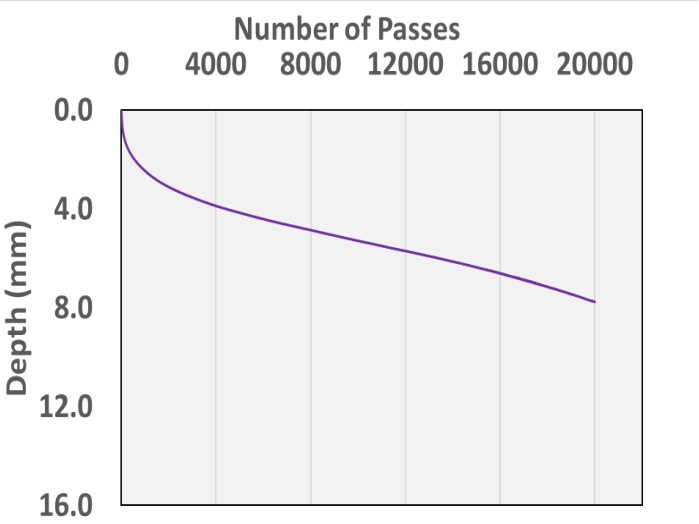

Figure 12. Graph. Typical HWTT test result.

STATISTICAL ANALYSIS

The final phase of the study focused on performing statistical analyses to investigate the relationship between binder rheological and HMA cracking potential parameters. The goal was to develop a predictive model for HMA cracking potential (e.g., FI, post-peak slope, G_f) using binder test result parameters (e.g., 1PAV ΔT_c, 2PAV ΔT_c, $\Delta|G^*|_{peak\ \tau}$, S-value, m-value). The following steps were completed:

1. Database Compilation and Preprocessing: A laboratory test database was developed. The database comprises measured binder rheological parameters and corresponding HMA cracking potential parameters. The dataset included HMA with different binder PG, RAP

content, and softener type. Data preprocessing techniques, including normalization, were employed to ensure comparability and to address data variability.

2. Exploratory Statistical Analysis: Correlation analysis was conducted to explore potential relationships between binder parameters and HMA cracking potential metrics. Normality tests were performed to confirm the suitability of statistical assumptions for subsequent modeling.

3. Regression Modeling: Statistical modeling techniques, including multiple linear regression, were applied to establish a predictive model of HMA fracture from binder rheology. This will also guide future model refinement.

4. Nonlinear Modeling: For parameters exhibiting weak linear relationships, nonlinear modeling techniques, such as support vector regression, were utilized. Validation methods ensured robust and accurate prediction.

5. Integrated Prediction of FI: Integrated modeling approaches, combining predictions from linear and nonlinear methods to estimate FI values effectively, were utilized to support the practical application of the model.

CHAPTER 4: CHARACTERIZATION OF MODIFIED BINDERS

MODIFIED BINDER STABILITY AND MASS LOSS

This study involved various modifications to asphalt binder (e.g., softening, polymer modification, and polymer-softener modification), so the stability of modified binders was critical to ensure optimal HMA performance. Therefore, both storage and thermal stability were investigated. The results of the cigar tube test, conducted in accordance with ASTM D7173 to evaluate storage stability, are presented in Table 5. Homogeneity indices (the difference between the top and bottom parts of a tested specimen) were calculated using Figure 5.

Table 5. Cigar Tube Test Results

Modifier	Blend	Temperature (°C)	Portion	Average G*/sinδ (kPa)	Homogeneity Index
S	G+3.5S	76	Top	1.515	**0.97**
			Bottom	1.560	
C	G+3C+5S	76	Top	1.870	**1.01**
			Bottom	1.845	
F	G+3.5F+4.7S	76	Top	1.920	**1.01**
			Bottom	1.900	
M	G+5M+5S	70	Top	2.715	**0.99**
			Bottom	2.725	
N	B+5.2S+5N	76	Top	1.400	**1.01**
			Bottom	1.390	

Blends with a high PG of 76°C were selected for each softener, as they contain the highest dosage of SBS and the highest risk of separation and storage instability. The homogeneity indices of blends were between 0.97 and 1.01, suggesting no separation. Homogeneity indices between 0.8%–1.2% are typically considered acceptable (Kumar et al., 2021; Al-Abdul Wahhab et al., 2017). Hence, all modified binder blends were considered stable against separation under static heated storage conditions.

The binder mass loss on RTFO-aged binder was used to evaluate thermal stability of softened binders. Results of three replicates and their averages are presented in Table 6. Mass loss was 0.08%, 0.22%, 0.14%, and 1.07% for blends made with softeners F, C, M, and N, respectively. Based on the results, softener F was the most thermally stable, while softener N was the least stable. AASHTO M 320 sets a maximum threshold of 1.0% for acceptable mass loss. While softeners F, C, and M met this criterion, softener N exceeded the limit, indicating high volatility. The elevated mass loss of softener N was further supported by the strong, unpleasant odor released during RTFO aging.

Softener F, the most stable, is a vegetable oil–based softener, while softener N, a glycol-amine–based softener, resulted in a mass loss about seven times higher than other softeners. These findings align with results reported by Singhvi et al. (2021), where a glycol-amine–based softener, G, had a mass loss of 2.98% (about six times greater than other softeners in the study), while a vegetable oil–based

softener had the lowest mass loss (0.36%). These findings emphasize the volatility of glycol-amine–based softeners, highlighting the caution for their use in binder modification.

Table 6. Binder Mass Loss Results

Softener	S1	S2	S3	Average (%)
F	0.02	0.03	0.19	**0.08**
C	0.20	0.22	0.24	**0.22**
M	0.07	0.22	0.14	**0.14**
N	1.05	1.08	1.08	**1.07**

THERMOGRAVIMETRIC ANALYSIS OF MODIFIED BINDER

Thermogravimetric analysis (TGA) was used as a secondary thermal stability technique after binder mass loss. TGA measures changes in the mass of a material as a function of temperature or time. The following section presents the result of the two types of TGA conducted: ramp and heat-and-hold.

The ramp TGA involved heating the softeners from room temperature to 600°C at a ramp of 20°C/min. Heat-and-hold TGA involves heating the softener to a certain temperature and holding it for a specific duration. The heat-and-hold ramp TGA directly affects storage durations for modified binders. When binders are stored at a specific temperature for an extended period due to factors such as construction delays or site distance, thermal stability of the modifier content becomes crucial. Additionally, prolonged heating times could be restricted for thermally unstable blends.

The test data and accompanying thermograms are presented in Table 7 and Figure 13, respectively.

Table 7. Ramp TGA Results

Softener ID	Base	Percent remaining at 163°C (%)	Temp at 1% loss (°C)
F	Vegetable Oil	100.00	348.93
C	Fatty Acid/Tall Oil	99.92	216.03
M	Aromatic Oil	100.00	207.33
N	Glycol Amine	99.11	167.25

From Figure 13, softener M lost 100% of its content at a lower temperature (~366°C) than that of softener N (~455°C). However, there are no practical instances for the usage of binders above 300°C. From the ramp TGA, softener F was the most thermally stable, while softener N was the least stable, using two criteria: temperature at which they lose 1% of material and the percent remaining at 163°C. 163°C is an important temperature, as this is the RTFO temperature and curing temperature used for polymer-modified binders. Although there are no current specifications or thresholds for the TGA of softeners, the ramp TGA results agreed with binder mass loss data.

For the heat-and-hold TGA, the temperature was 163°C and the hold was for 1 hour. The test data and accompanying thermograms are presented in Table 8 and Figure 14, respectively. After a 1-hour hold at 163°C, the remaining percentage was 99.85%, 96.30%, 87.20%, and 81.70% for softeners F, C,

M, and N, respectively. There was agreement between both stability investigations: thermal and storage stability. In general, from a stability perspective, the softeners are ranked as follows: F, C, M, and then N, where F is the most stable.

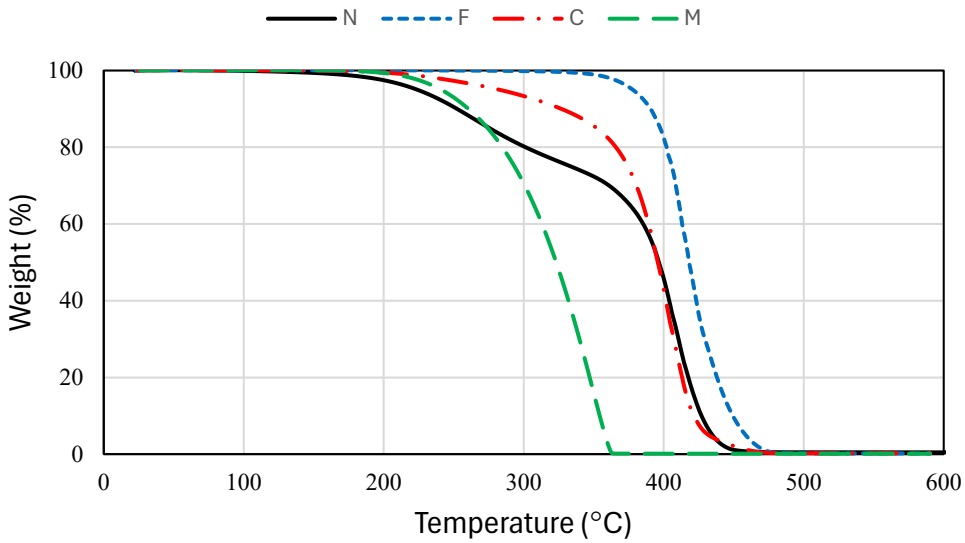

Figure 13. Graph. Thermograms of ramp TGA.

Table 8. Heat-and-Hold TGA Results

Softener ID	Base	Percent Remaining after 1 Hour Hold at 163°C (%)
F	Vegetable Oil	99.85
C	Fatty Acid/Tall Oil	96.30
M	Aromatic Oil	87.20
N	Glycol Amine	81.70

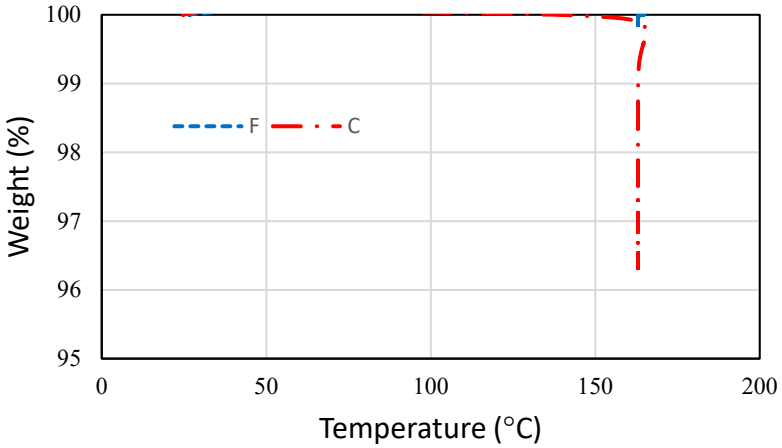

A. Softeners F and C

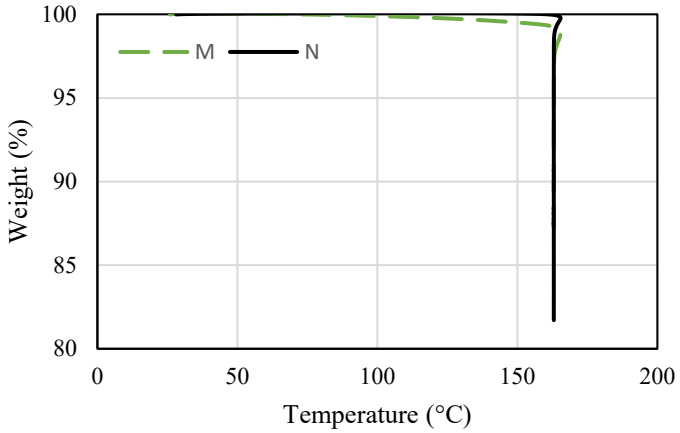

B. Softeners M and N

Figure 14. Graph. Thermograms of heat-and-hold TGA.

While softener N was the least stable softener, there was no current classification for it using the TGA. In addition, its binder mass loss of 1.07% was quite marginal compared to the 1.00% threshold. However, its instability raised a major concern with polymer-softening modification whenever softener N was used. All polymer-softener-modified blends maintained their low-PG temperature designation except when softener N was used. The increase in true low-PG temperature indicated a reduction in stress relaxation.

For example, the softened binder with softener N (B+5N) met the target low PG of −28 (−28.6°C). However, upon the SBS modification of this softened binder, the low-temperature PG increased from −28.6°C to −26.4°C. While this is just a 2.2°C difference, the blend may no longer be designated PG-28. To investigate this softening loss, samples were tested for low-temperature PG at 6-hour intervals (i.e., 0, 6, 12, and 18 hours), as presented in Table 9.

Table 9. Low-Temperature PG of Softener N in Polymer-Softener-Modified Binders

ID	Curing Duration (hr)	Temp (°C)	m-value	S (MPa)	True PG, m (°C)	True PG, S (°C)	True PG (°C)	ΔT_c (°C)
B+5N	N/A	−18	0.308	285	−28.6	−28.4	−28.4	0.3
		−24	0.236	647				
B+5N+5.5S	0	−18	0.277	238	−25.4	−30.1	−25.4	−4.6
		−24	0.223	463				
	6	−18	0.273	257	−24.6	−29.5	−24.6	−4.9
		−24	0.224	484				
	12	−18	0.270	239	−26.4	−32.0	−26.4	−5.8
		−24	0.221	452				
	18	−18	0.286	196	−26.4	−32.0	−26.4	−5.6
		−24	0.232	374				

The binder became more m-controlled during the curing period. Although a progressive reduction in ΔT_c was observed during the 16-hour curing period, a major loss of the softening effect happened before curing started, as the binder low-temperature PG had already increased by 3°C and switched from S-controlled to m-controlled at 0 hours of curing. Softener evaporation took place when the softened binder was modified with polymer (shearing at 4,500 rpm and 185°C for about 1 hour) and had caused the blend to fail the low-temperature PG.

To overcome evaporation and subsequent loss of softening, the polymer-softener modification protocol was reversed. Instead of modifying a softened binder with polymer, a polymer-modified binder was softened post-polymerization. This revised approach successfully preserved the desired low-PG designation, as presented in Table 10. This change in protocol was also shown in the designation: G+4S+5N indicates a blend obtained from base binder G, polymer modified with 4% of SBS, and then softened with 5% of softener N.

Regarding the preferred sequence of adding polymer and softener to binders to produce polymer-softener-modified binders, an industry survey was conducted with binder suppliers. Of the respondents, 60% reported they polymer modify an already softened binder while 20% indicated they soften an already polymer-modified binder. The remaining 20% use either of the two sequences.

Table 10. Low-Temperature PG of Softener N in Polymer-Softener-Modified Binders (Alternate Protocol)

Superpave PG	Designation	Temp (°C)	m-value	S (MPa)	True PG, m (°C)	True PG, S (°C)	True PG (°C)	ΔT_c (°C)
70-28	G+4S+5N	−18	0.314	290	−29.2	−28.3	−28.3	0.9
		−24	0.245	618				
	B+4S+5N	−18	0.310	235	−29.0	−30.1	−29.0	−1.1
		−24	0.251	472				
76-28	G+5.2S+5N	−18	0.318	289	−29.5	−28.3	−28.3	1.1
		−24	0.246	573				
	B+5.2S+5N	−18	0.312	216	−29.5	−30.8	−29.5	−1.3
		−24	0.265	436				

MODIFIED BINDER RHEOLOGICAL PARAMETERS

The true PG of the base and modified binder are reported in Table 11, in accordance with AASHTO M 320.

Table 11. True PG of Base and Modified Binders

Blend Type	ID	True High PG	True Low PG	PG	1PAV ΔT_c	2PAV ΔT_c
Base Binders (Experimental)	G	67.0	−23.5	64-22	0.8	−1.4
	B	66.3	−24.1	64-22	−2.1	−7.6
Base Binders (Comparison)	58-28G	60.8	−30.1	58-28	0.7	−3.2
	58-28B	62.9	−30.6	58-28	0.0	−4.8
Softened Binders	G+4F	60.3	−29.9	58-28	1.2	−0.2
	B+4F	59.8	−29.7	58-28	−1.8	−6.1
	G+4C	59.4	−28.4	58-28	4.1	0.9
	B+4C	58.8	−31.4	58-28	−0.3	−4.5
	G+5M	60.7	−27.9	58-28	1.2	−0.7
	B+5M	60.4	−29.0	58-28	−1.2	−4.6
	B+5N	62.0	−28.4	58-28	0.3	−1.5
Polymer-Modified Binders	G+1.8S	71.8	−24.5	70-22	0.3	N/A
	B+1.8S	73.3	−24.0	70-22	−2.9	N/A
	G+3.5S	77.0	−25.6	76-22	−0.1	N/A
	B+3.5S	78.9	−24.6	76-22	−3.8	N/A
Polymer-Softener-Modified Binders	G+4F+3.6S	70.5	−31.7	70-28	−0.1	−2.2
	B+4F+3.6S	73.4	−31.3	70-28	−2.4	−5.6
	G+4C+3.6S	70.1	−30.7	70-28	0.6	−0.5
	B+4C+3.5S	70.5	−31.3	70-28	−2.0	−3.0
	G+4M+3.5S	72.8	−28.9	70-28	0.6	−1.5
	B+5M+3.4S	73.1	−30.1	70-28	−2.1	−6.7
	G+4S+5N	71.7	−28.3	70-28	0.9	1.0
	B+4S+5N	72.9	−29.0	70-28	−1.1	−2.5
	G+3.5F+4.7S	76.7	−31.3	76-28	−0.9	−0.6
	B+3.5F+4.1S	77.2	−30.0	76-28	−3.2	−6.0
	G+3C+5S	76.1	−29.0	76-28	−0.6	−0.8
	B+3C+5S	78.6	−28.9	76-28	−3.2	−5.4
	G+5M+5S	76.6	−30.7	76-28	0.1	−0.8
	B+4.9M+4.2S	77.1	−29.0	76-28	−3.9	−5.6
	G+5.2S+5N	80.0	−28.3	76-28	1.1	0.5
	B+5.2S+5N	76.3	−29.5	76-28	−1.3	−3.0

All modified binders achieved their target PG. The Superpave PG system classifies binders using small-strain tests at a particular temperature. However, the Superpave method may not adequately determine the performance characteristics of modified binders. Modified binders may be classified as neat binders PG, although the former may have a distinct performance at both binder and HMA levels.

Delta-TC (ΔT_c)

ΔT_c is the difference between the critical low PG temperatures, as presented in Figure 1. The critical temperature from stiffness, $T_{C,s}$, and m-value, $T_{C,m}$, are measured in the BBR test. ΔT_c indicates the relaxation properties of asphalt binder, which can contribute to non-load-related cracking or other age-related distresses in HMA pavement (Baumgardner, 2021). The following sections present the results of ΔT_c for base binders, softened binders, polymer-modified binders, and polymer-softener-modified binders. The minimum ΔT_c thresholds are usually −2°C and −5°C for PAV- and 2PAV-aged binders, respectively (Asphalt Institute, 2019).

The ΔT_c values for base binders are presented in Table 1 and Figure 15. Based on the ΔT_c values, the experimental base binders are more distinct (larger ΔT_c difference) than the comparison base binders. As expected, ΔT_c values decreased from 1PAV to 2PAV. For both base binders, the good binder has a higher ΔT_c value than the borderline binder. For the experimental base binders, the good binder passes both 1PAV and 2PAV thresholds, while the borderline binder fails them.

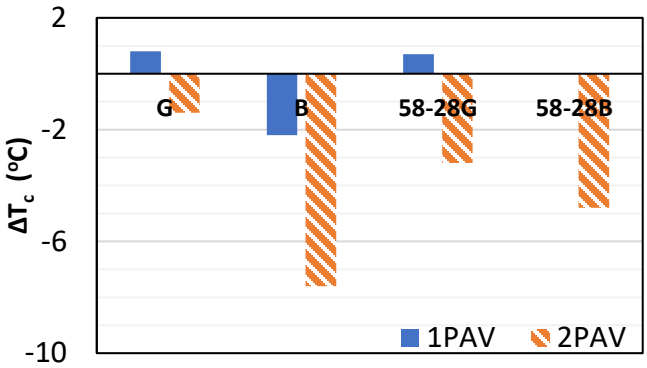

Figure 15. Bar plot. ΔT_c values for 1PAV- and 2PAV-aged base binders.

The ΔT_c values for softened binders compared to base binders (experimental) are presented in Figure 16. For all softener types, at both 1PAV and 2PAV, ΔT_c values increased compared to the base. Softeners decreased the S-value and increased the m-value, with a more pronounced effect on the m-value, leading to an aggregate increase in ΔT_c. All softened binders passed the 1PAV and 2PAV thresholds except softener F (vegetable oil), which failed the 2PAV threshold with the borderline binder. At a particular aging condition, 1PAV or 2PAV, the ranking of softened binders was not consistent for good and borderline binders. This shows the difference in compatibility of different softeners with base binders. However, across binders and aging conditions, softener C, the fatty acid–based softener, showed the highest change in ΔT_c values. Softener F, the vegetable oil–based softener, showed the lowest change.

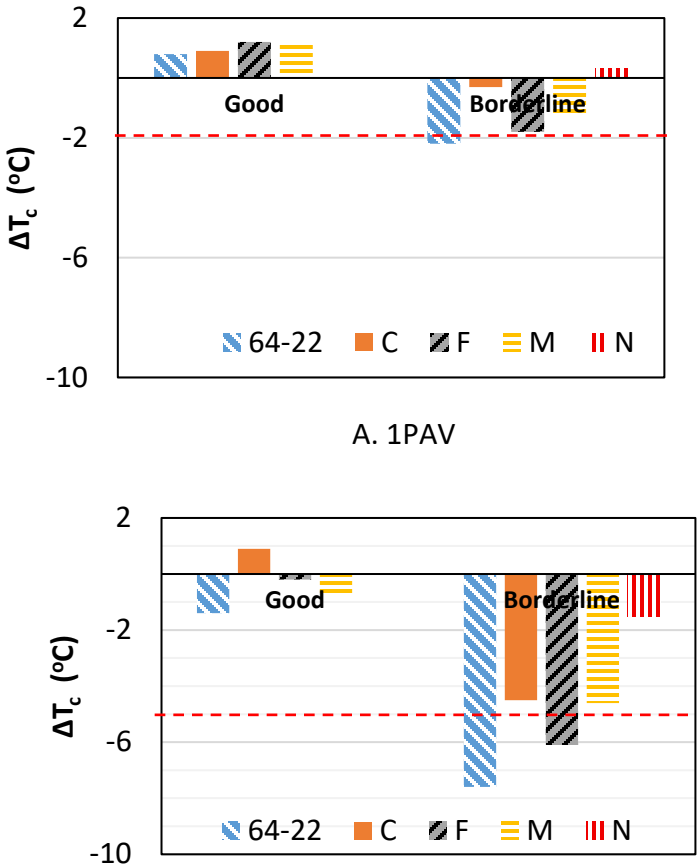

Figure 16. Bar plot. 1PAV and 2PAV ΔT_c values for softened binders.

The ΔT_c values for polymer-modified binders compared to base binders (experimental) are presented in Figure 17. To achieve a PG 70 and PG 76, 1.8% and 3.5% SBS were added to the base binders, respectively. Polymer modification reduces ΔT_c values when compared to the base. An increase in SBS dosage from PG 70 to PG 76 led to further reduction of ΔT_c. Like softeners, SBS decreased the S-value and increased the m-value. However, unlike softeners, the S-value was more pronounced than the m-value, leading to an aggregate decrease in ΔT_c. All good binder blends still had higher ΔT_c than borderline binders.

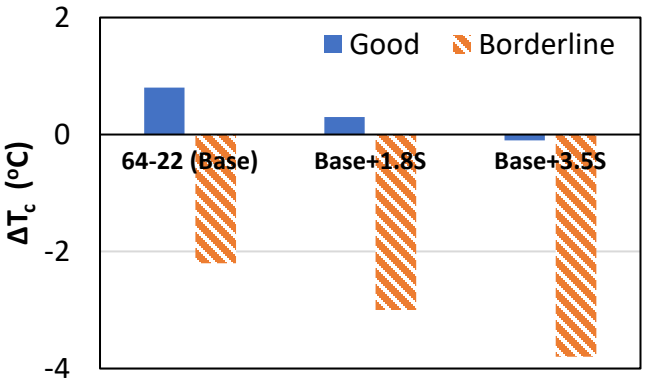

Figure 17. Bar plot. 1PAV ΔT_c values for polymer-modified binders.

The ΔT_c values for polymer-softener-modified binders compared to base binders (experimental) are presented in Figure 18 (PG 70-28) and Figure 19 (PG 76-28).

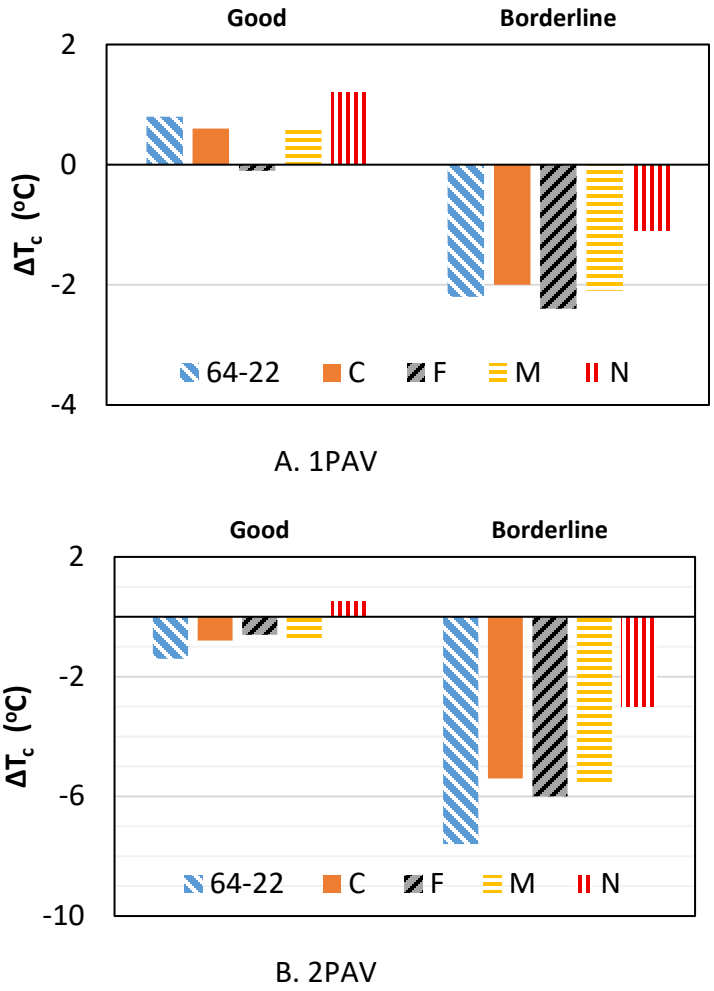

Figure 18. Bar plots. 1PAV and 2PAV ΔT_c values for polymer-softener-modified binders (PG 70-28).

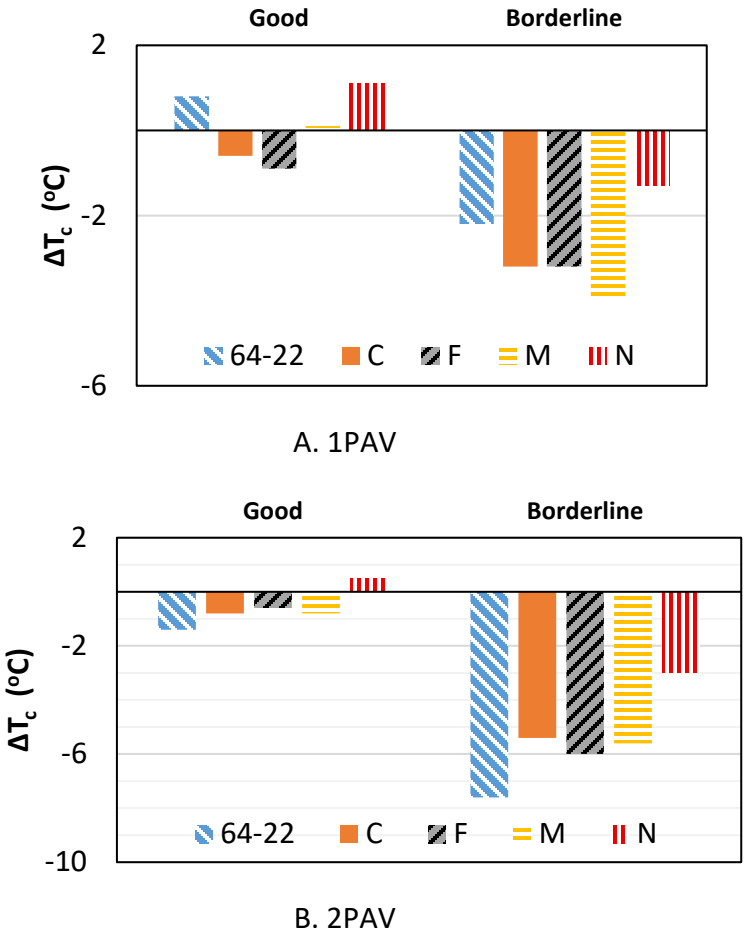

Figure 19. Bar plot. 1PAV and 2PAV ΔT_c values for polymer-softener-modified binders (PG 76-28).

From the above results, softeners increased ΔT_c while polymers decreased ΔT_c. The combination of softening and polymer modification as in polymer-softener-modified binders led to balancing both effects. Hence, ΔT_c values became like those of base binders. For the same softener, ΔT_c values decreased when comparing PG 70 blends to PG 76 blends. This is due to the additional SBS content required to meet the higher PG requirement. All modified good binders passed their required thresholds (−2°C and −5°C for PAV- and 2PAV-aged binders, respectively). For borderline modified binders, softeners C and N of PG 70 blends passed their required thresholds. However, only softener N of the PG 76 blends passed the required ΔT_c thresholds. An alternate blending protocol was used for the polymer-softener-modified binders of softener N.

Delta-G-Star ($\Delta|G^*|_{peak\tau}$)

$\Delta|G^*|_{peak\,\tau}$ is the reduction in complex shear modulus, $|G^*|$, from the start of the linear amplitude sweep (LAS) test until the peak shear-stress condition is reached. This parameter has been used to describe the effect of aging and modification on binder fatigue tolerance (García Mainieri et al., 2021). It provides a comparison criterion for binders, suggesting relative performance under field conditions. The LAS test was used to study the damage characteristics of modified and unmodified

binders at extended long-term aging conditions (2PAV). A higher $\Delta|G^*|_{peak\,\tau}$ indicates better fatigue damage tolerance. The following sections present the results of $\Delta|G^*|_{peak\,\tau}$ for base binders, softened binders, polymer-modified binders, and polymer-softener-modified binders. The $\Delta|G^*|_{peak\,\tau}$ values were compared at intermediate PG temperature (i.e., LAS is an intermediate temperature test).

The LAS test utilizes the DSR to assess the fatigue behavior of binders by applying cyclic loading at increasing amplitudes (AASHTO, 2018). $\Delta|G^*|_{peak}$ measures the decay in modulus. It relies on peak stress, not to define failure, but as a cut-off point at which the capacity to resist shear loading begins to deteriorate. $\Delta|G^*|_{peak\,\tau}$ values for base binders are presented in Table 1. Unlike with ΔT_c, there are no major distinctions between good and borderline binders with respect to $\Delta|G^*|_{peak\,\tau}$. This conclusion holds for both experimental and comparison binders. Comparison binders, which are relatively softer, have a higher $\Delta|G^*|_{peak\,\tau}$, and hence fatigue tolerance, than experimental binders.

The $\Delta|G^*|_{peak\,\tau}$ values for softened binders compared to base binders (experimental) are presented in Figure 20. There is a slight increase in $\Delta|G^*|_{peak\,\tau}$ values for softened binder compared to the base binder except for good binder modified with softener C. Generally, softening led to a ~1.5% increase in fatigue tolerance. This is regardless of the ~6°C reduction in intermediate temperature (yellow dots) when binders are softened from PG 64-22 to PG 58-28, highlighting a deficiency in the conventional PG system. Softener F, the vegetable oil–based softener, showed the highest increase in $\Delta|G^*|_{peak\,\tau}$ values, while softener M, the aromatic oil–based softener, showed the lowest increase.

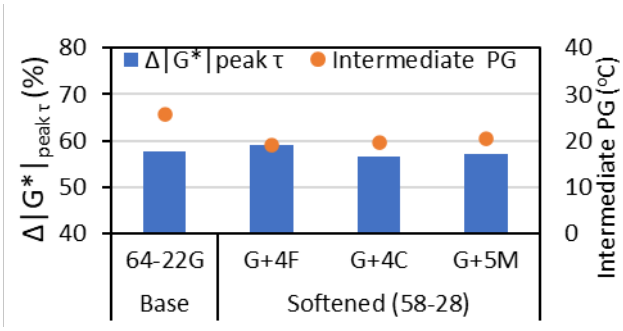

A. Good

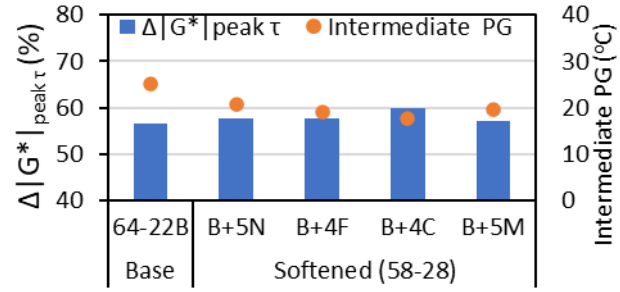

B. Borderline

Figure 20. Bar plot. 2PAV $|\Delta G^*|_{peak\,\tau}$ values for softened binders.

The $\Delta|G^*|_{peak\,\tau}$ values for polymer-modified binders compared to base binders are presented in Figure 21 (experimental base) and Figure 22 (comparison base). Unlike softener modification, where there was a slight increase in $\Delta|G^*|_{peak\,\tau}$ values, polymer modification led to a clear increase in $\Delta|G^*|_{peak\,\tau}$ values, for all SBS modification and dosages. Generally, polymer modification led to a ~10.5% increase in fatigue tolerance. While ΔT_c is sensitive to polymer modification and is negatively impacted, $\Delta|G^*|_{peak\,\tau}$ showed the benefits of polymer. An increase in SBS dosage from PG 70 to PG 76 led to further increase in $\Delta|G^*|_{peak\,\tau}$. However, it was a comparatively smaller increase in fatigue tolerance, indicating a nearness to an optimal dosage.

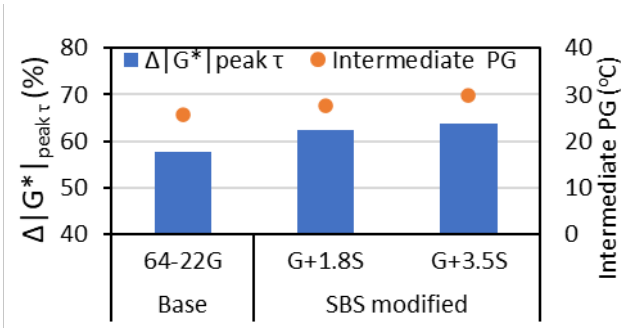

A. Good

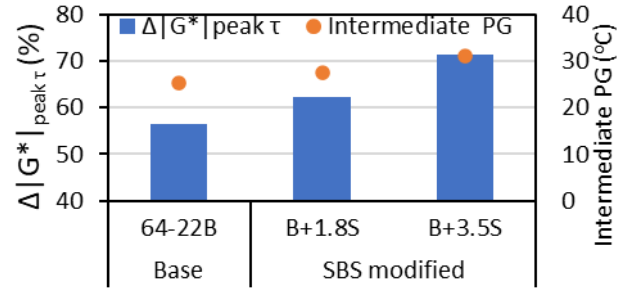

B. Borderline

Figure 21. Bar plot. 2PAV $\Delta|G^*|_{peak\,\tau}$ values for polymer-modified binders (experimental base).

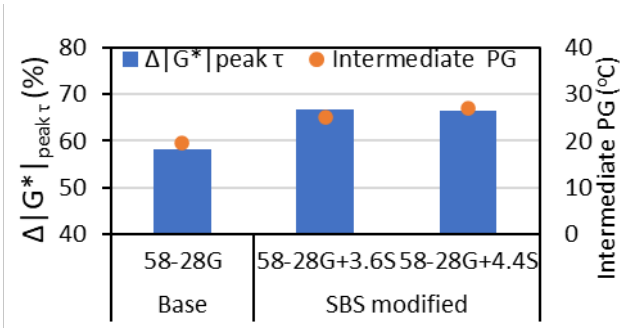

A. Good

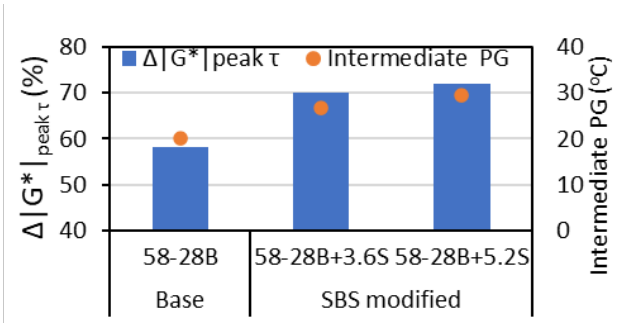

B. Borderline

Figure 22. Bar plot. 2PAV $\Delta|G^*|_{peak\,\tau}$ values for polymer-modified binders (comparison base).

As presented in Figure 21 and Figure 22, fatigue tolerance and intermediate PG temperature follow the same trend. This is the reverse of the observations in Figure 20, where they follow different trends. From laboratory tests and field observations, polymer modification has been shown to reduce fatigue cracking potential (Lewandowski, 1994). Figure 23 presents the stress-strain behavior for typical base, softened, and polymer-modified binder (PMB), as well as the shear modulus change with the number of cycles.

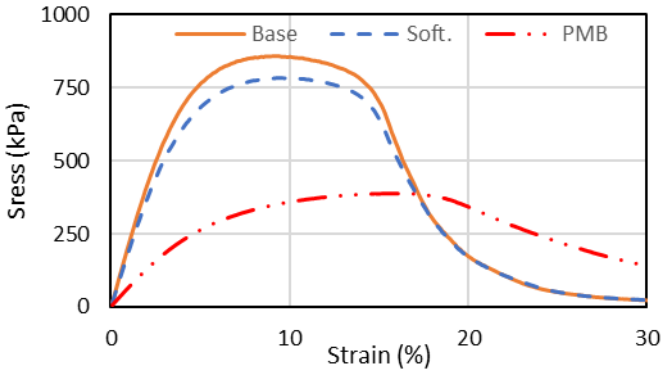

A. Stress vs Strain

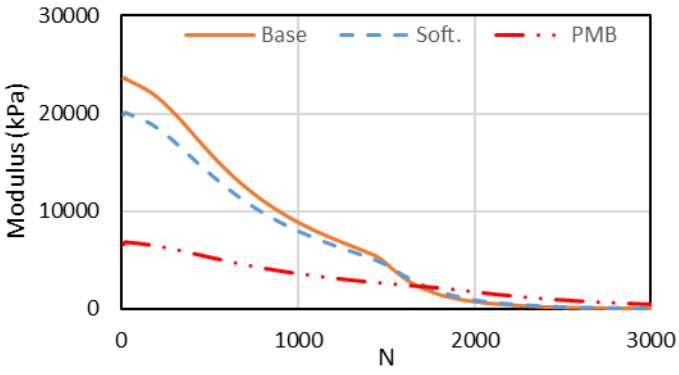

B. Modulus vs number of cycles

Figure 23. Graph. Binder behavior during the LAS.

The stress-strain curve demonstrates the polymer-modified binder has a lower peak shear stress, but most importantly, a longer plateau at this peak stress. This plateau indicates there is more energy dissipation without damage. Also, from the plot of modulus with the number of cycles (N), the polymer-modified binder has a lesser slope, indicating less damage accumulation or that damage accelerates slower. This occurs even though the polymer-modified binder has a lower modulus. These phenomena, while also present in softened binders, are less easy to see.

The $\Delta|G^*|_{peak\,\tau}$ values for polymer-softener-modified binders compared to base and softened binders are presented in Figure 24. S+PMB are PG 70 blends, while S+PMB (high) are PG 76 blends, which have higher dosage. From the $\Delta|G^*|_{peak\,\tau}$ analysis, polymers increased the $\Delta|G^*|_{peak\,\tau}$ and softeners also increased the $\Delta|G^*|_{peak\,\tau}$, albeit slightly. The combination of softening and polymer modification as in polymer-softener-modified binders led to better fatigue tolerance than a simple summation. For the same softener, $\Delta|G^*|_{peak\,\tau}$ values increased when comparing PG 70 blends to PG 76 blends due to the additional SBS content required to meet the higher PG requirement.

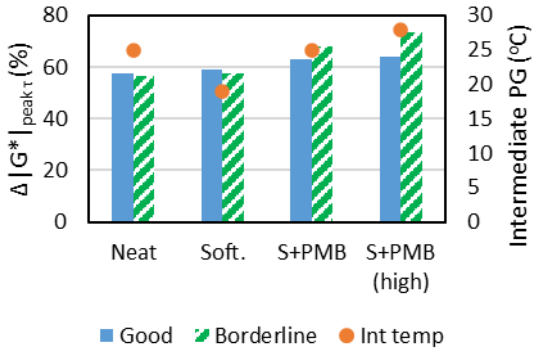

A. Softener F

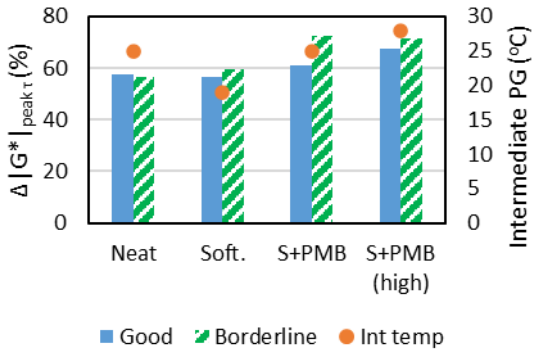

B. Softener C

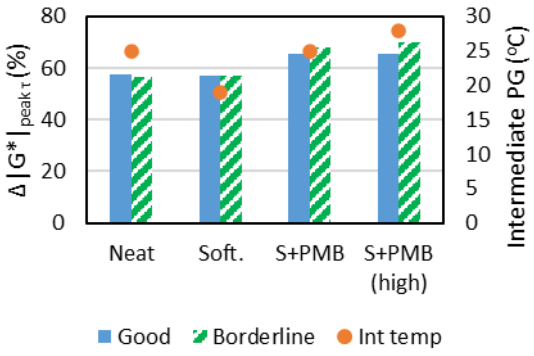

C. Softener M

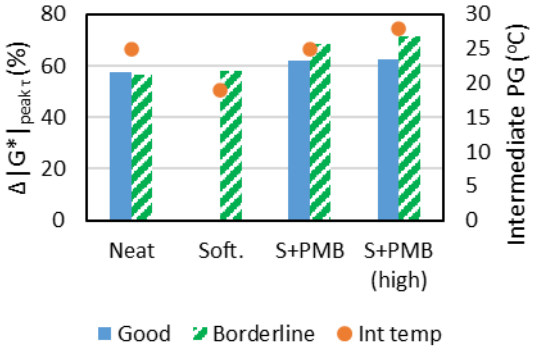

D. Softener N

Figure 24. Bar plot. 2PAV $\Delta|G^*|_{peak\,\tau}$ values for polymer-softener-modified binders.

Figure 24 summarizes findings from the fatigue tolerance investigations, as evaluated using $\Delta|G^*|_{peak\tau}$ (clustered columns) in comparison with the conventional intermediate PG (yellow dots). The progression from base to softening to polymer-softener modification led to consecutive increases in fatigue tolerance, highlighting the beneficial effects of these modifiers to asphalt binder as evident by both laboratory and field performance (Behnood & Gharehveran, 2019; Bennert et al., 2014; Liu et al., 2018; Yildirim, 2007). However, for intermediate PG, softening may be adverse to intermediate temperature performance. The IDOT *Bureau of Design and Environment* manual special provision uses a threshold of 54%. All binders (base, softened, polymer-softener-modified) tested in this study passed this threshold.

Multiple Stress Creep Recovery

The MSCR test was used to evaluate elastic recovery and nonrecoverable deformation behaviors of asphalt binder. J_{nr} indicates the permanent deformation susceptibility of the binder, while R indicates the elastic response of the binder. The higher the J_{nr} values, the greater the rutting potential, while higher R values indicate better elastic recovery. Table 12 presents the MSCR results for binder blends.

Table 12. MSCR Values for Binder Blends

Blend Type	ID	True High PG	R @ 0.1 kPa (%)	R @ 3.2 kPa (%)	J_{nr} @ 0.1 kPa (kPa^{-1})	J_{nr} @ 3.2 kPa (kPa^{-1})	Traffic Level Grade
Base Binders (Experimental)	G	66.9	3.4	1.5	1.9	2.0	H
	B	66.3	7.9	3.8	1.2	1.3	H
Softened Binders	G+4F	60.3	4.0	1.9	1.7	1.8	H
	B+4F	59.8	7.9	3.8	1.2	1.3	H
	G+4C	59.4	3.0	1.3	2.0	2.2	S
	B+4C	58.8	6.0	2.6	1.5	1.7	H
	G+5M	60.7	5.1	2.8	1.2	1.3	H
	B+5M	60.4	9.4	5.2	0.9	1.0	V
	B+5N	62.0	7.3	3.0	1.3	1.4	H
Polymer-Modified Binders	G+1.8S	71.8	27.7	14.7	1.4	1.9	H
	B+1.8S	73.1	35.0	20.2	1.1	1.5	H
	G+3.5S	77.0	64.1	41.2	0.8	1.0	V
	B+3.5S	78.9	69.4	53.3	0.5	0.8	V
Polymer-Softener-Modified Binders	G+4F+3.6S	70.5	69.5	51.4	0.5	0.9	V
	B+4F+3.6S	73.4	77.1	65.2	0.3	0.5	V
	G+4C+3.6S	70.1	70.3	50.1	0.5	1.0	V
	B+4C+3.5S	70.5	70.0	52.8	0.5	0.9	V
	G+4M+3.5S	72.8	60.4	43.4	0.6	1.0	V
	B+5M+3.4S	73.1	69.7	56.7	0.4	0.7	V
	G+4S+5N	71.6	63.8	40.1	0.7	1.4	H
	B+4S+5N	72.9	67.1	48.5	0.6	1.0	V
	G+3.5F+4.7S	76.7	80.2	56.8	0.3	0.9	V
	B+3.5F+4.1S	77.2	78.5	60.8	0.4	0.7	V
	G+3C+5S	76.1	74.0	43.1	0.4	1.1	H
	B+3C+5S	78.6	86.5	75.3	0.2	0.4	E
	G+5M+5S	76.6	76.7	58.2	0.4	0.8	V
	B+4.9M+4.2S	77.1	74.7	57.5	0.5	0.9	V
	G+5.2S+5N	77.0	74.5	40.3	0.7	1.9	H
	B+5.2S+5N	78.1	80.2	58.2	0.4	0.9	V

The J_{nr} and R values were both measured at 0.1 kPa and 3.2 kPa. As expected, the R values decreased, while the J_{nr} values increased from 0.1 kPa to 3.2 kPa. The borderline binder experienced higher percent recovery and lesser nonrecoverable creep compliance than the good binder. This foretells a consistent pattern in which the borderline binders (with respect to cracking) leverage modification more efficiently (with respect to rutting) than the good binders. This observation is valid for all forms of modification of base binders (softening, polymer-modification and polymer-softener modification), except for the PG 76-28 w/M binder. This emphasizes the importance of base binder quality on the performance of any type of modified binder produced using the base binder.

The traffic level grade in Table 12 is in accordance with AASHTO M 332 (2021), with "S," "H," "V," and "E" representing standard (< 10 million equivalent single axle load [ESALs]), heavy (10–30 million ESALs), very heavy (> 30 million ESALs), and extremely heavy (> 30 million ESALs and standing) traffic levels, respectively. While most softeners kept the "H" traffic grade, softener C with the good binder bumped down the grade to "S," while softener M with the borderline binder bumped up the grade to "V." Polymer modification had an "H" and "V" traffic grade. The "V" traffic grade was due to an increase in SBS dosage to 3.5%. For the polymer-softener modification, most blends led to a bump up to "V." At PG 76 using softener C, the good binder blend kept the "H" grade, while the borderline blend bumped up to "E." Softener N, with good binder, kept the "H" grade at both PG 70 and PG 76. Polymer-softener-modified binders using softener N were produced using the alternate reversed protocol: a polymer-modified binder was softened post-polymerization. From the foregoing, softeners C and N were the worst performing softeners.

Effect of Modifiers on MSCR

Effect of Softening

Figure 25 presents the $R_{3.2}$ for the base and softened binders. Two softeners (F and M) had positive effects (increasing $R_{3.2}$) while the other two softeners (C and N) had negative effects (decreasing $R_{3.2}$).

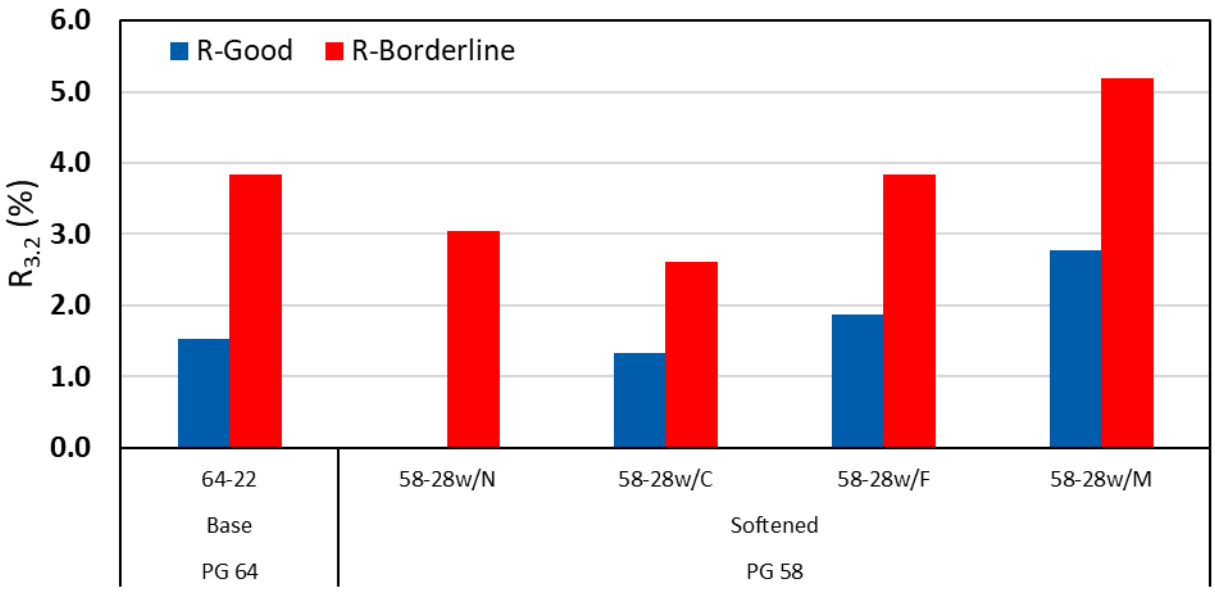

Figure 25. Bar plot. $R_{3.2}$ values for base and softened binders.

Figure 26 presents the $J_{nr\,3.2}$ for the base and softened binders. Similar conclusions to that in Figure 25 can be reached. The same two softeners (F and M) had positive effects (decreasing $J_{nr\,3.2}$), while the other two softeners (C and N) had negative effects (increasing $J_{nr\,3.2}$). Softeners reduce binder stiffness, restore ductility, and improve low-temperature performance. However, they reduce high-temperature viscosity and consequently increase rutting potential.

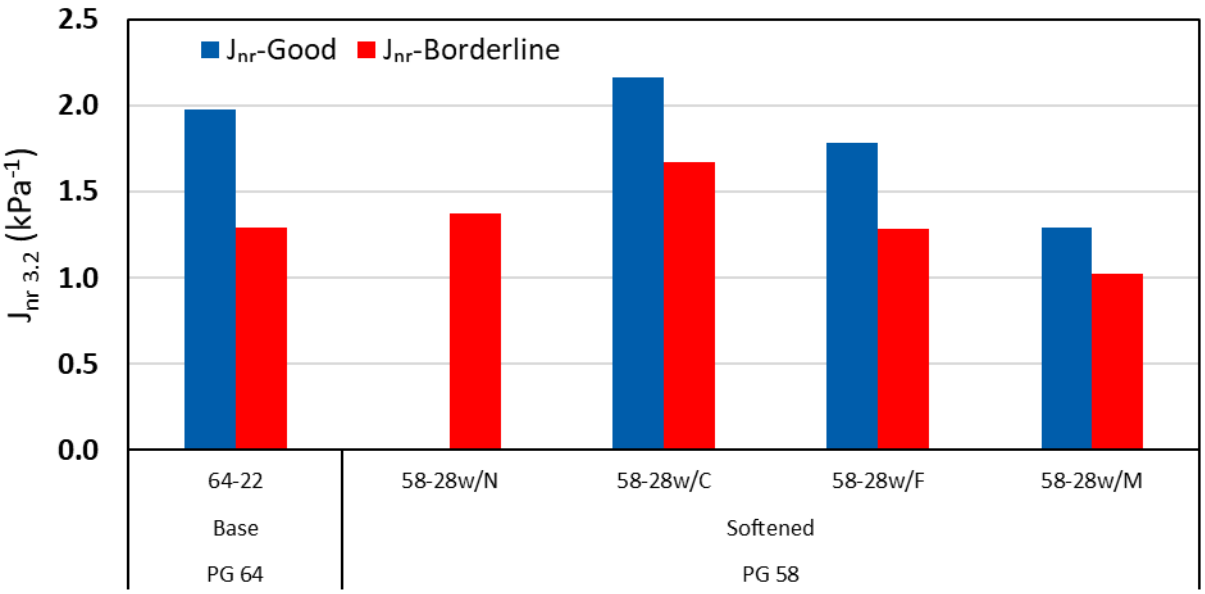

Figure 26. Bar plot. $J_{nr\ 3.2}$ values for base and softened binders.

Effect of Polymer Modification

The effect of polymer modification is more pronounced than that of softening. Figure 27 and Figure 28 present the $R_{3.2}$ and $J_{nr\ 3.2}$ values for binder blends, respectively. Polymer modification (either alone or with softeners) had a positive effect on binder rutting potential, increasing R and decreasing J_{nr}, with a higher effect on R. This is case for all binder blends containing polymer, except the SBS 70-22 borderline binder, which had a slight increase in $J_{nr\ 3.2}$.

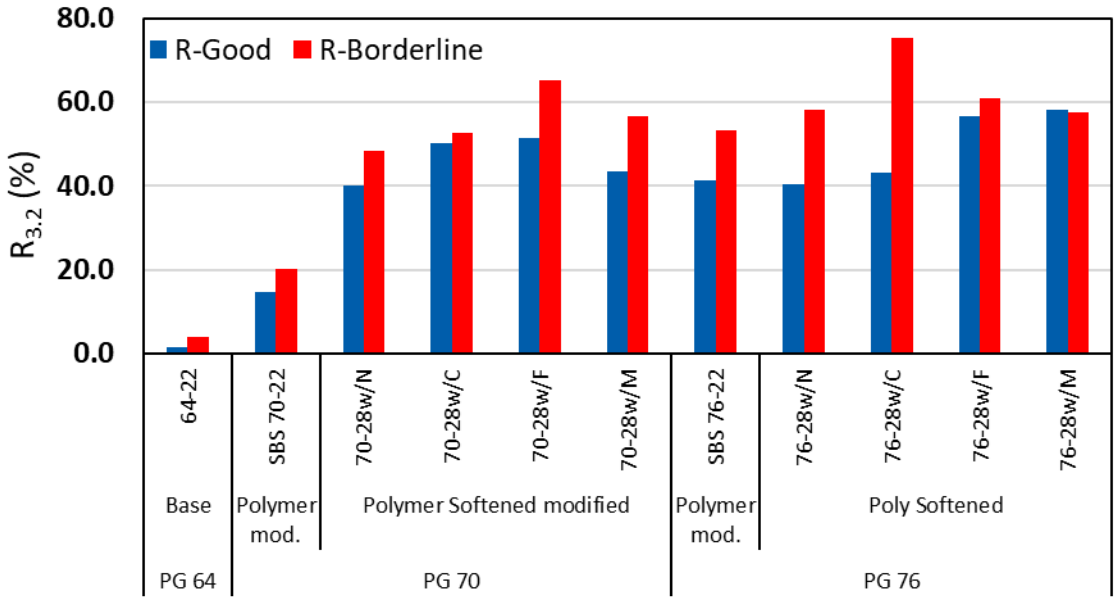

Figure 27. Bar plot. $R_{3.2}$ values for base and binder blends containing polymer.

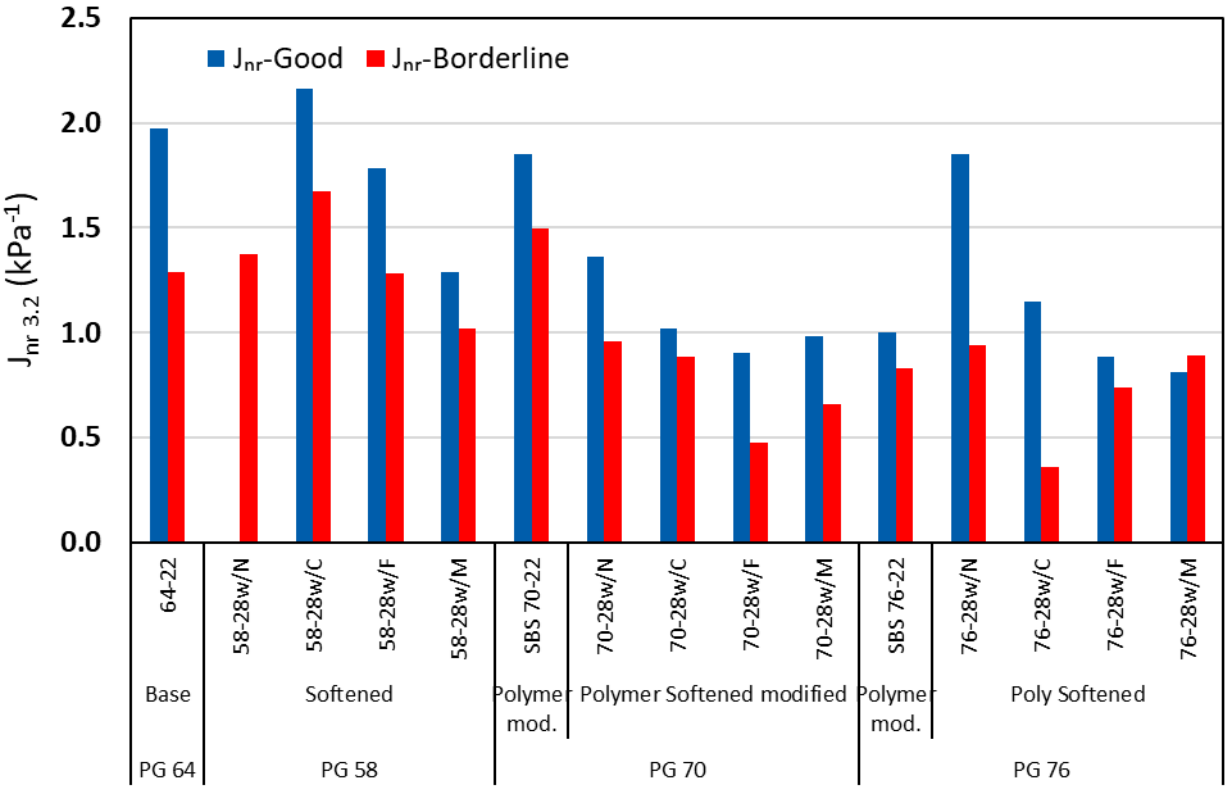

Figure 28. Bar plot. $J_{nr\ 3.2}$ values for base and binder blends containing polymer.

Unmodified (neat) binders behaved mostly viscous at high stresses. They deformed and did not recover, leading to a lower $R_{3.2}$. Polymers form an elastic network within the asphalt binder matrix. Under stress, this network stretches and stores energy like a spring. When the load is removed, the network helps the binder recover, reducing permanent strain. Hence, the higher the polymer dosage, the stronger and more continuous the elastic network becomes. This increases percent recovery at high stress ($R_{3.2}$) (Pipintakos et al., 2025; DuBois et al., 2014). $J_{nr\ 3.2}$ decreases with polymer addition because polymers introduce a resilient elastic network that resists rutting under heavy loads. The more polymer present, the more effective this network becomes, reducing nonrecoverable strain and making the binder much more rut resistant (D'Angelo & Dongré, 2009).

Effect of Polymer-Softener Modification

Per the MSCR test, it appears the dual modification is beneficial. Figure 29 shows the plot of $R_{3.2}$ vs $J_{nr\ 3.2}$ for binder blends as well as the AASHTO R92 boundary which "defines binders that have significant elastic response for the associated value of non-recoverable creep compliance (indicating that the asphalt binder has been modified by an elastomeric polymer)" (AASHTO, 2022). As expected, the base and softened binders plot within the boundary, while blends with polymer are outside the boundary.

A higher $R_{3.2}$ and lower $J_{nr\ 3.2}$ are characteristic of binders with good elastic response and lower permanent deformation susceptibility. Hence, from Figure 29, low rutting potential binders would

plot in the upper left corner of the graph. At the same PG, polymer-softener modification causes a shift toward this upper left corner of the graph when compared to ordinary polymer modification, highlighting the benefit of the dual modification process.

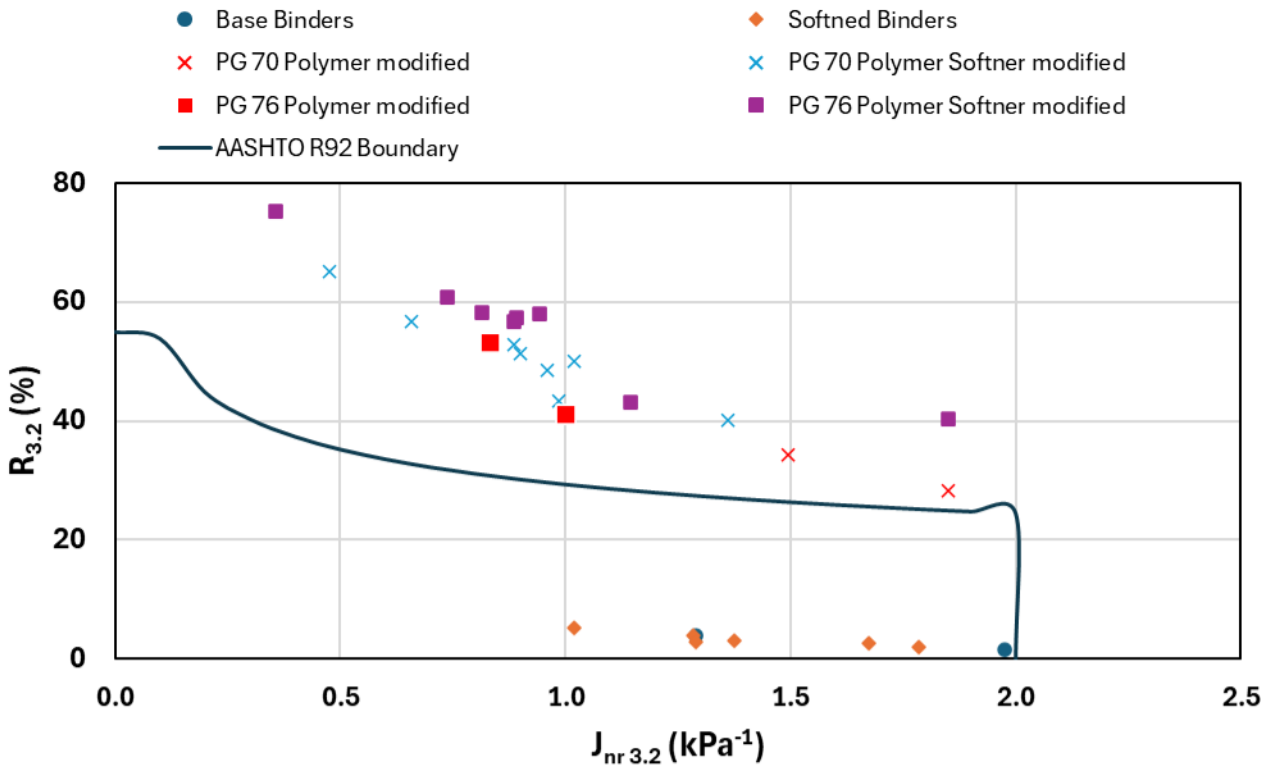

Figure 29. Graph. $R_{3.2}$ vs $J_{nr\ 3.2}$ for binder blends.

Percentage Difference in R and J_{nr}

Although the R and J_{nr} at both stress levels (0.1 kPa and 3.2 kPa) are important parameters to characterize binders, the percentage difference in R and J_{nr} between these two stress levels is important and is a significant parameter. R_{diff} indicates how much a binder's elastic recovery capacity deteriorates under a higher stress. A lower value means the binder maintains its recovery ability even when traffic load increases, reflecting a stable polymer network. A higher value signals that recovery falls off at higher stresses, suggesting the binder's elastic response is "overwhelmed" by heavier loads. Because recovery is linked to a binder's ability to resist rutting, a binder with lower R_{diff} is considered more reliable for heavy traffic applications. Specifically, for polymer-modified binders, a smaller R_{diff} is often used as evidence of an effective elastic network that continues to function under stress (Hossain et al., 2016; Wang et al., 2022).

The differences are calculated using Figure 30 and Figure 31 for R_{diff} and $J_{nr\ diff}$, respectively. Table 13 presents the percentage difference in R (R_{diff}) and J_{nr} ($J_{nr\ diff}$) for binder blends. Figures 32 and 33 present the R_{diff} and $J_{nr\ diff}$ values for binder blends, respectively.

$$R_{diff} = \frac{R_{0.1} - R_{3.2}}{R_{0.1}} * 100$$

Figure 30. Equation. Percent difference between average recovery, R_{diff}.

$$J_{nr\,diff} = \frac{J_{nr,3.2} - J_{nr,0.1}}{J_{nr,0.1}} * 100$$

Figure 31. Equation. Percent difference between nonrecoverable creep compliance, $J_{nr\ diff}$.

Table 13. Percentage Difference in R and J_{nr}

Blend Type	ID	True High PG	R_{diff} (%)	$J_{nr\ diff}$ (%)
Base Binders (Experimental)	G	66.9	55.3	6.2
	B	66.3	51.5	8.5
Softened Binders	G+4F	60.3	53.4	6.7
	B+4F	59.8	51.2	8.3
	G+4C	59.4	56.1	6.0
	B+4C	58.8	56.5	9.0
	G+5M	60.7	46.1	5.7
	B+5M	60.4	44.6	7.9
	B+5N	62.0	57.8	9.8
Polymer-Modified Binders	G+1.8S	71.8	47.0	28.3
	B+1.8S	73.1	42.2	34.3
	G+3.5S	77.0	35.7	45.0
	B+3.5S	78.9	23.2	68.3
Polymer-Softener-Modified Binders	G+4F+3.6S	70.5	26.0	76.8
	B+4F+3.6S	73.4	15.4	63.9
	G+4C+3.6S	70.1	28.8	86.4
	B+4C+3.5S	70.5	24.6	73.1
	G+4M+3.5S	72.8	28.1	55.8
	B+5M+3.4S	73.1	18.7	54.0
	G+4S+5N	71.6	37.1	84.4
	B+4S+5N	72.9	27.7	71.0
	G+3.5F+4.7S	76.7	29.2	160.0
	B+3.5F+4.1S	77.2	22.5	104.9
	G+3C+5S	76.1	41.8	159.7
	B+3C+5S	78.6	12.9	98.2
	G+5M+5S	76.6	24.2	104.7
	B+4.9M+4.2S	77.1	23.0	84.5
	G+5.2S+5N	77.0	45.9	180.6
	B+5.2S+5N	78.1	27.5	137.2

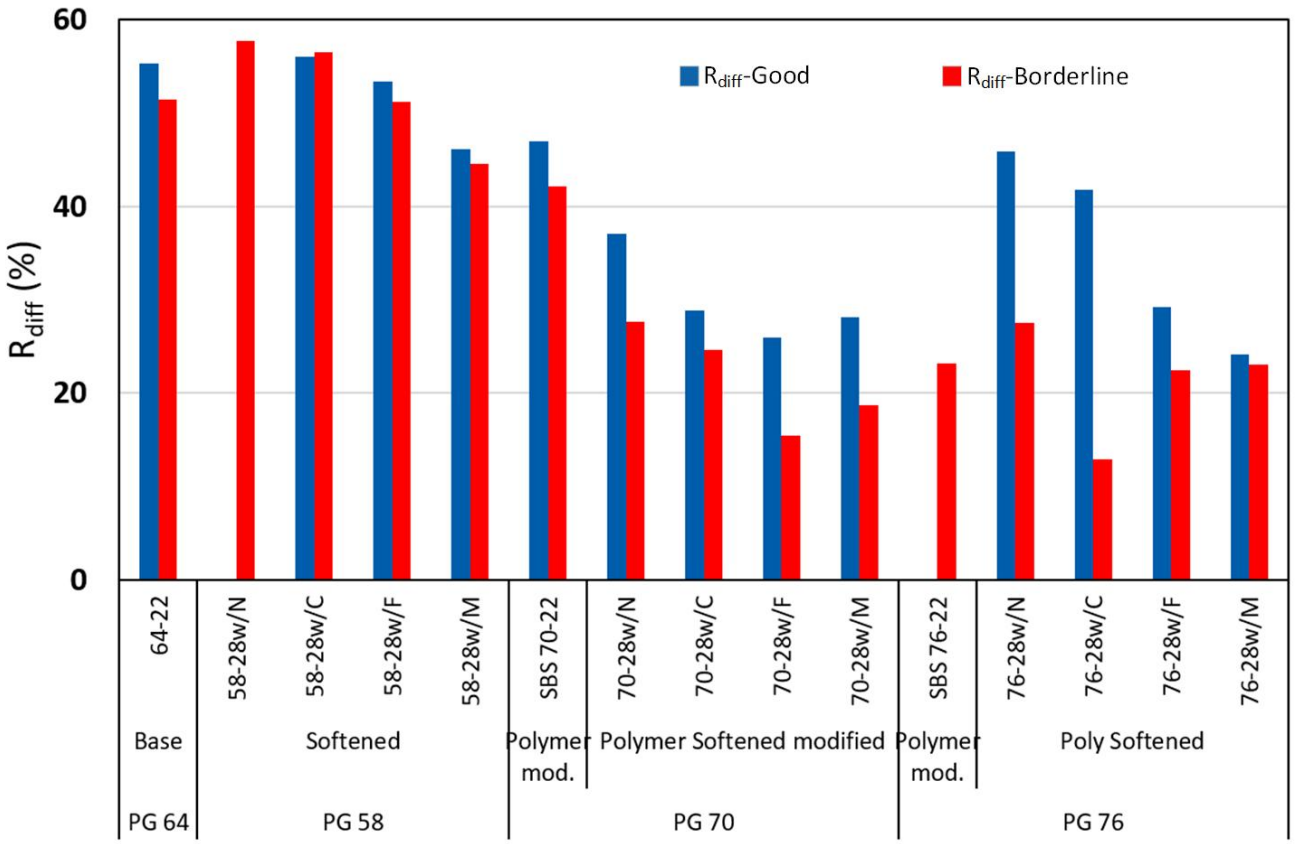

Figure 32. Graph. R_{diff} values for binder blends.

Consistent with previous findings ($R_{3.2}$ and $J_{nr\ 3.2}$), softeners F and M reduced the R_{diff} while softeners N and C slightly increased the R_{diff}. With polymer modification to a PG 70, there was a significant decrease in R_{diff} for all softeners and SBS contents. However, with a higher SBS dosage to PG 76, most blends had an increase or insignificant decrease in R_{diff}. This observation agrees with earlier findings from the mixes' FI results, which suggest an optimal SBS dosage exists between SBS 70-28 to SBS 76-28, beyond which additional polymer content may not offer commensurate cracking resistance benefit.

SBS dosage magnifies nonlinearity. At low SBS content, the binder behaves almost like a neat asphalt binder, where elastic recovery is limited between 0.1 kPa and 3.2 kPa. At low stress (0.1 kPa), the network remains largely intact, so recovery is moderate and proportional to the polymer content. However, at higher stress (3.2 kPa), more of the polymer network is "activated," leading to a disproportionately higher recovery compared to low stress and a relatively lower R_{diff}. However, at higher SBS content, the binder gains a stronger elastic component. Under small stresses, only a portion of this elastic network is engaged, but at relatively high stresses the network stretches and recovers more fully. This rises in recovery at 3.2 kPa relative to 0.1 kPa, increasing R_{diff}. In other words, the stronger the polymer network, the more nonlinear its response, which increases R_{diff}. Hence, this supports the notion of the existence of an optimal SBS dosage.

High R_{diff} may not necessarily be bad for polymer-modified binders or polymer-softener-modified binders, as it indicates that the polymer structure contributes more under heavy traffic loads. Also, unlike $J_{nr\ diff}$, there are no thresholds for R_{diff} in specifications. R_{diff} may primarily be useful as an analytical indicator of polymer network strength and contribution under stress. Hence, this helps in distinguishing between effective and ineffective modification.

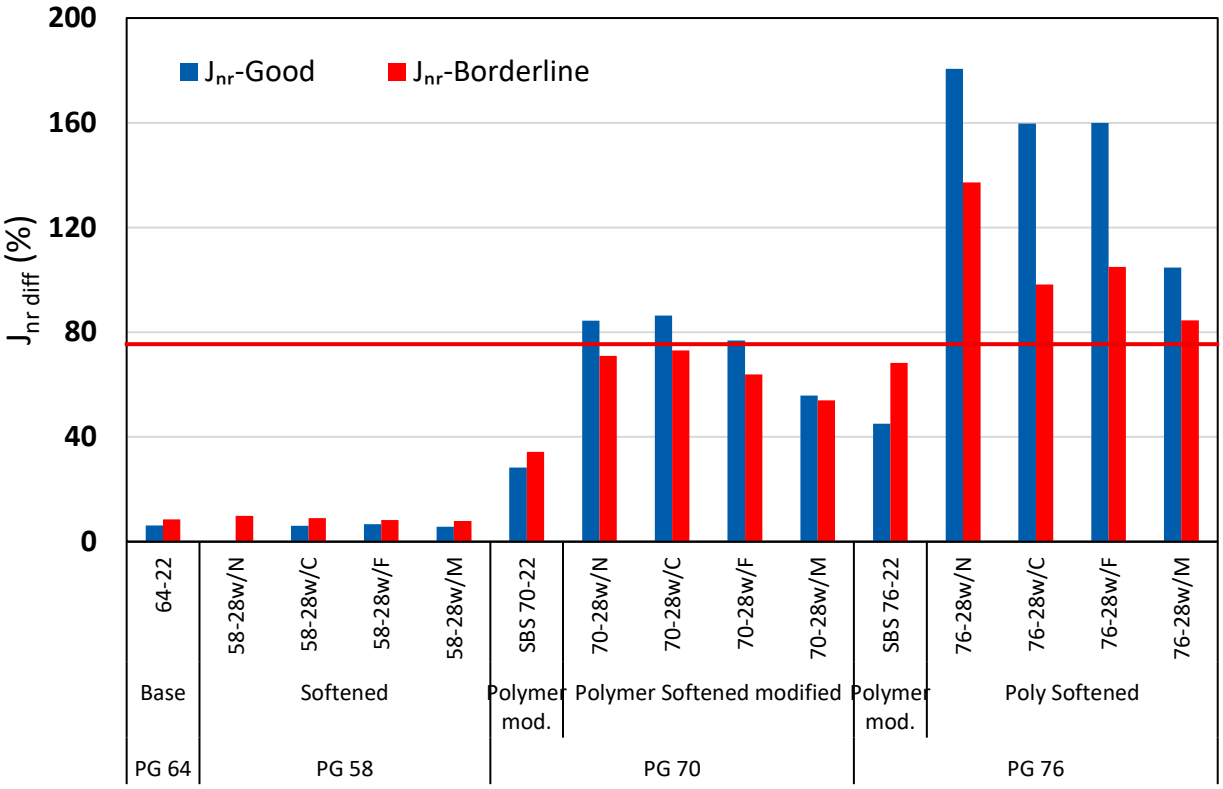

Figure 33. Graph. $J_{nr\ diff}$ values for binder blends.

$J_{nr\ diff}$ indicates the sensitivity of a binder's rutting potential to stress level. A low $J_{nr\ diff}$ indicates that binder accumulates permanent strain at a consistent rate across light and heavy loads, which is desirable for varied traffic conditions, as rutting potential is more predictable in service. A high $J_{nr\ diff}$ means the binder is more deformable at higher stresses, suggesting vulnerability under heavy or slow-moving loads. AASHTO M332 explicitly uses $J_{nr\ diff}$ of ≤ 75% for binder acceptable. Figure 33 presents the $J_{nr\ diff}$ values for binder blends.

Generally, in consistency with previous findings ($R_{3.2}$, $J_{nr\ 3.2}$, and R_{diff}), softeners F and M slightly reduced the $J_{nr\ diff}$, while softeners N and C slightly increased the $J_{nr\ diff}$. With polymer modification to a PG 70, there is a significant increase in $J_{nr\ diff}$ for all softener and SBS content. Also, for a higher SBS dosage to PG 76, there is a further increase in $J_{nr\ diff}$ for all softener and SBS content. This shows a linearity between SBS dosage and $J_{nr\ diff}$. In other words, the stronger the polymer network, the greater the contrast between low-stress and high-stress nonrecoverable creep compliance. As

illustrated with the red line in Figure 33, with respect to AASHTO M332, it appears that limit has been established for polymer modification without considering the effect of softening.

Summary

The MSCR test was used to evaluate the effect of softening, polymer modification, and polymer-softener modification on the stress-dependent rutting potential of binder blends. Generally, borderline binders had less rutting potential than their good counterparts. Although this may appear to contradict the definition of "good" and "borderline" binders, the definition is based on ΔT_c, a parameter strongly indicative of low-temperature cracking potential. Borderline binder is expected to resist rutting more, as it is stiffer.

Cracking potential is governed largely by a binder's flexibility and relaxation capacity, which allows it to dissipate stresses without fracturing, while rutting potential requires a binder to be stiff and resistant to permanent deformation, especially under high temperatures and heavy traffic loading. This could be illustrated by that fact that the two softeners (F and M) with the best performance in the MSCR tests ($R_{3.2}$, $J_{nr\ 3.2}$, R_{diff}, and $J_{nr\ diff}$) at PG 58, PG 70, and PG 76 had consistently the lowest ΔT_c values (both 1PAV and 2PAV) at PG 58-28, PG 70-28, and PG 76-28, as shown in Table 11.

This has been observed in the mixture phase. While the good binders demonstrated lower cracking potential than the borderline binders, as shown in the I-FIT results, the borderline binders had lower rutting potential than the good binders, as shown in the HWTT results. This trade-off underscores the importance of balanced mix design, where both cracking and rutting thresholds are enforced through performance-based tests, ensuring that no binder or mixture is optimized for one distress at the expense of the other.

Fourier-Transform Infrared Spectroscopy

Effect of Modification

Softening

The binders' FTIR spectral changes with softening, depending on the type of softener used. Figure 34 presents typical spectra with four softeners compared with the base binder. Generally, for each softened binder, both spectra (base and softened) follow the same pattern. Peaks are around the same wavenumber, albeit with slight differences in peak height or width. However, at characteristic wavenumbers, the softened binders show peaks that are absent from the base binder. The peak around 1,735 cm^{-1} (Figure 34-a) represents carbonyl from the acid or ketone group (Tarhan et al., 2017). Figure 34-b shows a characteristic peak at 1,743 cm^{-1}, which represents carbonyl stretching (C=O) in the vegetable oil–based softeners like softener F. The peak at 1,160 cm^{-1} reflects the presence of C-O from triglycerides (Shi et al., 2017; Rohman & Man, 2013). Figure 34-c shows peaks at 1,212 and 1,736, which represent C-O stretching and C=O stretching, respectively. In Figure 34-d, the peak at 1,645 represents N-H bending of the amine, which can be found in glycol-amine softeners like N (Sigma Aldrich).

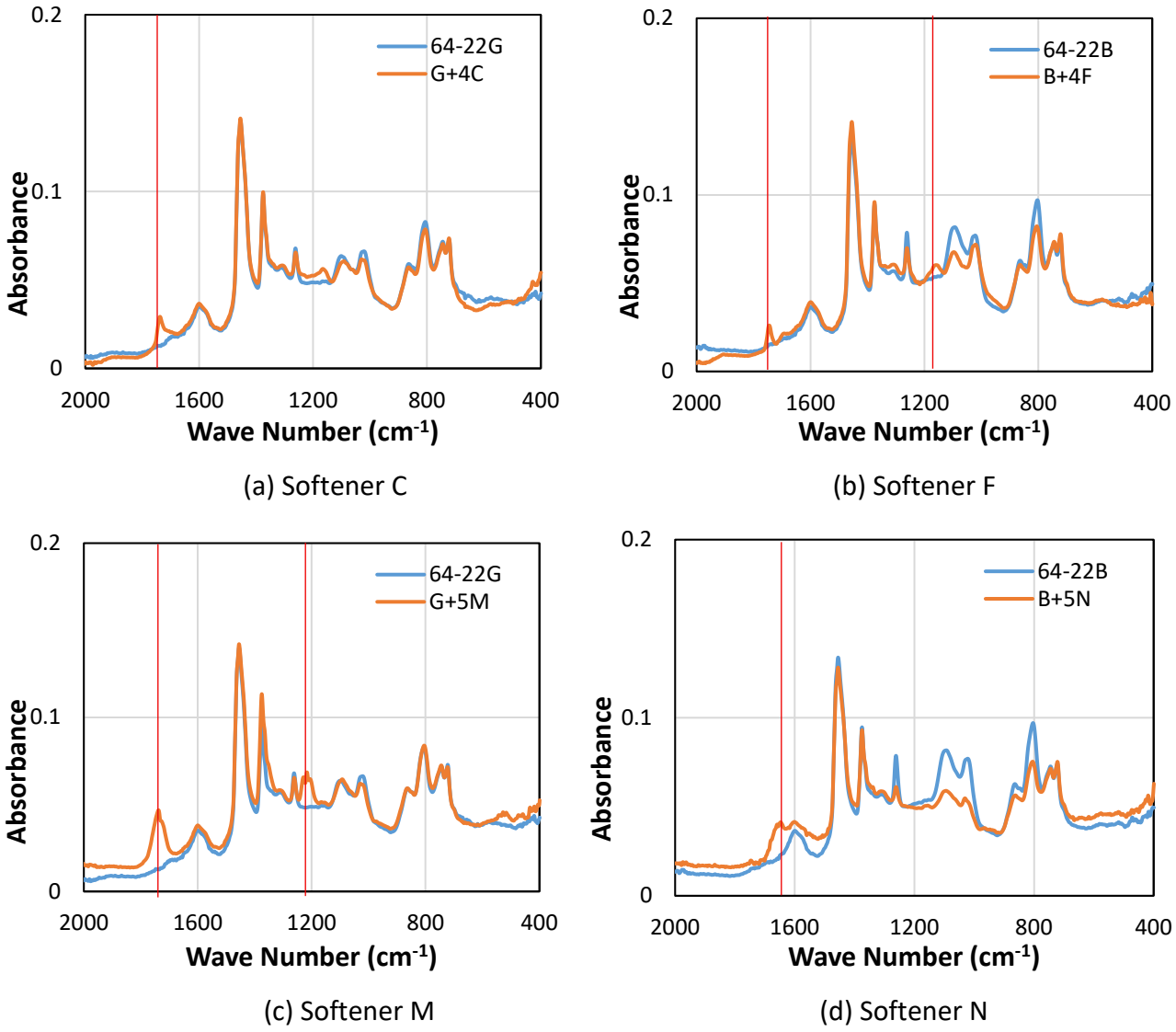

Figure 34. Graph. Typical FTIR spectra for softened binders.

Polymer Modification

Figure 35 demonstrates typical spectra of polymer-modified binders compared with the base binder. Peaks around 699 cm^{-1} and 966 cm^{-1} are characteristic of polybutadiene (PB) and polystyrene (PS), respectively (Yut & Zofka, 2011; Lin et al., 2017). Also, the peak heights at these wavenumbers increased as SBS dosage increased from 1.8% to 3.5%.

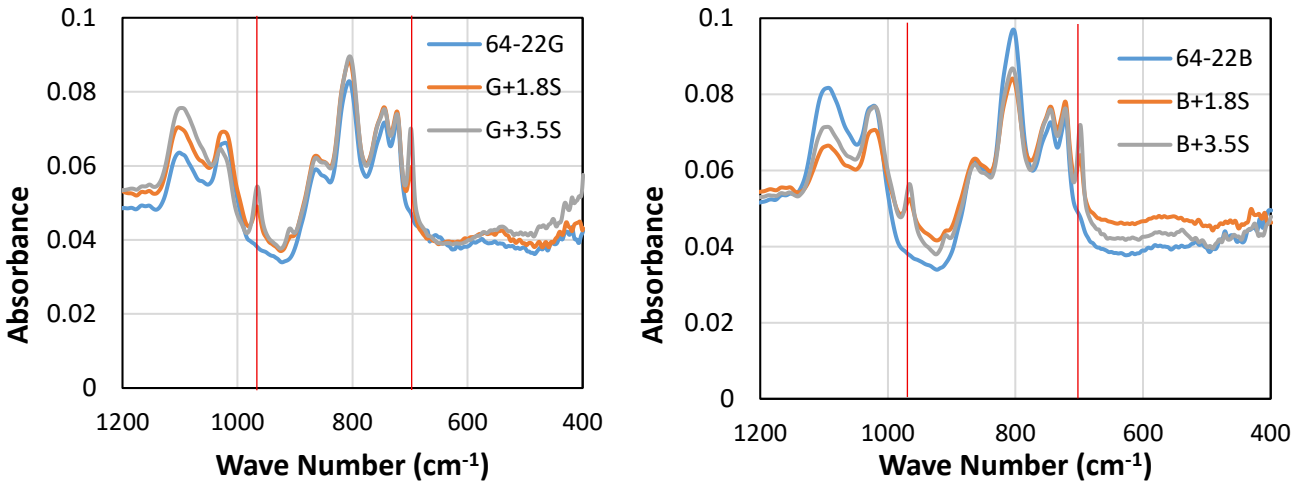

(a) Good Binder (b) Borderline Binder

Figure 35. Graph. Typical FTIR spectra for polymer-modified binders.

Aging Evaluation

Oxidation Indices

Two aging indices, Figure 36 and Figure 37, were used to qualify the effect of laboratory aging. Generally, indices use the area under functional groups' peaks that correlate well and undergo significant changes with oxidation. The areas are normalized with other more stable peaks that do not experience significant change with oxidation. Normalization is essential to eliminate the differences caused by changes in the order of magnitude in absorbance peaks. Figure 36 shows an index that uses the carbonyl peak ($A_{C=O}$), while Figure 37 uses both the carbonyl and sulfoxide ($A_{S=O}$) peaks. Both indices are normalized using the aromatic ($A_{C=C}$) and aliphatic (A_{C-H}) peaks.

$$I_{C=O} = \frac{A_{C=O}}{A_{C=C} + A_{C-H}}$$

Figure 36. Equation. Carbonyl-based FTIR oxidation index.

$$I_{C=O+S=O} = \frac{A_{C=O} + A_{S=O}}{A_{C=C} + A_{C-H}}$$

Figure 37. Equation. Carbonyl- and sulfoxide-based FTIR oxidation index.

where $A_{C=O}$, $A_{S=O}$, $A_{C=C}$, and A_{C-H} is the area under FTIR spectra between 1,670–1,725 cm^{-1}, 980–1,070 cm^{-1}, 1,535–1,650 cm^{-1}, and 1,325–1,515 cm^{-1}, respectively.

Effect on Aging

Figure 38 and Figure 39 present the aging evolution of binder blends, showing original binder (OB), PAV, and 2PAV conditions. Figure 38 shows aging evolution using the $I_{C=O}$ index while Figure 39 uses the $I_{C=O+S=O}$ index.

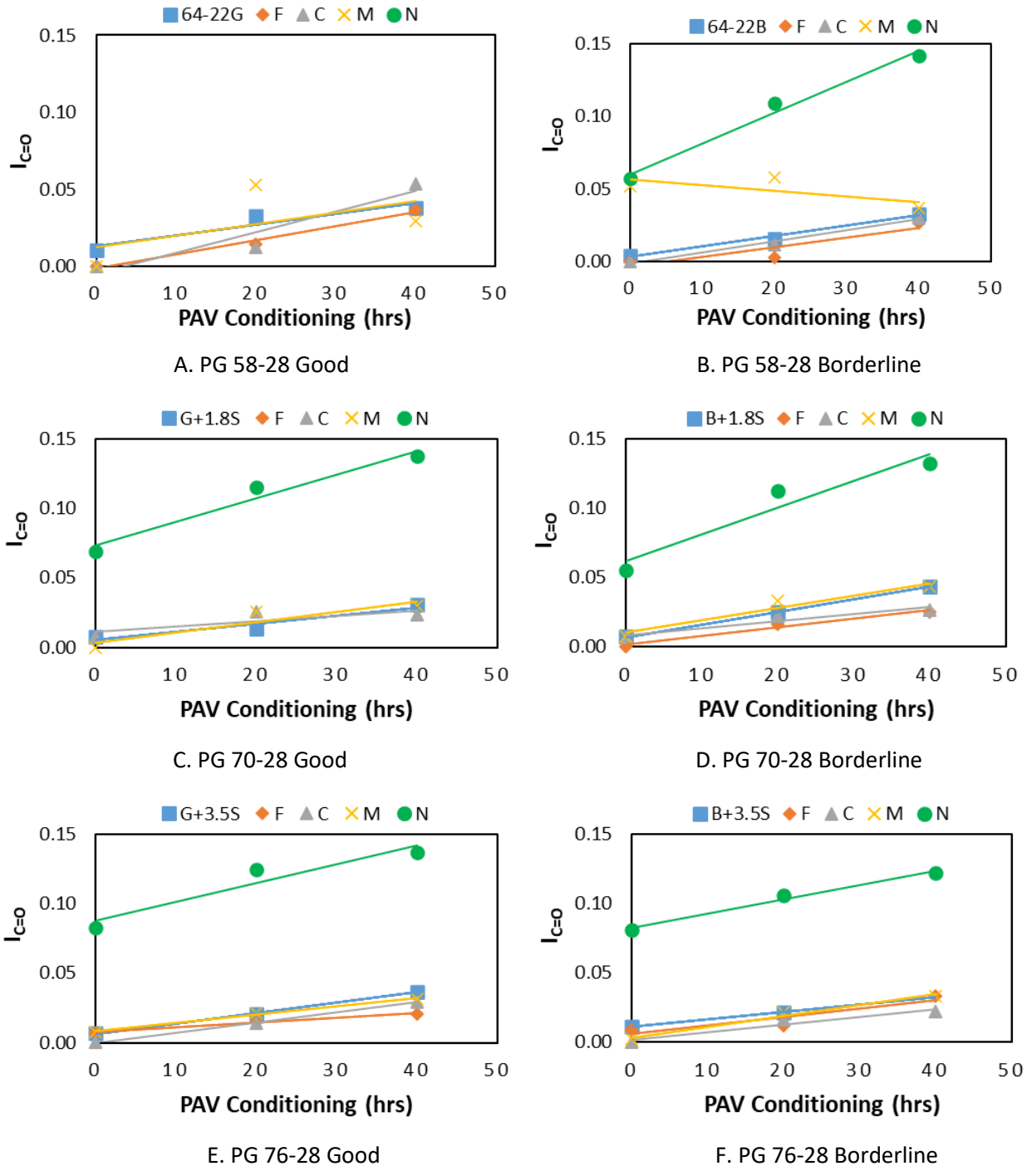

A. PG 58-28 Good

B. PG 58-28 Borderline

C. PG 70-28 Good

D. PG 70-28 Borderline

E. PG 76-28 Good

F. PG 76-28 Borderline

Figure 38. Graph. Aging evolution for binder blends using $I_{C=O}$.

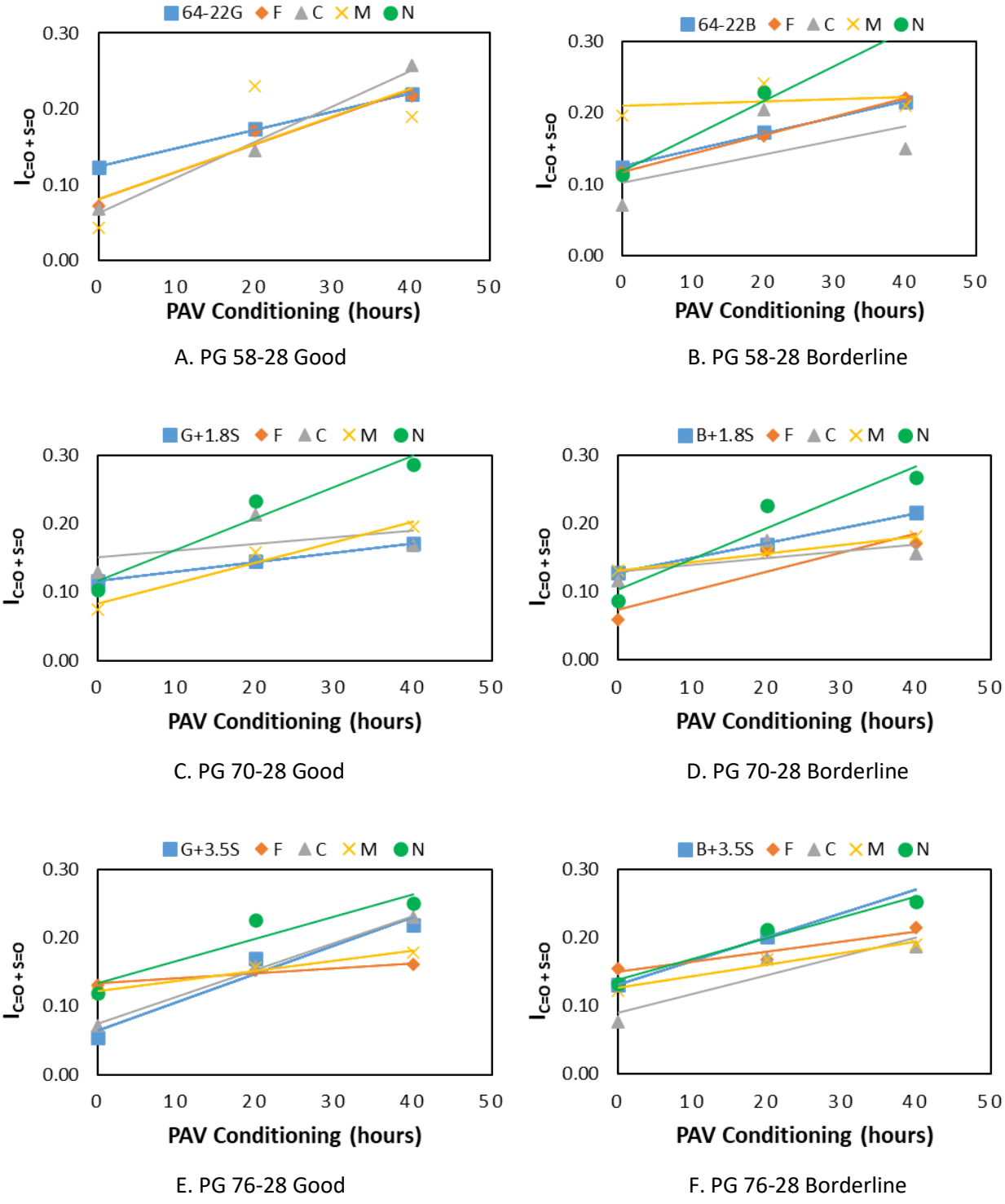

A. PG 58-28 Good

B. PG 58-28 Borderline

C. PG 70-28 Good

D. PG 70-28 Borderline

E. PG 76-28 Good

F. PG 76-28 Borderline

Figure 39. Graph. Aging evolution for binder blends using $I_{C=O+S=O}$.

In summary, across PG, while $I_{C=O}$ showed similar oxidation rates (slope of line) from OB to PAV and PAV to 2PAV between the four softeners, the oxidation rates varied for different softeners, as shown by $I_{C=O+S=O}$. While softener N does not necessarily have a higher rate of change for the $I_{C=O}$ index compared to other softeners, it had higher lower values for oxidation indices at different aging conditions. For both PG 58-28 binder types and corresponding indices, softener M had an increase from OB to PAV and then a decrease from PAV to 2PAV. While counterintuitive, this could be due to volatilization or degradation of oxidized compounds and phase separation in modified binders.

Polymer Degradation Evaluation

Degradation Indices

Polymer degradation was quantified using the degradation index, Figure 40. The index uses the butadiene peak (A_B), which is normalized by the styrene peak (A_S). The PB segment is targeted by oxygen, due to the unsaturated C=C bond, leading to its oxidation and subsequent degradation. The relative stability, under oxidation, of the PS segment makes it suitable as a normalization parameter (Wang et al., 2015; Yan et al., 2018; Lin et al., 2020).

$$I_{B/S} = \frac{A_B}{A_S}$$

Figure 40. Equation. Butadiene- and styrene-based FTIR degradation index.

where A_B and A_S is area under FTIR spectra between 937–977 cm^{-1} and 679–709 cm^{-1} respectively.

Figure 41 presents the SBS degradation of binder blends, showing OB, PAV, and 2PAV conditions.

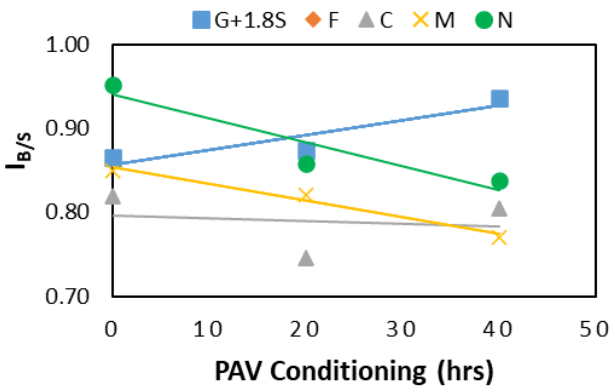

A. PG 70-28 Good

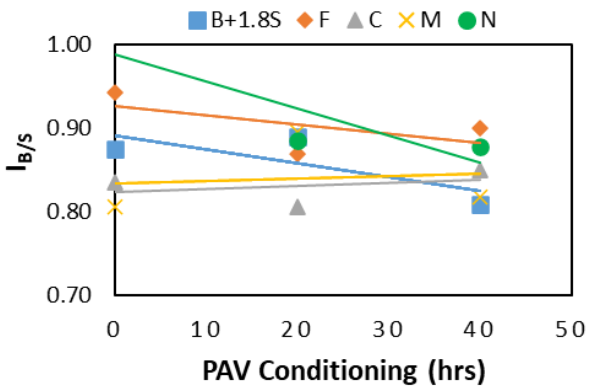

B. PG 70-28 Borderline

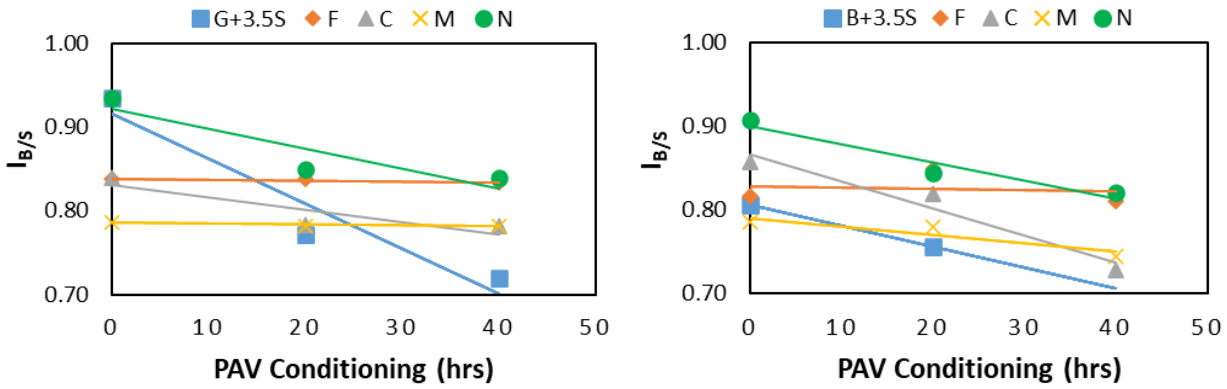

C. PG 76-28 Good

D. PG 76-28 Borderline

Figure 41. Graph. Polymer degradation for binder blends using $I_{B/S}$.

In summary, the $I_{B/S}$ index decreased with aging, highlighting the degradation of the SBS. Generally, apart from PG 70-28 Good (Figure 41-a), the degradation rate (slope of line) of the polymer-modified binders is higher than the polymer-softener-modified counterparts. Hence, softeners appear to slow SBS degradation, with Softener F having the lowest rate of change for the $I_{B/S}$ index compared to other softeners.

CHAPTER 5: MIXTURE POTENTIAL PERFORMANCE

ILLINOIS FLEXIBILITY INDEX TEST

A set of binders (Table 5), representing different types of modifiers and PG binders, was used in HMA with different ABRs, as presented in Table 4. Mixes were evaluated for their cracking potential, as per the Illinois Modified AASHTO T 393 (IDOT, 2024), under short- and long-term aging conditions (compacted and prepared I-FIT specimens for 3 days at 95°C in a conventional forced draft oven) (Al-Qadi et al., 2019). The FI indicates HMA cracking potential, with a higher value representing lower cracking potential. Table 14 and Table 15 present the FI values for the limestone-based and traprock-based mixes, respectively.

From Figure 42, all mixes, except one (traprock-high ABR-borderline-PG 58-28 w/N-LTA), passed their required FI threshold (5.0 for LTA, 8.0 for STA). As expected, there was a reduction in FI from STA to LTA for all mixes and binder types. The two lines in Figure 42 indicate the thresholds identified by IDOT for the STA (top line, where FI = 8.0) and LTA (the bottom line, where FI = 5.0) of dense-graded HMA in the mix design phase. All good binders had higher FI than borderline counterparts at both STA and LTA conditions. The distinction of a binder as good or borderline is based on the ΔT_c parameter. Hence, the ΔT_c parameter was able to capture brittleness and indicate potential cracking.

The limestone-based mixes had greater FI, in general, than their traprock-based counterparts. This difference is dependent on the mix's ABR. However, while mixes with no ABR were twofold, the mixes with relatively high ABR were similar, especially for SBS-modified binders. The relative ranking of softeners and binders remained similar when comparing limestone- and traprock-based mixes. For both mix classifications, SBS PG 76-28 w/M was higher than SBS PG 76-28 w/C at no ABR; SBS PG 70-28 w/F was higher than SBS PG 70-28 w/N at moderate ABR; and PG 58-28 w/C was higher than PG 58-28 w/N at high ABR.

The fracture energy and the post-peak slopes for the selected mixes are presented in Figure 43 and Figure 44, respectively. The results resemble the conclusions noted for FI values. Generally, good binders have higher fracture energies than borderline binders. Borderline binders have a higher slope than their good binder counterparts, indicating an increased crack propagation rate. The higher FI values of the limestone-based mixes compared to their traprock-based counterparts can be explained by their higher fracture energies and lesser slope values.

Table 14. FI Values for Selected Mixes (Limestone Mix)

	Base Binder PG 64-22					Base Binder PG 58-28				
		Good		Borderline			Good		Borderline	
Mix Type	Binder	STA	LTA	STA	LTA		STA	LTA	STA	LTA
High ABR	*PG 58-28 w/C*	25.3	13.9	18.7	8.6					
	PG 58-28 w/N	N/A	N/A	14.7	7.2					
						Neat PG 58-28	20.7	6.3	13.6	7.6
Moderate ABR	*SBS PG 70-28 w/N*	38.4	16.8	23.6	13.9					
	SBS PG 70-28 w/F	57.2	33.3	30.1	17.3					
						SBS PG 70-28	36.2	14.0	25.1	11.9
No ABR	*Neat PG 64-22*	39.1	18.5	33.2	14.0					
	SBS PG 76-28 w/C	84.5	41.6	58.2	32.2					
	SBS PG 76-28 w/M	83.6	42.4	63.0	33.4					
						Neat PG 58-28	38.2	19.9	28.7	14.5
						SBS PG 70-28	66.7	28.3	46.5	26.4
						SBS PG 76-28	58.1	21.3	44.4	27.9

Table 15. FI Values for Selected Mixes (Traprock Mix)

	Base Binder PG 64-22					Base Binder PG 58-28				
		Good		Borderline			Good		Borderline	
Mix Type	Binder	STA	LTA	STA	LTA		STA	LTA	STA	LTA
High ABR	*PG 58-28 w/C*	20.2	8.8	17.1	7.2					
	PG 58-28 w/N	N/A	N/A	9.7	4.5					
						Neat PG 58-28	16.6	6.4	13.0	7.1
Moderate ABR	*SBS PG 70-28 w/N*	20.1	7.21	14.2	6.4					
	SBS PG 70-28 w/F	25.3	14.8	19.0	10.3					
						SBS PG 70-28	21.9	7.3	15.7	6.2
No ABR	*SBS PG 76-28 w/C*	34.1	22.4	23.5	15.3					
	SBS PG 76-28 w/M	43.8	18.8	24.6	12.2					
						Neat PG 58-28	21.5	17.1	19.5	12.6
						SBS PG 70-28	27.7	18.8	21.5	15.1
						SBS PG 76-28	41.9	18.9	23.6	15.7

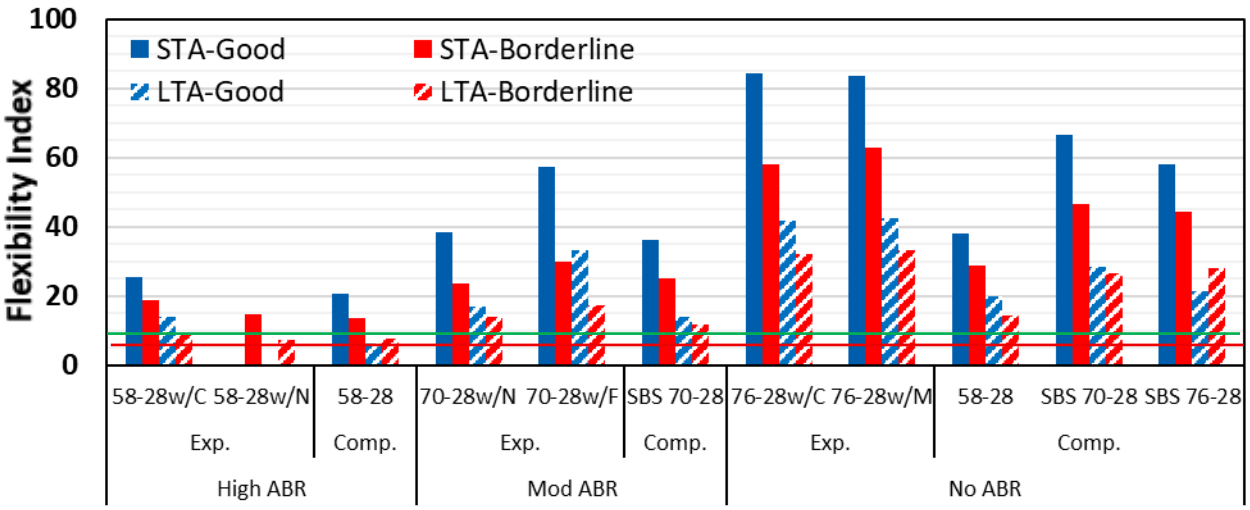

A. Limestone Mix

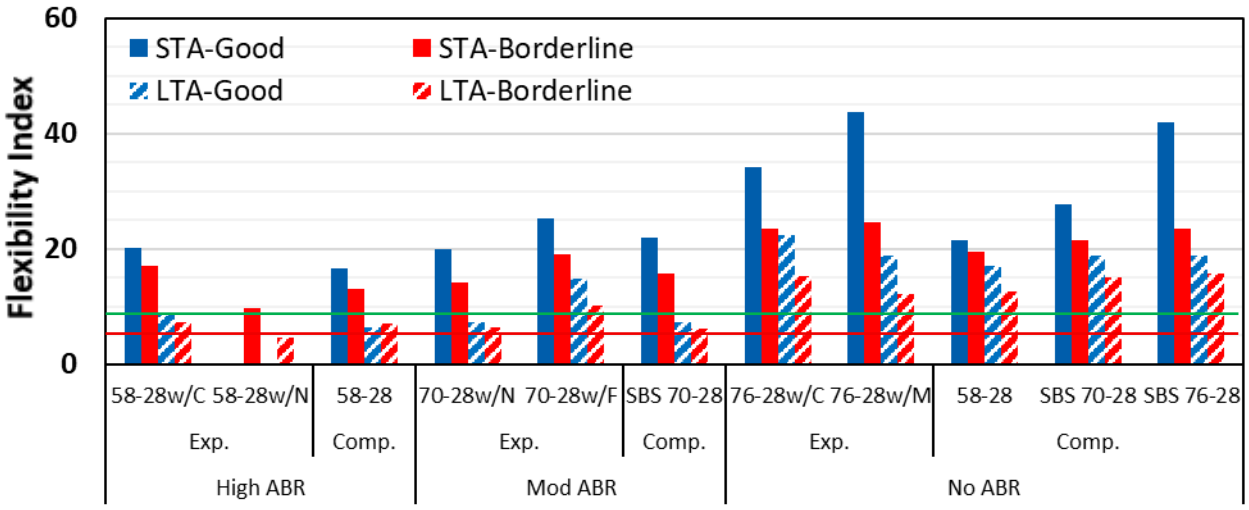

B. Traprock Mix

Figure 42. Bar plot. FI values for selected mixes.

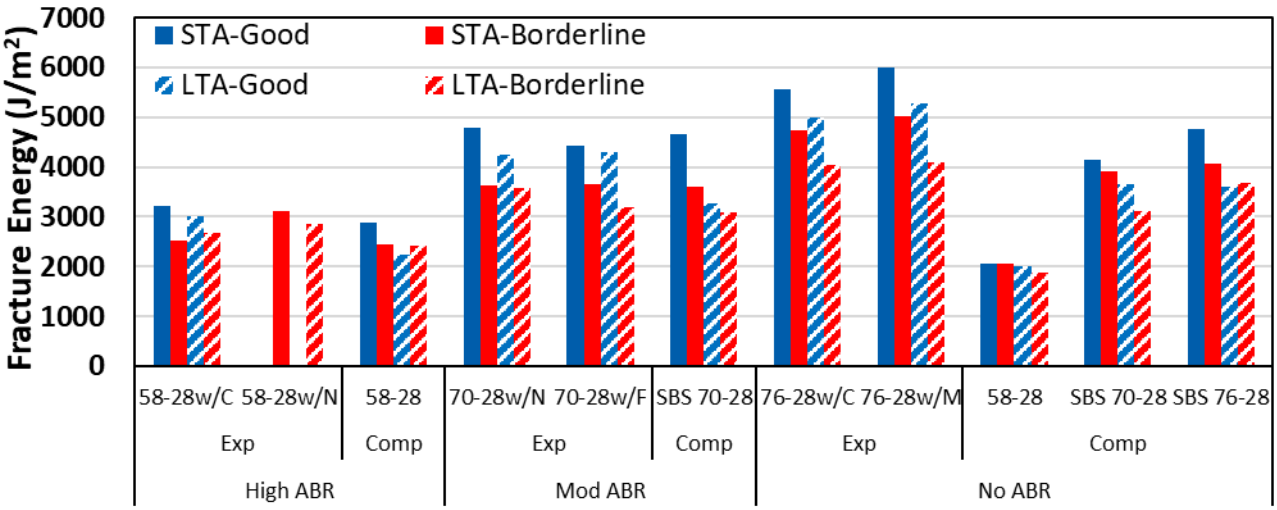

A. Limestone Mix

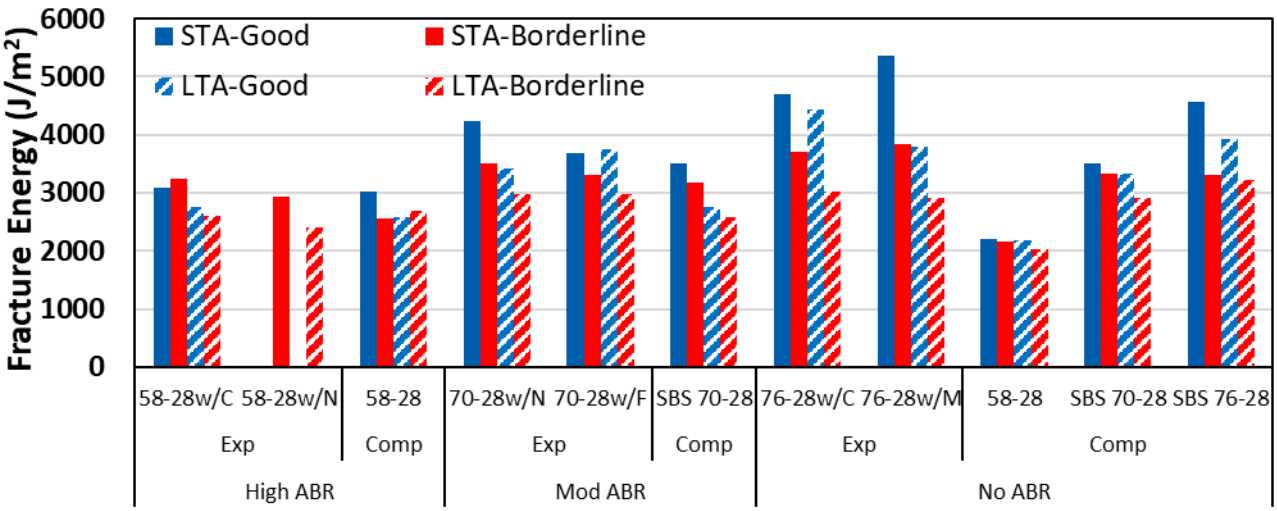

B. Traprock Mix

Figure 43. Bar plot. Fracture energy values for selected mixes.

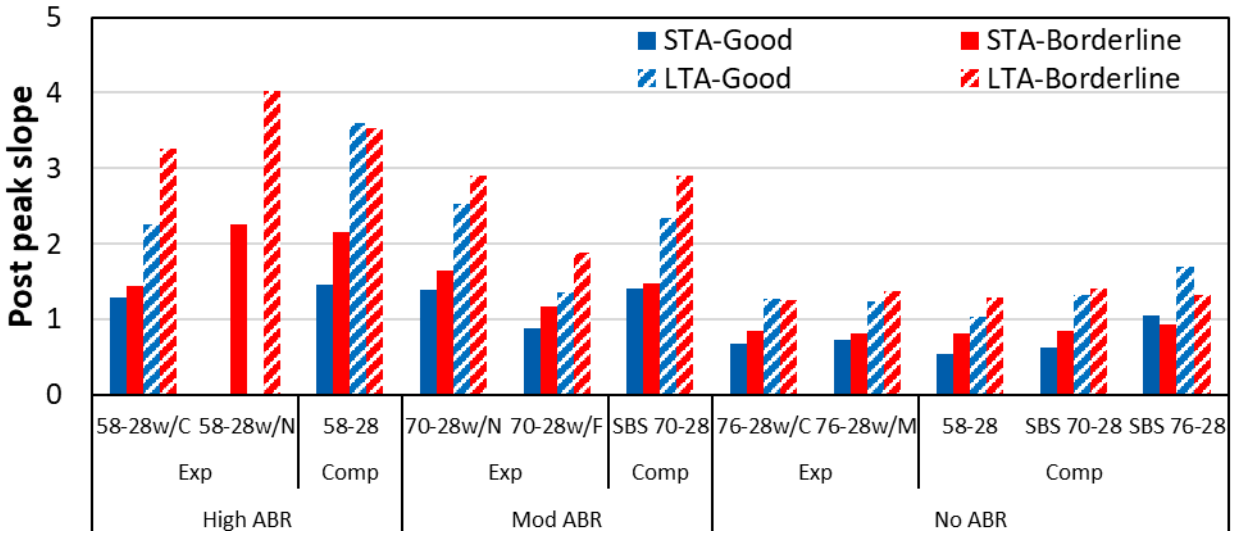

A. Limestone Mix

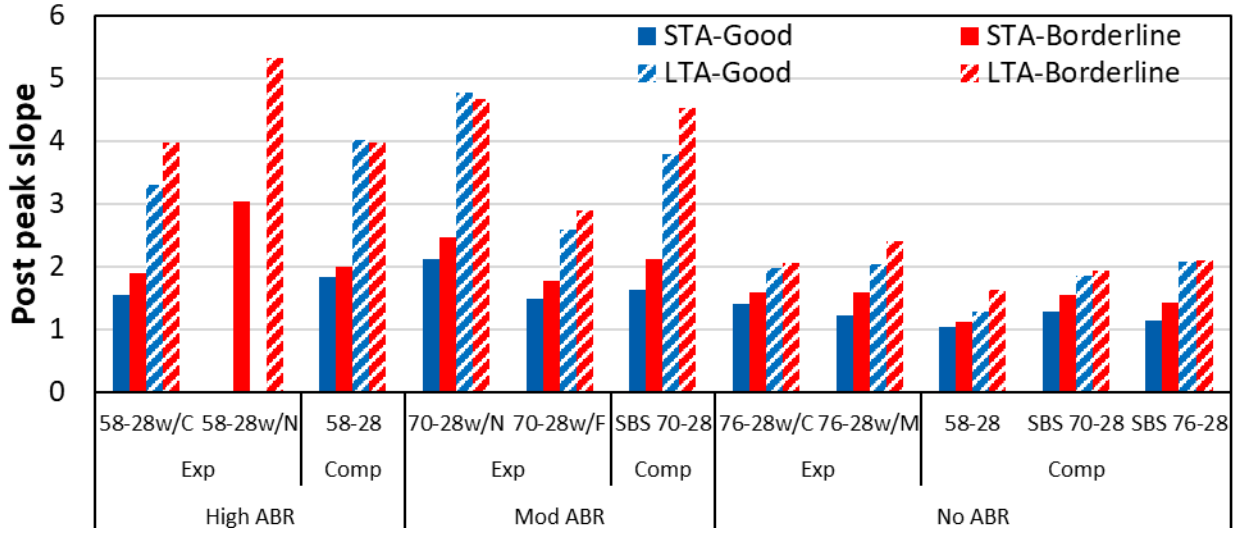

B. Traprock Mix

Figure 44. Bar plot. Post-peak slope values for selected mixes.

Effect of Binder Modifiers on HMA Flexibility Index

Softeners are used in HMA to enhance flexibility by reducing binder stiffness, thereby minimizing cracking potential, particularly at low temperatures. The softeners are expected to lower binder viscosity and reduce glass transition temperature (T_g), resulting in improved ductility and strain tolerance (Zhou et al., 2020). Figure 45 illustrates the impact of softeners on high ABR mixes. The softened binders (patterned bars) had a higher FI than the neat binder (solid bars). The mixes with fatty acid C-modified binder outperformed both mixes with neat and with softener N (glycol amine) in controlling potential cracking. These findings align with the results reported by Singhvi et al. (2021). However, this is in contrast with the rheological data, which suggested a favorable performance when

a glycol-amine–based softener is used (Table 8). Glycol-amine–based softeners are highly volatile, which may result in losing softening components during binder modification and aging. In addition, they are more susceptible to moisture at the mixture level (Singhvi et al., 2021).

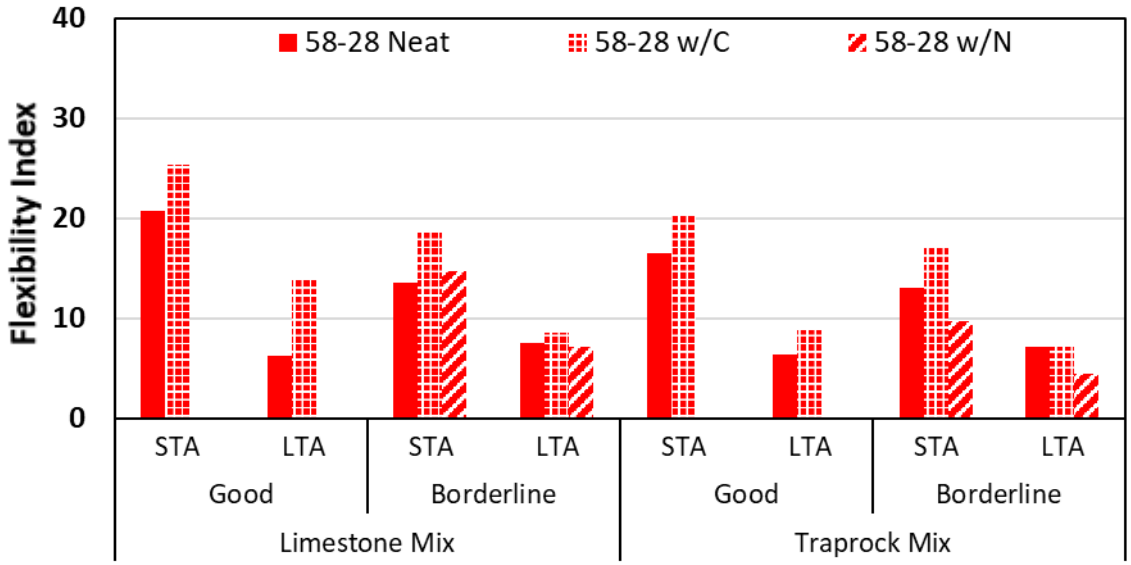

Figure 45. Bar plot. FI values for mixes with relatively high ABR.

Figure 46 (moderate ABR) and Figure 47 (no ABR) present the effect of softening when SBS is present. The trends observed in Figure 46 align with the earlier discussion regarding the superior performance of F-modified mixes (vegetable oil) over N-modified mixes. This contrasts with the binder rheology results, where softener N exhibited better performance. The presence of softeners increases FI, when comparing patterned bars with their accompanying solid bar. From Figure 47 and for the traprock-based mixes, under STA conditions, softener M (aromatic oil) performed better than softener C (fatty acid), whereas under LTA conditions, softener C slightly outperformed softener M.

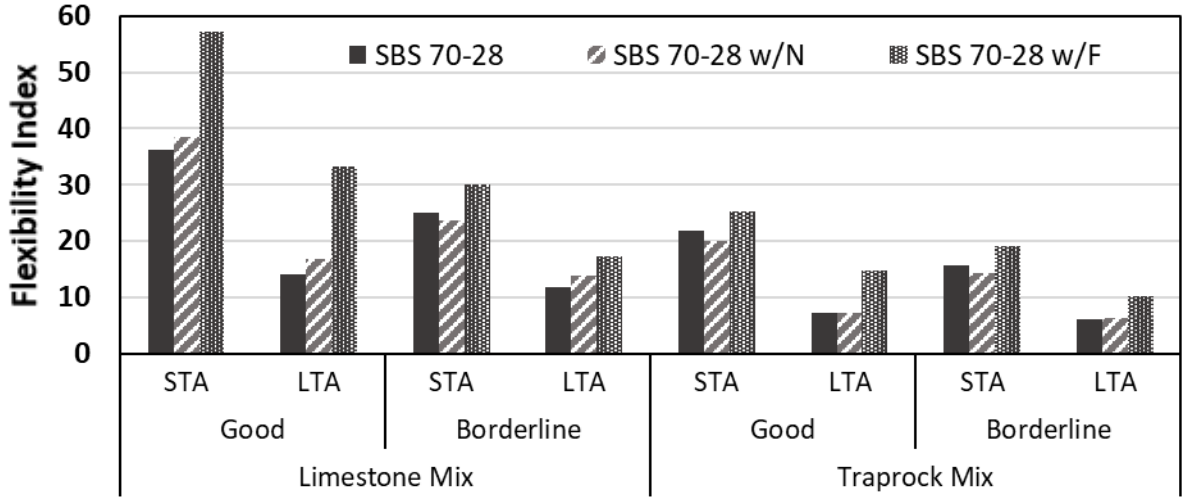

Figure 46. Bar plot. FI values for mixes with moderate ABR.

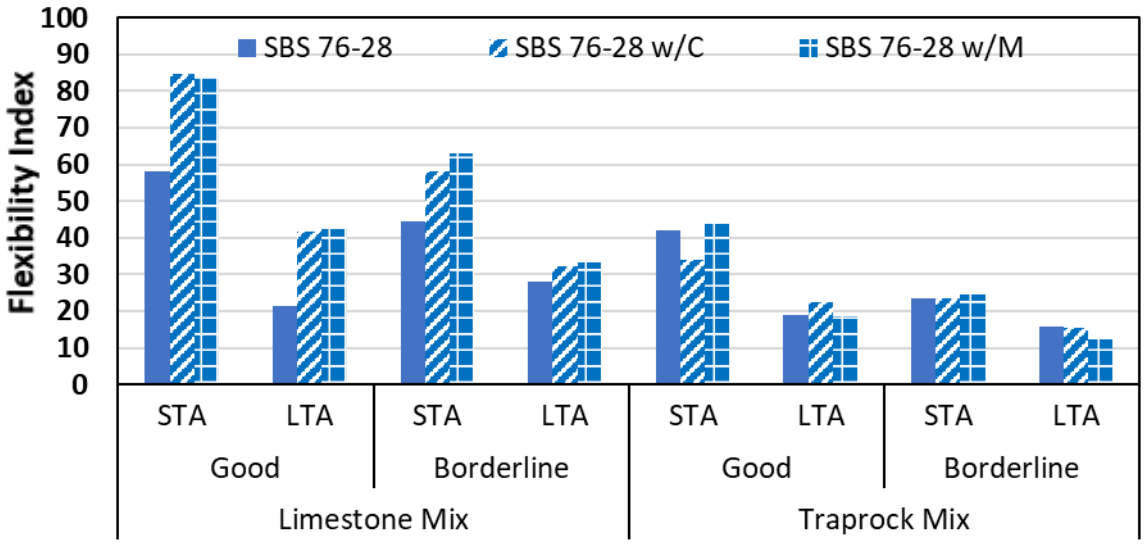

Figure 47. Bar plot. FI values for no ABR mixes (SBS 76-28, SBS 76-28 w/C, and SBS 76-28 w/M).

The incorporation of polymers, particularly SBS, into HMA is expected to enhance its flexibility and to reduce cracking potential. SBS-modified HMA exhibits remarkable elasticity, enabling it to withstand various stressors without cracking, even under extreme weather conditions. This elasticity is attributed to the elastomeric properties of SBS, which improve the binder's ability to recover its original shape after deformation, thereby enhancing pavement's resistance to fatigue and extending its service life (Behnood & Modiri Gharehveran, 2019; DuBois et al., 2014; D'Angelo and Dongré, 2009).

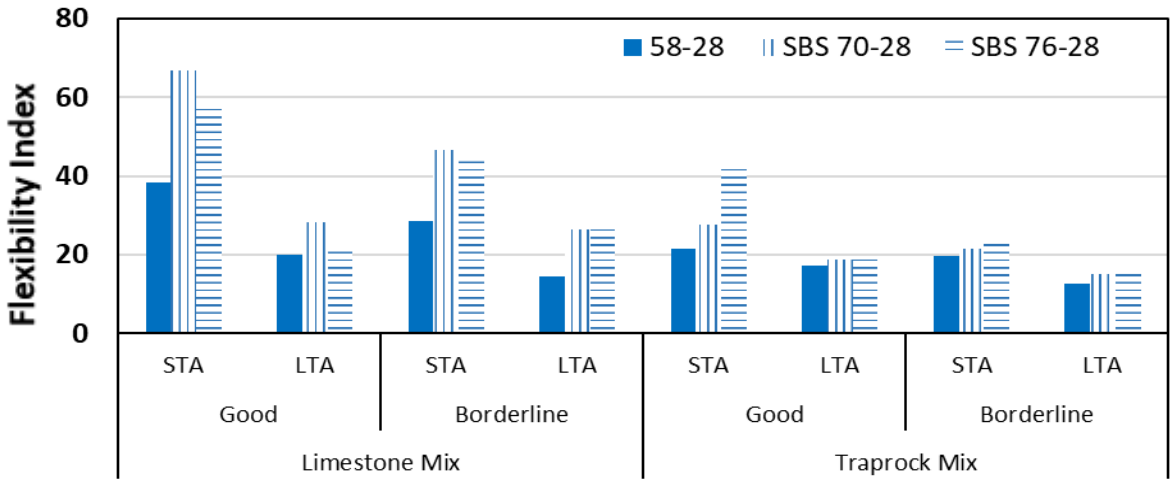

Figure 48. Bar plot. FI values for no ABR mixes (58-28, SBS 70-28, and SBS 76-28).

From Figure 48, there was a significant increase in FI from 58-28 to the polymer-modified SBS 70-28, indicating the positive effect of polymer modification on cracking potential. However, with the limestone-based mix, an increased dosage from SBS 70-28 to SBS 76-28 led to no additional benefit; a reduction was observed in most cases. With the traprock-based mix, an increased dosage from SBS

70-28 to SBS 76-28, there was a partial additional benefit. However, in this case, the increase in FI is less than when comparing an unmodified binder to a modified binder. These two observations suggest an optimal SBS dosage exists, beyond which additional polymer content may not offer commensurate cracking-resistance benefits. Polymer addition after this point may lead to increased stiffness in the mastic, accelerating crack propagation rather than mitigating it. Therefore, an SBS dosage sufficient to achieve PG 70 appears adequate to control cracking potential. However, if stiffer HMA is desired to control rutting, softener may be needed to provide a balance to control potential cracking.

Unlike softeners and SBS, the effect of the combination of SBS and softeners, as in polymer-softener-modified binders, on the flexibility of HMA is not present in the literature at the time of this study. Figure 49 compares a neat binder (solid fill) with its polymer-softener-modified counterpart (patterned fill). As shown, the effect of modifiers (SBS and softeners) lead to a significant increase in the FI values. The increase is greater when compared to the individual effect of softeners and SBS, highlighting the combinatory effect of both modifiers. The combination of both modifiers led to a greater increase in fatigue tolerance that exceeds a simple summation of each modifier.

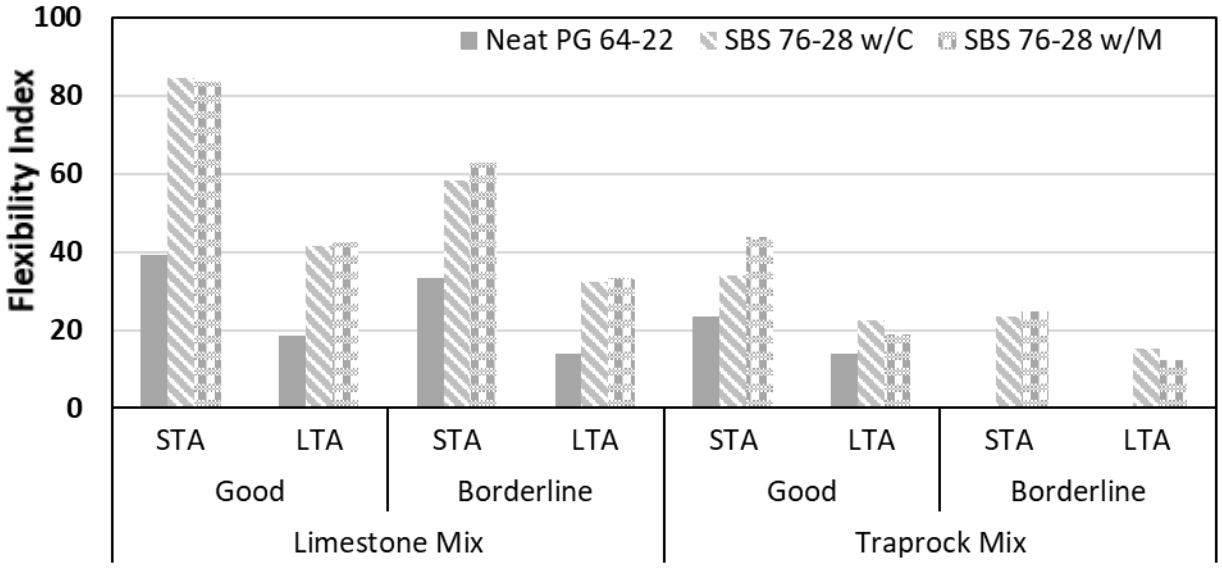

Figure 49. Bar plot. FI for no ABR mixes (neat 64-22, SBS 76-28 w/C, and SBS 76-28 w/M).

Effect of ABR on HMA Flexibility Index

As expected, the incorporation of RAP into HMA significantly affects flexibility, reducing it due to the aged and stiffened nature of the recycled binder. As RAP content increases, the mixture tends to exhibit higher stiffness and lower ductility, leading to an increased susceptibility to cracking, particularly in colder climates (Al-Qadi et al., 2007). The effect of RAP on all mixes' FI values was evident, as presented in Figure 50 and Figure 51. For all cases (binder type, aging duration, and PG), the FI decreases with increasing ABR. The reduced flexibility is primarily attributed to oxidative aging of the RAP binder, which results in a loss of maltenes and an increase in asphaltenes, making the binder more brittle. However, as observed in this study, the negative impact on flexibility can be

mitigated by incorporating softener or softer virgin binders, which help restore the rheological properties of the aged asphalt and reduce cracking potential (Cavalli et al., 2018; Fatmehsari et al., 2019; Nguyen et al., 2024). Adding the appropriate modification in mixes with RAP resulted in regaining the FI values to values like those of neat binder.

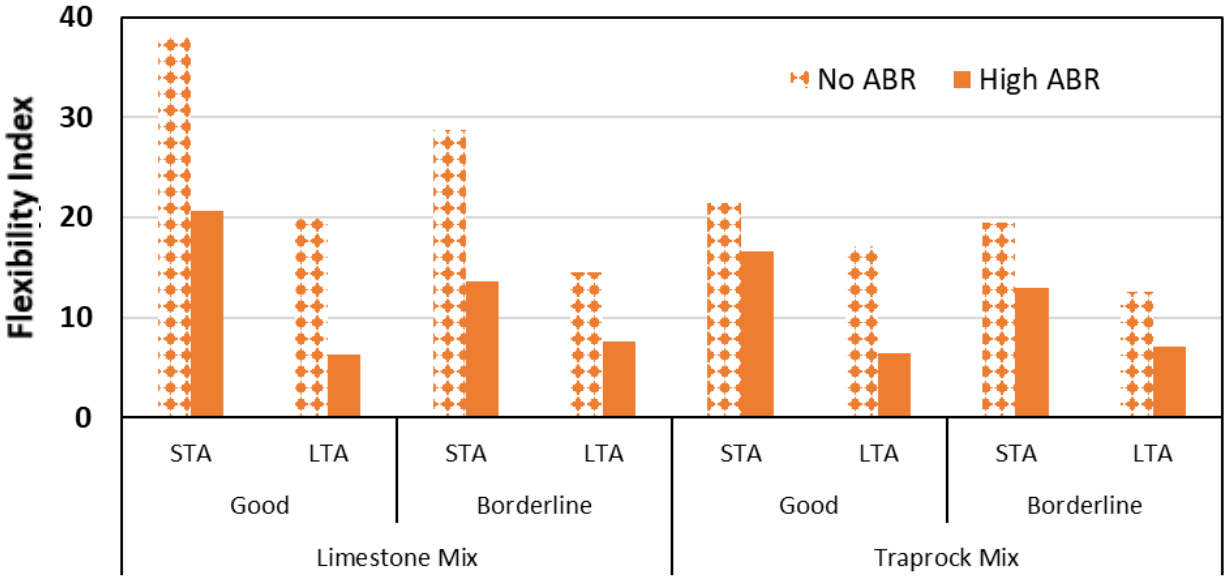

Figure 50. Bar plot. FI values for neat 58-28 (no and high ABR).

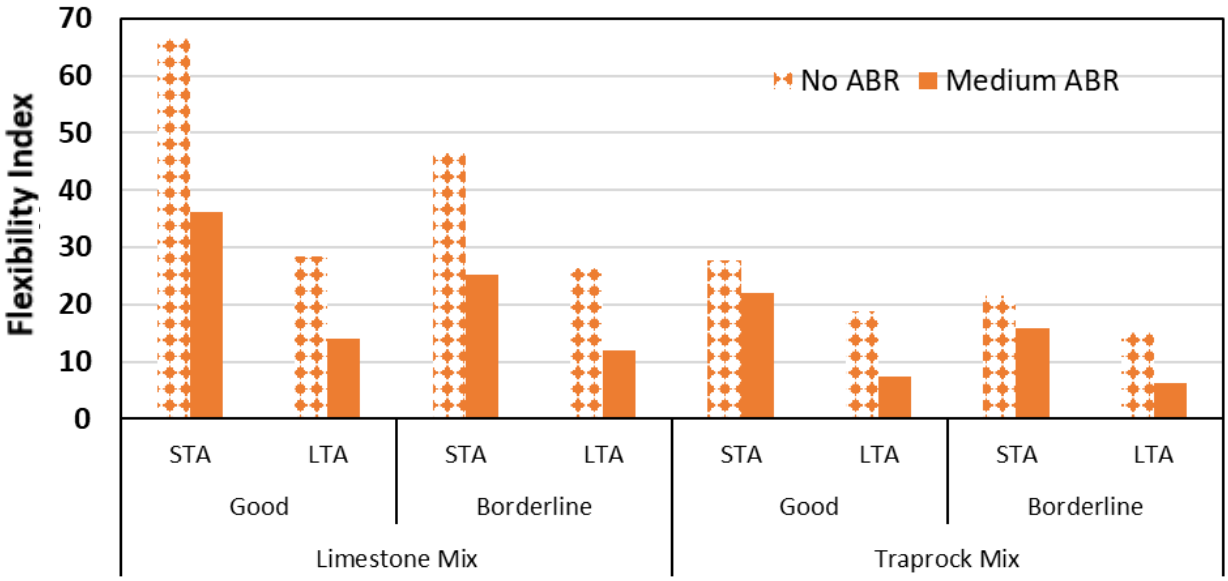

Figure 51. Bar plot. FI values for SBS PG 70-28 (no and medium ABR).

Statistical Analysis of the Binder Modification Effect

While modifiers, SBS and softeners, improve high-temperature stiffness and flexibility, respectively, the intrinsic properties of the base binder (e.g., viscosity, aging susceptibility, and chemical composition) play a crucial role in determining overall HMA cracking potential. A statistical test was conducted to determine which of the two components (base binder and modifier) primarily affects cracking potential. The test is in the form of an independent (two-sample) t-test.

The t-test is a statistical method used to determine whether there is a significant difference between the means of two groups. It is particularly useful when comparing small sample sizes and assessing whether observed differences are due to chance or an actual effect. The test statistics are calculated as the difference between the sample means divided by the standard error of the difference. The resulting value is compared against a critical t-value from the t-distribution to determine statistical significance. A p-value less than the chosen significance level (e.g., 0.05) indicates the difference between the groups is statistically significant (Kim, 2015).

For each ABR level, the mixes were grouped by base binder type and by modifier type. A significance level (α) of 0.1 was assumed. From Table 16, the t-test results showed that when mixes were grouped by base binder, except for the high ABR mix (0.2430), the p-values were less than 0.1. This finding indicates that the difference between the groups is statistically significant. Hence, the distinction due to base binders is evident in the cracking potential regardless of the type of modification. However, when mixes were grouped by modifier type, all p-values were much greater than 0.1, indicating that the difference between the groups was not statistically significant. This suggests that base binder is critical in the modification, and the impact of modification could be limited by the type of binder used.

Table 16. T-test p-values for FI Values

	Grouped by Base Binder	Grouped by Modifier Type
High ABR	0.2430	0.3480
Moderate ABR	0.0424	0.5660
No ABR (with SBS)	0.0113	0.7940

HAMBURG WHEEL-TRACKING TEST

The HWTT was conducted to confirm that the designed and FI-evaluated mixes would have low rutting potential. Mixes with RAP have less rutting potential, as the aged binder provides stability. Hence, only mixes without RAP were evaluated using both the limestone- and traprock-based mixes. A total of 10 binders were used per mix; results are presented in Table 17 (limestone) and Table 18 (traprock).

Table 17. HWTT Results for Mixes with No ABR (Limestone Mix)

Binder	Binder Type	Minimum # of Passes	Rut Depth at Minimum # of Passes (mm)	Passes to 12.5 mm Criteria
Neat PG 58-28	Good	5,000	Failed (> 15)	NA
Neat PG 58-28	Borderline	5,000	Failed (> 15)	1,980
SBS PG 70-28	Good	15,000	Failed (> 15)	7,220
SBS PG 70-28	Borderline	15,000	Failed (> 15)	7,980
SBS PG 76-28	Good	20,000	Failed (> 15)	12,240
SBS PG 76-28	Borderline	20,000	Failed (> 15)	13,360
SBS PG 76-28 w/C	Good	20,000	Failed (> 15)	14,500
SBS PG 76-28 w/C	Borderline	20,000	Failed (> 15)	15,860
SBS PG 76-28 w/M	Good	20,000	Failed (> 15)	15,800
SBS PG 76-28 w/M	Borderline	20,000	Failed (> 15)	12,580

Table 18. HWTT Results for Mixes with No ABR (Traprock Mix)

Binder	Binder Type	Minimum # of Passes	Rut Depth at Minimum # of Passes (mm)	Passes to 12.5 mm Criteria
Neat PG 58-28	Good	5,000	Failed (> 12.5)	2,600
Neat PG 58-28	Borderline	5,000	Failed (> 12.5)	2,496
SBS PG 70-28	Good	15,000	5.97	> 20,000
SBS PG 70-28	Borderline	15,000	5.12	> 20,000
SBS PG 76-28	Good	20,000	4.44	> 20,000
SBS PG 76-28	Borderline	20,000	4.63	> 20,000
SBS PG 76-28 w/C	Good	20,000	4.65	> 20,000
SBS PG 76-28 w/C	Borderline	20,000	4.42	> 20,000
SBS PG 76-28 w/M	Good	20,000	4.92	> 20,000
SBS PG 76-28 w/M	Borderline	20,000	4.68	> 20,000

For the limestone mix, all tested mixes had a rut depth higher than 12.5 mm at their required number of load passes, indicating that they failed their rutting requirement. In an opposite trend to that observed in the I-FIT, borderline binders performed better than good binders except in the case of SBS PG 76-28 w/M. There are no HWTT data for the good-neat PG 58-28 binder, as the compacted pills fell apart about 30 minutes after compaction.

For the traprock mix, all tested mixes, except the two PG 58-28 binders, passed the 12.5 mm rut depth requirement at their required number of load passes. The effect of SBS is evident, as the PG 76-28 mixes have lesser rut depth than the PG 70-28 mixes. Like the limestone mixes, borderline binders performed better in rutting than good binders, except in the case of the neat PG 58-28, where the good binder showed less rutting than the borderline.

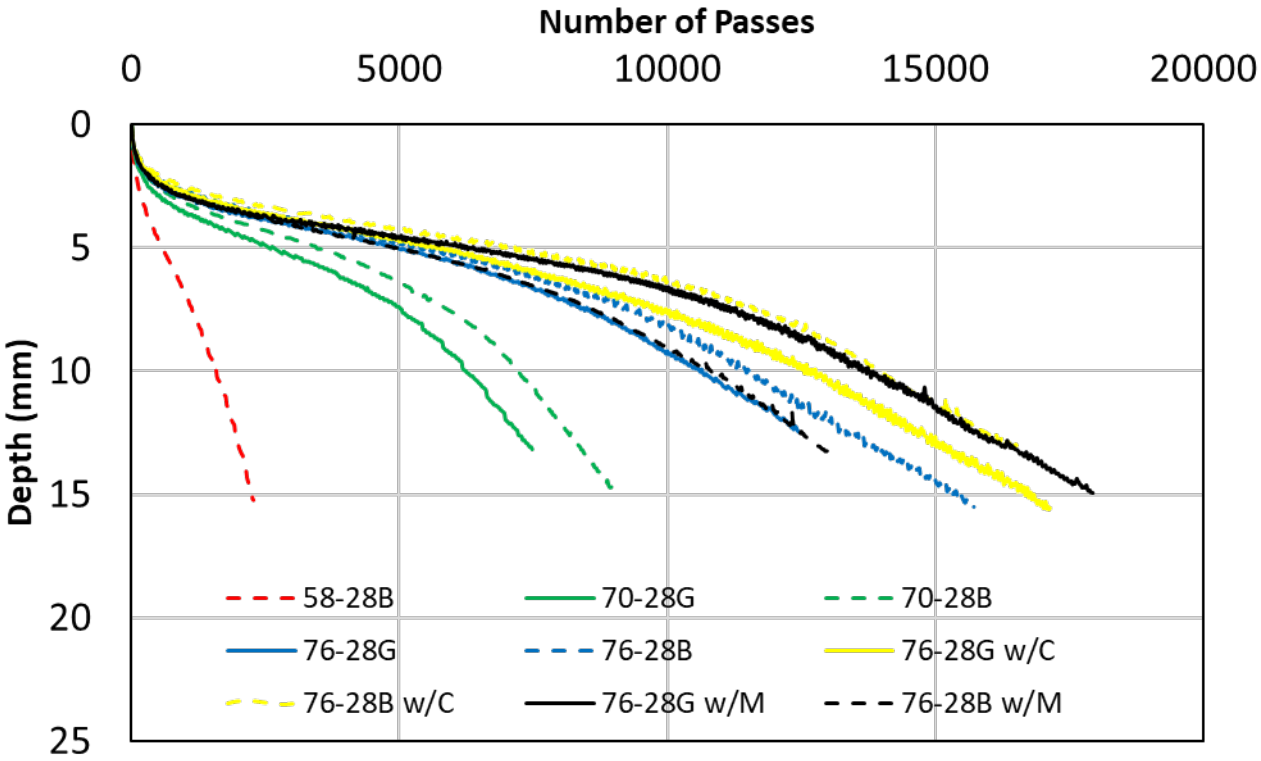

Figure 52. Graph. HWTT results for mixes with no ABR (limestone mix).

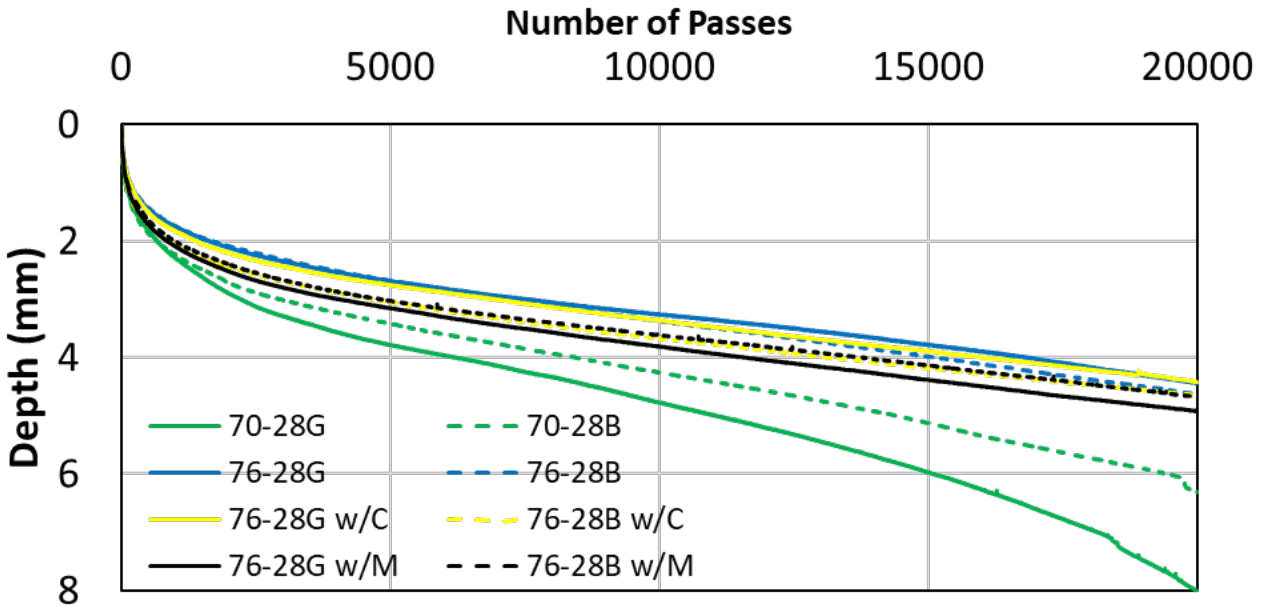

A. SBS mixes

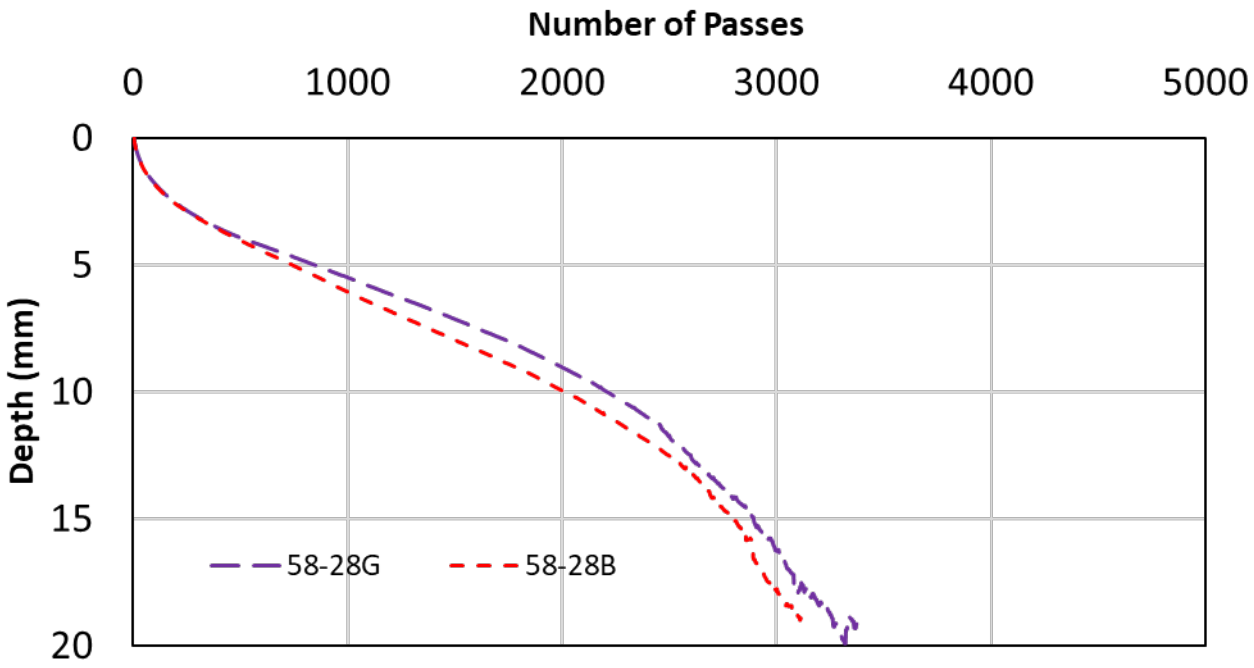

B. PG 58-28 mixes

Figure 53. Graph. HWTT results for mixes with no ABR (traprock mix).

Figure 52 and Figure 53 show the rut progression for the limestone and traprock mixes, respectively. Generally, for each of the 10 binder types, the limestone mixes had significantly higher rutting potential than the traprock mixes. However, with cracking potential, the limestone mixes had significantly less cracking potential than the traprock mixes. This is consistent with the findings of the ICT-IDOT project R27-231: Evaluation of the Asphalt Mixture Design Framework for Airfield Pavements in Illinois (Sulaiman et al., 2023). The project found an inverse relationship between cracking and rutting potential for airport and highway mixes. Airport mixes had less cracking and higher rutting potential compared to highway mixes. This may be attributed to the absence of RAP and the presence of manufactured sand in these airport mixes.

CHAPTER 6: CRACKING POTENTIAL OF HOT-MIX ASPHALT FROM BINDER RHEOLOGICAL PARAMETERS

The aim was to develop a scientific prediction of HMA cracking potential from binder performance test parameters (e.g., 1PAV ΔT_c, 2PAV ΔT_c, $\Delta|G^*|_{peak\,\tau}$, S-value, and m-value). The HMA cracking potential parameters are flexibility index (FI), post-peak slope (slope), and fracture energy (G_f) from I-FIT. To achieve that, laboratory test data were processed, and statistical analysis was applied to identify linear and/or nonlinear relationships between HMA cracking potential and binder rheological parameters.

DATA SOURCE AND PREPROCESSING

The total number of HMA samples in the database is 52 (Table 19); however, 46 samples were considered in the analysis. The nominal maximum aggregate size (NMAS) of the aggregates in all mixes is 9.5 mm and the asphalt content (AC) ranges from 5.7% to 6.3%. Cases 1 through 46 are laboratory-designed with the number of gyrations at 50, 70, and 90, and the design air void content is 3.9–4.1. Cases 1–23 use traprock aggregates, while cases 24–46 use limestone mixes. The number of gyrations and design air void for cases 47–52 are 70 gyrations and 4.5%, respectively. Those cases were obtained from data provided by Singhvi et al. (2021) from ICT-IDOT project, R27-196-HS: Rheology-Chemical Based Procedure to Evaluate Additives/Modifiers Used in Asphalt Binders for Performance Enhancements: Phase 2.

Table 19. Mix Design Characteristics of Hot-Mix Asphalt

Case	Binder ID	RAP	ABR	Binder	Softener	SBS	PG	AC (%)	AV[1] (%)	N Design
1	G+4C	27.8	High	G[2]	C	No	58-28	5.9	4.1	70
2	B+4C	27.8	High	B[3]	C	No	58-28	5.9	4.1	70
3	B+5N	27.8	High	B	N	No	58-28	5.9	4.1	70
4	58-28G	27.8	High	G	No	No	58-28	5.9	4.1	70
5	58-28B	27.8	High	B	No	No	58-28	5.9	4.1	70
6	G+4S+5N	17.5	Moderate	G	N	Yes	70-28	5.8	4	70
7	B+4S+5N	17.5	Moderate	B	N	Yes	70-28	5.8	4	70
8	G+4F+3.6S	17.5	Moderate	G	F	Yes	70-28	5.8	4	70
9	B+4F+3.6S	17.5	Moderate	B	F	Yes	70-28	5.8	4	70
10	58-28G+3.5S	17.5	Moderate	G	No	Yes	70-28	5.8	4	70
11	58-28B+3.4S	17.5	Moderate	B	No	Yes	70-28	5.8	4	90
12	G+3C+5S	0	No	G	C	Yes	76-28	5.7	3.9	90
13	B+3C+5S	0	No	B	C	Yes	76-28	5.7	3.9	90
14	G+5M+5S	0	No	G	M	Yes	76-28	5.7	3.9	90
15	B+4.9M+4.2S	0	No	B	M	Yes	76-28	5.7	3.9	90
16	58-28G	0	No	G	No	No	58-28	5.7	3.9	90
17	58-28B	0	No	B	No	No	58-28	5.7	3.9	90

Case	Binder ID	RAP	ABR	Binder	Softener	SBS	PG	AC (%)	AV[1] (%)	N Design
18	58-28G+3.5S	0	No	G	No	Yes	70-28	5.7	3.9	90
19	58-28B+3.4S	0	No	B	No	Yes	70-28	5.7	3.9	90
20	58-28G+4.5S	0	No	G	No	Yes	76-28	5.7	3.9	90
21	58-28B+4.4S	0	No	B	No	Yes	76-28	5.7	3.9	90
22	64-22G	0	No	G	No	No	64-22	5.7	3.9	90
23	64-22B	0	No	B	No	No	64-22	5.7	3.9	90
24	G+4C	29.5	High	G	C	No	58-28	6	4	50
25	B+4C	29.5	High	B	C	No	58-28	6	4	50
26	B+5N	29.5	High	B	N	No	58-28	6	4	50
27	58-28G	29.5	High	G	No	No	58-28	6	4	50
28	58-28B	29.5	High	B	No	No	58-28	6	4	50
29	G+4S+5N	19.01	Moderate	G	N	Yes	70-28	6.2	4	50
30	B+4S+5N	19.01	Moderate	B	N	Yes	70-28	6.2	4	50
31	G+4F+3.6S	19.01	Moderate	G	F	Yes	70-28	6.2	4	50
32	B+4F+3.6S	19.01	Moderate	B	F	Yes	70-28	6.2	4	50
33	58-28G+3.5S	19.01	Moderate	G	No	Yes	70-28	6.2	4	50
34	58-28B+3.4S	19.01	Moderate	B	No	Yes	70-28	6.2	4	50
35	G+3C+5S	0	No	G	C	Yes	76-28	6.1	4	50
36	B+3C+5S	0	No	B	C	Yes	76-28	6.1	4	50
37	G+5M+5S	0	No	G	M	Yes	76-28	6.1	4	50
38	B+4.9M+4.2S	0	No	B	M	Yes	76-28	6.1	4	50
39	58-28G	0	No	G	No	No	58-28	6.1	4	50
40	58-28B	0	No	B	No	No	58-28	6.1	4	50
41	58-28G+3.5S	0	No	G	No	Yes	70-28	6.1	4	50
42	58-28B+3.4S	0	No	B	No	Yes	70-28	6.1	4	50
43	58-28G+4.5S	0	No	G	No	Yes	76-28	6.1	4	50
44	58-28B+4.4S	0	No	B	No	Yes	76-28	6.1	4	50
45	64-22G	0	No	G	No	No	64-22	6.1	4	50
46	64-22B	0	No	B	No	No	64-22	6.1	4	50
47	C	25	High	N/A[4]	196 - C	No	58-28	6.3	4.5	70
48	S5	25	High	N/A	No	No	58-28	6.3	4.5	70
49	H	25	High	N/A	196 - H	No	58-28	6.3	4.5	70
50	F	25	High	N/A	196 - F	No	58-28	6.3	4.5	70
51	K	25	High	N/A	196 - K	No	58-28	6.3	4.5	70
52	G	25	High	N/A	196 - G	No	58-28	6.3	4.5	70

AV[1]: Air Voids; G[2]: Good; B[3]: Borderline; N/A[4]: Not Available

Figure 54 shows the asphalt binder performance parameters and corresponding HMA cracking potential parameters. The parameter data vary widely in scale. For example, G_f values span several thousand units, whereas m-values and ΔT_c have much narrower ranges. Notably, the S-values include obvious outliers, which could distort regression results due to scale dominance. Similarly, extremely high FI values that could bias the regression were also removed from the dataset. Hence, this chapter focuses on cases where FI is less than or equal to 40 (STA FI) and values less than or equal to 30 (LTA FI). $\Delta|G^*|_{peak\ \tau\ 2}$, $S(m=0.3)_2$, and $m(S=300)_2$ denote $\Delta|G^*|_{peak\ \tau}$, S(m=0.3), and m(S=300) measured under 2PAV conditions.

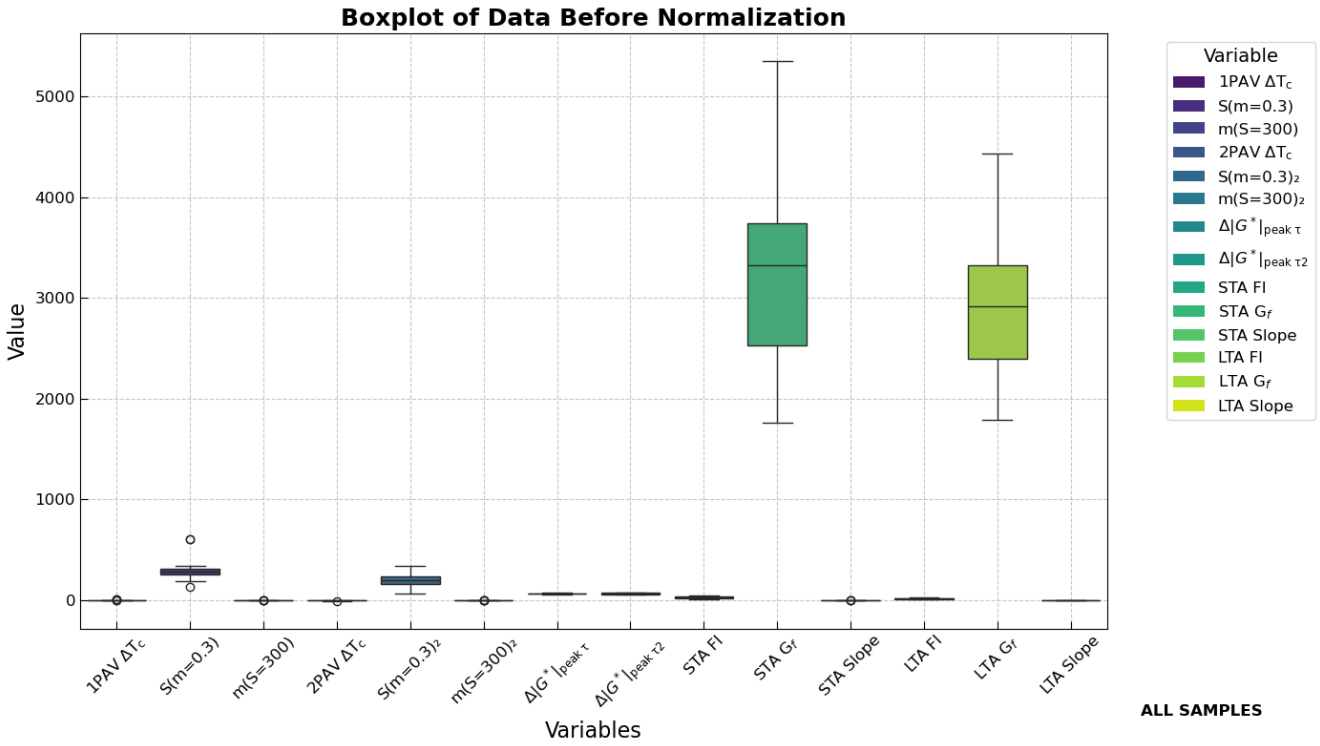

Figure 54. Graph. Distribution of binder and HMA parameters.

To address the varied range, min-max normalization was applied to scale all variables into a 0–1 range. Figure 55 presents the normalized distribution. Most variables fall between 0.1 and 0.8. Outputs, such as FI and G_f (STA and LTA), are skewed lower, while 1PAV ΔT_c and 2PAV ΔT_c tend to skew higher. Despite normalization, variable distributions remain distinct. A few mild outliers remain, especially for m-values, indicating residual variability. Normalization enhances comparability across features while preserving their individual distribution patterns.

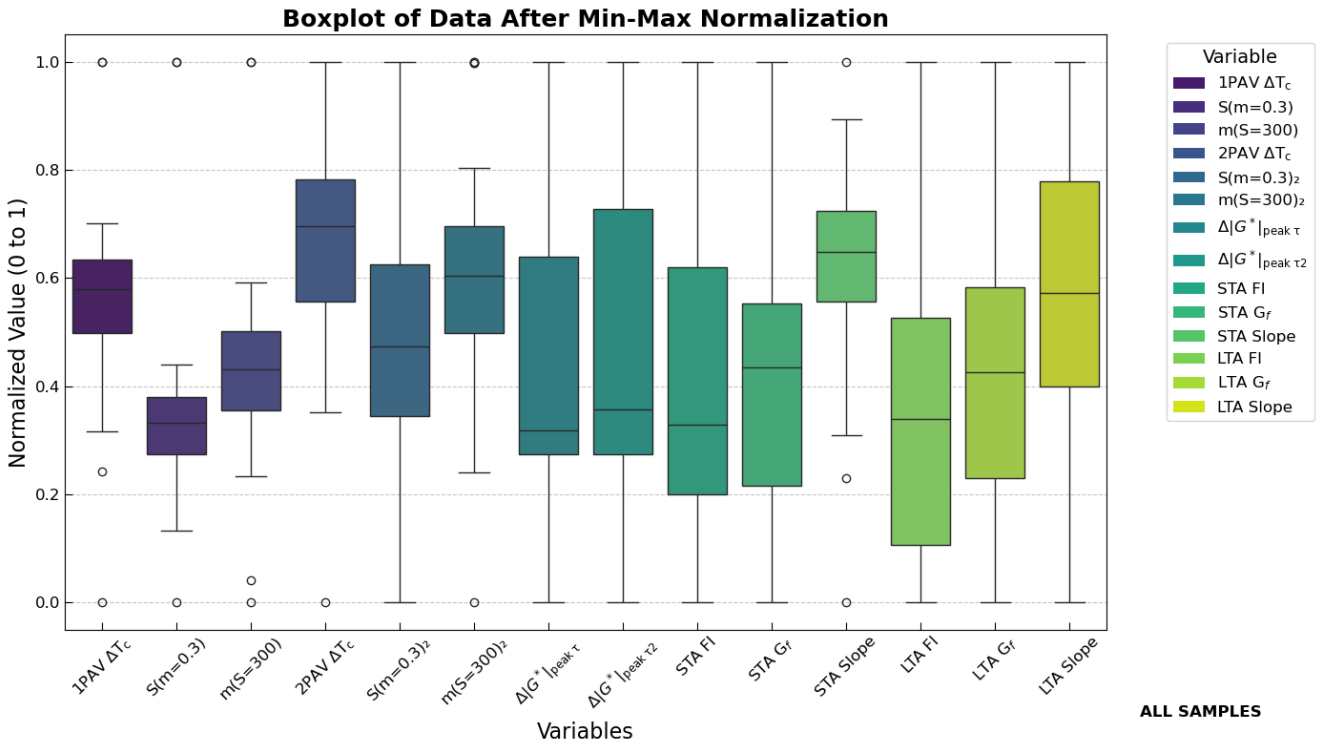

Figure 55. Graph. Distribution of normalized binder and HMA parameters.

STATISTICAL EVALUATION OF BINDER-MIXTURE RELATIONSHIPS

Correlation Analysis

Binder Recovery and Extraction

In line with the aim of the project, a simple linear relationship between binder rheological parameters and FI was investigated. Binder parameters were used as the independent variable, while FI values were used as the dependent variable. The ABR would impact the FI value; however, it was not considered part of the input parameters to predict FI values for HMA with RAP.

The following example utilized ΔT_c as an input variable and FI as an output variable. The 58-28G has a ΔT_c of 0.7. For the limestone mix, its corresponding FI value would be 20.7 when used in a high ABR mix. The FI increased to 38.2 when used in a mix with no ABR. Hence, to consider ABR in the prediction process, binder extraction and recovery were conducted to determine the binder rheology of the RAP binder.

Recovered RAP binders were blended with virgin binders at the same ratio as the ABR of the mix. This blend was thereafter conditioned, and its rheological parameters were determined. The no ABR 58-28G has a ΔT_c of 0.7 and its FI is 38.2. On the other hand, the high ABR 58-28G has a ΔT_c of -0.6 and an FI of 20.7.

While binder recovery and extraction results illustrated the effect of RAP, it would be unfeasible for practitioners and contractors to carry on this approach to select binders for mixes. HMA contractors may not always have access to binder recovery and extraction equipment. Hence, ABR was considered as a parameter in the model rather than the rheology properties of the RAP binder.

Pearson Correlation

To examine the relationship between binder rheological and HMA I-FIT parameters, Pearson correlation coefficients (R) were calculated. Table 20 presents the results for all samples. Overall, G_f and FI exhibited moderate to strong linear correlations with several binder parameters. In contrast, slope showed weaker or inconsistent correlations, suggesting possibly complex or nonlinear interactions. Notably, $\Delta|G^*|_{peak\,\tau\,2}$ consistently demonstrated strong positive correlations with both STA G_f (R = 0.57) and LTA G_f (R = 0.60), and a moderate correlation with FI for LTA (R = 0.54), while the correlation with STA FI (R = 0.20) was relatively weak. 2PAV ΔT_c and $S(m=0.3)_2$ also showed moderate correlations with G_f, but their predictive strength for FI remained limited. The relative high correlations between $\Delta|G^*|_{peak\,\tau}$ and G_f support its utility as a stiffness-related indicator with meaningful implication for cracking potential. Hence, $\Delta|G^*|_{peak\,\tau}$ may serve as a promising binder parameter for predicting HMA cracking potential.

Table 20. Correlation Matrix for I-FIT and Binder Parameters

	Metrics	1PAV ΔT_c	2PAV ΔT_c	S(m=0.3)	$S(m=0.3)_2$	m(S=300)	$m(S=300)_2$	$\Delta\|G^*\|_{peak\,\tau}$	$\Delta\|G^*\|_{peak\,\tau\,2}$
STA	G_f	0.14	0.45	0.11	0.45	0.12	0.32	0.29	**0.57**
	FI	0.12	0.17	0.11	0.17	0.13	0.08	0.10	0.20
	Slope	−0.04	−0.23	0.02	−0.21	0.00	−0.2	−0.09	−0.16
	Strain	0.10	0.42	0.05	0.41	0.06	0.32	0.25	0.48
LTA	G_f	0.15	**0.47**	0.09	**0.46**	0.11	0.34	0.18	**0.60**
	FI	0.04	0.16	−0.00	0.12	0.01	0.09	0.24	**0.54**
	Slope	−0.03	−0.06	−0.03	−0.10	−0.04	−0.06	0.19	0.30
	Strain	0.18	0.43	0.14	0.45	0.16	0.34	−0.01	0.15

Slope-related metrics (STA slope, LTA slope) consistently exhibited weak or no linear relationships with any binder parameters across all conditions. This implies that post-peak slope may not have a linear relationship with traditional binder rheology. Hence, nonlinear modeling or consideration of other factors, such as binder content (BC) or aggregate structure distribution, may be needed.

Normality checks using the Shapiro-Wilk test confirmed that none of the binder variables followed normal distributions (González-Estrada et al., 2019). Most variables showed skewness or extended tails. For example, 1PAV ΔT_c and 2PAV ΔT_c exhibited mild to moderate negative skewness, with long left tails. Some variables, such as $\Delta|G^*|_{peak\,\tau 2}$, showed a p-value of 0.00087, suggesting a non-normal distribution likely due to skewness or multimodality. For variables with strong skewness, logarithmic or exponential transformations are commonly used to mitigate their impact on regression modeling. Hence, considering multi-linear or nonlinear regressions was essential.

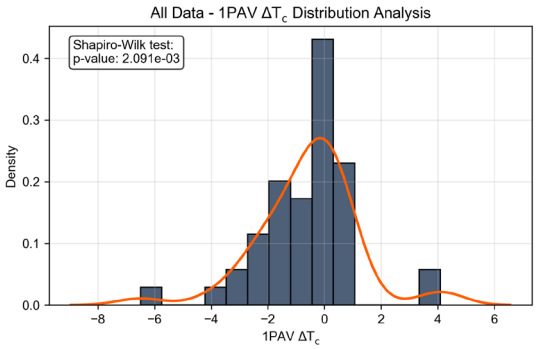

A. 1PAV ΔT_c

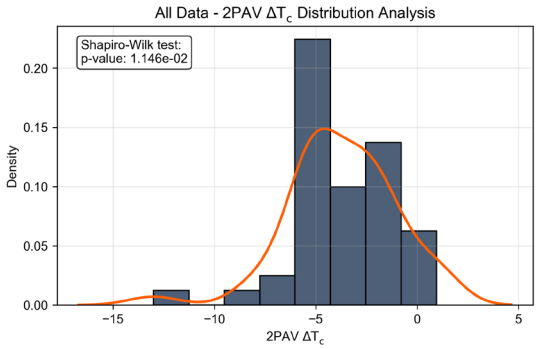

B. 2PAV ΔT_c

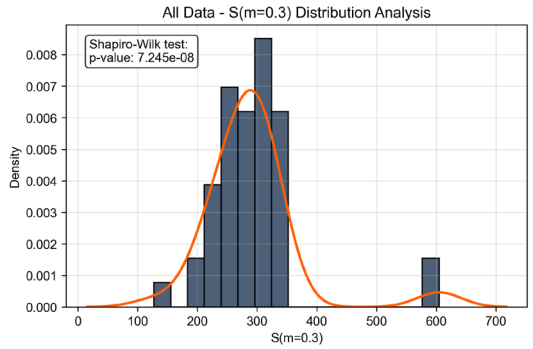

C. S(m=0.3)

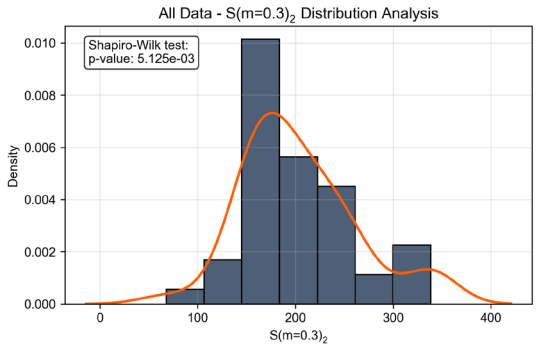

D. $S(m=0.3)_2$

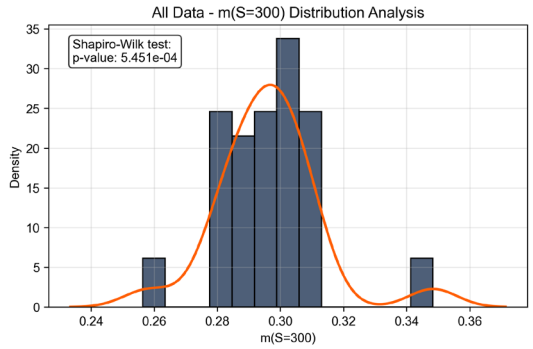

E. m(S=300)

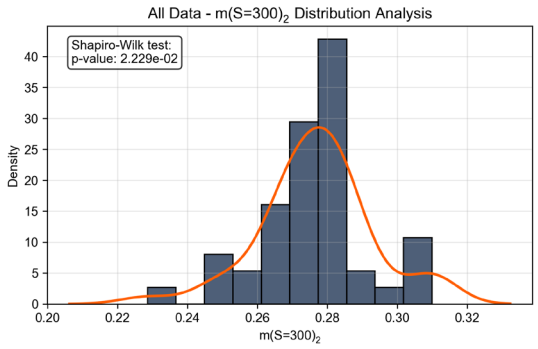

F. $m(S=300)_2$

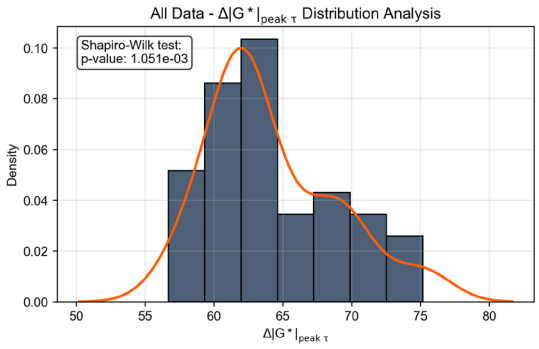

G. $\Delta|G^*|_{peak\ \tau}$

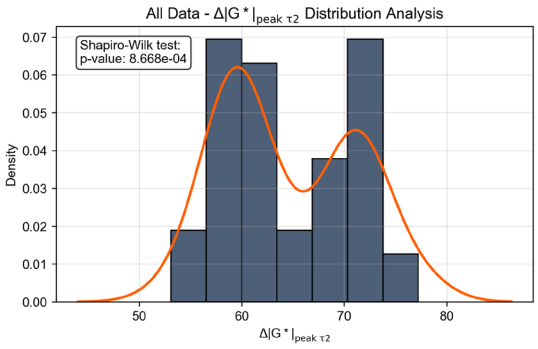

H. $\Delta|G^*|_{peak\ \tau\ 2}$

Figure 56. Graph. Shapiro-Wilk normality test results.

Initial Multi-Linear Statistical Analysis of I-FIT Parameters

To quantify the relationship between binder rheological properties and HMA I-FIT metrics, multi-linear regression was conducted using all samples. Regression models were first developed to predict G_f. For short-term aging (STA G_f), the key predictors selected based on statistical significance ($p < 0.05$) were $\Delta|G^*|_{peak\,\tau}$, ΔT_c, and S(m=0.3). For long-term aging (G_f LTA), significant predictors included $\Delta|G^*|_{peak\,\tau}$, S(m=0.3), and m(S=300). Data for 1PAV and 2PAV were used in STA and LTA, respectively.

The resulting models yielded $R^2 = 0.33$ for STA G_f and $R^2 = 0.68$ for LTA G_f. While the LTA model explains a substantial variability, the STA model shows a relatively weak fit. The F-statistic for the STA is 4.82, though statistically significant ($p < 0.001$), it suggests a marginal model fit and limited explanatory power. In contrast, the F-statistic for LTA (29.33) indicates a stronger model. Table 21 presents regression coefficients, p-values, and individual variable correlations.

Table 21. Multiple Linear Regression Results for STA G_f and LTA G_f

Metrics	STA G_f Model			LTA G_f Model		
Predictor	Coefficient	P-value	Correlation	Coefficient	P-value	Correlation
Const	−27510	0.02	–	3458.06	0.14	–
$\Delta\|G^*\|_{peak\,\tau}$ /$\Delta\|G^*\|_{peak\,\tau\,2}$	132.36	0.00	0.29	68.41	0.00	0.60
1PAV ΔT_c/ 2PAV ΔT_c	−1977.54	0.02	0.14	–	–	–
S(m=0.3)/ $S(m=0.3)_2$	73.86	0.01	0.14	12.77	0.00	0.46
m(S=300)/ $m(S=300)_2$	–	–	–	−27470	0.01	0.34
BC	–	–	–	–	–	–
ABR Content	–	–	–	–	–	–
R^2	0.33			0.68		
F-statistic	4.82			29.33		

All predictors were individually significant ($p < 0.05$), but $\Delta|G^*|_{peak\,\tau1}$ and $\Delta|G^*|_{peak\,\tau2}$ were the most, reinforcing their relevance to cracking potential. Regression was also applied to other I-FIT metrics, as presented in Table 22. Results varied by metric, aging condition, and gyration-related parameters. Predictions of slope yielded lower and less stable R^2 values across all cases, suggesting limitations of linear regression for the outputs, and were consistent with earlier findings, where slope exhibited relatively weak and less consistent correlations with binder parameters.

For FI models, BC, ABR content, and S-value consistently appeared as important predictors. However, when SBS modification was included, the models became less reliable, especially for FI, often yielding fewer than two significant predictors. In the full dataset, the STA FI model reached $R^2 = 0.548$ using binder content, ABR content, and S(m=0.3). For LTA FI, the best linear model included S(m=0.3), gyration, and RAP content ($R^2 = 0.758$).

Table 22. Multiple Linear Regression Results for FI and Slope

	SBS (Yes)		SBS (No)		All Samples	
Metrics	***R^2 (%)***	**Selected Predictors**	***R^2 (%)***	**Selected Predictors**	***R^2 (%)***	**Selected Predictors**
STA FI	0.52*	BC ABR content	0.613*	BC ABR content	**0.548**	BC ABR content S(m=0.3)
LTA FI	0.752*	BC ABR content	0.802*	ABR content $S(m=0.3)_2$	**0.758**	BC ABR content $\Delta\lvert G^*\rvert_{peak\,\tau\,2}$ $S(m=0.3)_2$
STA Slope	0.513*	BC ABR content	0.603*	BC ABR content	0.576*	BC ABR content
LTA Slope	0.810	BC ABR content $\Delta\lvert G^*\rvert_{peak\,\tau\,2}$ $m(S=300)_2$	0.651*	ABR content	0.655*	BC ABR content

* Unreliable prediction

Variable Screening and FI Model Development

Building on the initial regression analysis and the Shapiro-Wilk normality test results (Figure 56), a customized model selection framework was implemented to systematically explore combinations of input variables. Both linear and nonlinear regression were considered for predicting STA FI and LTA FI. Screening was performed on the variable (e.g., BC, ABR content, ΔT_c, S-value, and $\Delta\lvert G^*\rvert_{peak\,\tau}$) after transformation, including square, logarithmic, square root, exponential, and inverse forms. To ensure model robustness and interpretability, the following constraints were applied:

- Only one variable from each collinear group was allowed (e.g., S or S^2).
- Combinations were screened for multicollinearity using the variance inflation factor less than five (VIF < 5).
- All models were evaluated on both full dataset and using leave-one-out cross validation (LOOCV). LOOCV provides an estimate of model generalization to new, unseen data. It is particularly important for relatively small datasets. Only combinations meeting both performance thresholds, $R^2 > 0.70$ (full fitting) and $R^2 > 0.60$ (LOOCV), were retained.

In Illinois, basic binder rheology is available to contractors in the binder's certificate of analysis (COA). Hence, for practical reasons the developed model was tailored to binder parameters usually available to contractors. COAs typically provide the S- and m-values at one BBR temperature, while the $\Delta|G^*|_{peak\,\tau}$ is only available for softened binders. As shown in Table 23, two types of FI models were developed for both STA and LTA aging conditions:

- **Model A1**: Using directly measured binder values, including $\Delta|G^*|_{peak\,\tau}$, S, and m at one temperature.
- **Model A2**: Using interpolated binder parameters, such as ΔT_c, S(m = 0.3), and m(S = 300), derived from averaged or interpolated values across the dataset.

Table 23. Model Input Definitions for STA and LTA FI Prediction

Aging	Models	Values	*Parameters to select from*
STA FI (1PAV)	A1	Measured binder values	m, S, $\Delta\|G^*\|_{peak\,\tau}$, BC, ABR, Ngyr*
	A2	Interpolated values	ΔT_c, m (S=300), S (m=0.3), $\Delta\|G^*\|_{peak\,\tau}$, BC, ABR, Ngyr
LTA FI (2PAV)	A1	Measured binder values	m, S, $\Delta\|G^*\|_{peak\,\tau}$, BC, ABR, Ngyr
	A2	Interpolated values	ΔT_c, m (S=300), S (m=0.3), $\Delta\|G^*\|_{peak\,\tau}$, BC, ABR, Ngyr

* Number of Design Gyrations

Based on the automated screening framework, Table 24 summarizes the variable combinations that met the criteria for multi-linear regression modeling. While Model A2 incorporates interpolated binder rheological parameters, the standard deviations of input variables and residuals in Model A2 show signs of instability, which may increase the overall uncertainty of the model. From an engineering perspective, when R^2 values between A1 and A2 are similar, the use of A1 is recommended due to its reliance on directly measured parameters (e.g., S and m). This would enhance reliability and ease of implementation.

Table 24. Variable Combinations Selected for STA FI and LTA FI Prediction

Aging	Models	Variables	σ_{input}	$\sigma_{residual}$	*Intercept*	R^2	R^2 *LOOCV*
STA FI (1PAV)	A1	$\Delta\|G^*\|_{peak\,\tau}$, BC, Ngyr, ABR, log S, log m	**0.551**	**3.614**	**19.29**	**0.770**	**0.641**
		$\Delta\|G^*\|_{peak\,\tau}$, BC, √Ngyr, ABR, log S, log m	0.544	3.622	33.21	0.769	0.639
	A2	S(m=0.3), $\Delta\|G^*\|_{peak\,\tau}$, BC, Ngyr, ABR, $e^{\Delta Tc}$	1.311	3.103	−35.99	0.830	0.660
		m(S=300), $\Delta\|G^*\|_{peak\,\tau}$, BC, Ngyr, ABR	0.116	3.706	−4.94	0.758	0.655
LTA FI (2PAV)	A1	$\Delta\|G^*\|_{peak\,\tau}$, BC, Ngyr, S, log m, 1/ABR	**0.469**	**2.407**	**−14.65**	**0.835**	**0.763**
		S, $\Delta\|G^*\|_{peak\,\tau}$, BC, log m, 1/ABR	0.512	2.595	25.08	0.796	0.693
	A2	log m(S=300), BC, √ABR, $e^{\Delta Tc}$	0.008	2.986	−31.15	0.726	0.615
		$S(m=0.3)^2$, $\Delta\|G^*\|_{peak\,\tau}$, BC, 1/ABR	0.362	2.702	−71.37	0.776	0.702

FI Prediction Results

As presented in Table 24, applying transformations such as exponential, logarithmic, or inverse significantly improves FI prediction performance. To ensure model generalizability, avoid multicollinearity, and maintain interpretability, only variable combinations meeting screening criteria (e.g., VIF < 5 and acceptable model performance) were retained. Figure 57 and Figure 58 present the multi-linear regression equations for STA FI and LTA FI, respectively. For the STA FI equations, all rheological parameters are based on 1PAV data, whereas for the LTA FI equations, all rheological parameters are based on 2PAV cycle data.

Table 25 and Figure 59 present the predictive performance of the selected STA FI and LTA FI models. Even after cross-validation, the R^2 remains above 0.7. The LOOCV-based mean average error (MAE) is 3.368 for STA FI and 2.355 for LTA FI, respectively, which are close to full-sample errors. The models demonstrated relatively strong robustness.

$$FI\ (STA) = 19.29 + 0.2 \times \Delta|G^*|_{\text{peak }\tau} + 7.25 \times BC - 0.235 \times Ngyr - 0.67 \times \text{A}BR + 2.736 \times \log S + 39.32 \times \log m$$

Figure 57. Equation. Regression equation for STA FI.

$$FI\ (LTA) = -14.65 + 0.343 \times \Delta|G^*|_{\text{peak }\tau} + 6.23 \times BC - 0.07 \times \text{N}gyr + 10.42 \times (1/ABR) + 0.016 \times S + 30.5 \times \log m$$

Figure 58. Equation. Regression equation for LTA FI.

Table 25. Performance Metrics of STA and LTA FI Models (Full Sample vs. LOOCV)

Metrics	R^2	*MAE*	R^2 *LOOCV*	*MAE LOOCV*
STA FI	0.770	2.645	0.641	3.368
LTA FI	0.835	1.967	0.763	2.355

$\Delta|G^*|_{\text{peak }\tau}$ is required for softener-modified binders but not necessary for unsoftened binders. Although including this parameter typically improves model performance, additional models excluding $\Delta|G^*|_{\text{peak }\tau}$ were developed for unsoftened binders. These alternative models still achieved acceptable performance, with STA FI yielding $R^2 = 0.759$ and R^2 LOOCV = 0.636, and LTA FI yielding $R^2 = 0.770$ and R^2 LOOCV = 0.687.

$$FI\ (STA) = -9.65 + 77.02 \times m + 4.52 \times BC - 0.254 \times Ngyr - 0.678 \times \text{A}BR + 0.89 \times \log S$$

Figure 59. Equation. Regression equation for STA FI without $\Delta|G^*|_{\text{peak }\tau}$.

$$FI\ (LTA) = -23.5 + 0.013 \times S + 0.95 \times BC - 0.11 \times Ngyr - 0.54 \times ABR + 73.25 \times \sqrt{m}$$

Figure 60. Equation. Regression equation for LTA FI without $\Delta|G^*|_{\text{peak }\tau}$.

Figure 61 presents the prediction results and residual plots for both STA FI and LTA FI models. Overall, both models demonstrate good fit using the dataset. FI is affected by $\Delta|G^*|_{peak\,\tau}$, BC, and ABR content with corresponding aging. In addition, while S-value and m-value both affect STA FI and LTA FI, STA FI is expected to be used for binder screening, and LTA may be used for further validation.

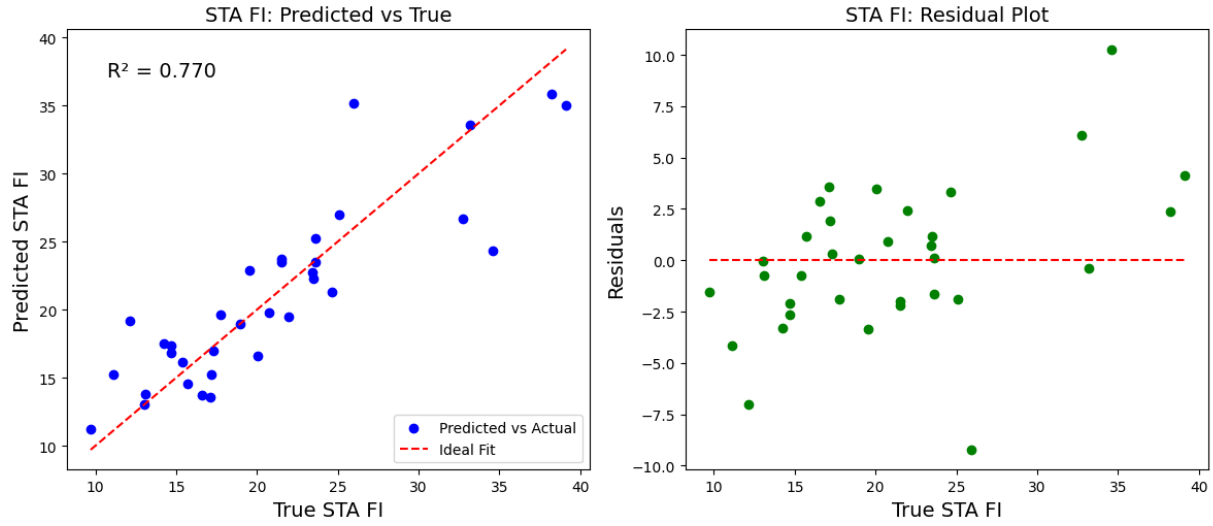

A. STA FI Predicted Results

B. STA FI Residual Plots

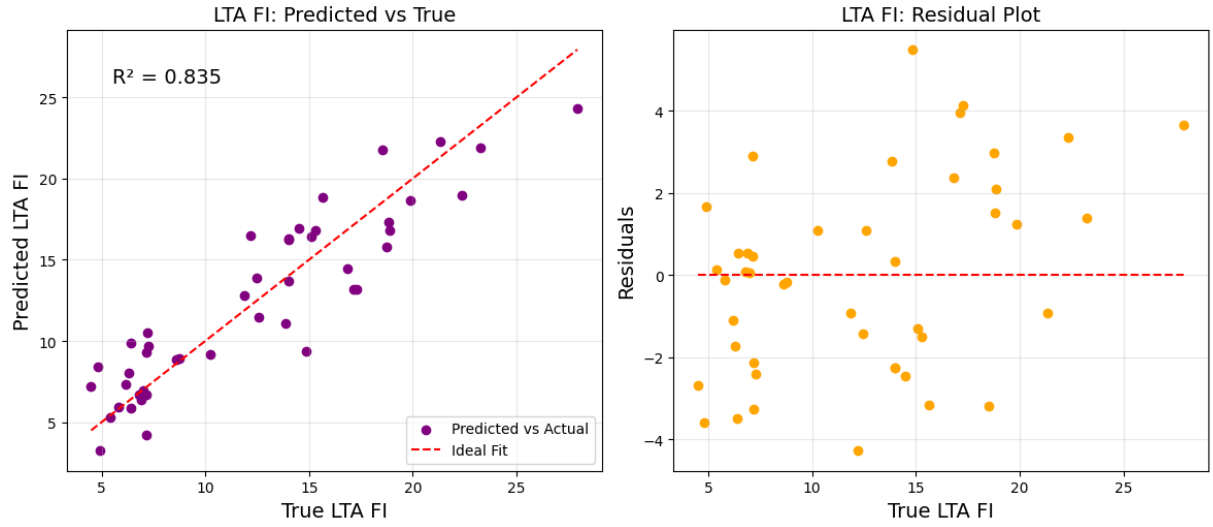

C. LTA FI Predicted Results

D. LTA FI Residual Plots

Figure 61. Graph. Prediction results vs. residual plots.

To assess the assumptions underlying the regression models, residual analyses were conducted separately for STA FI and LTA FI. As shown in Figure 62, the residual distributions for both models were evaluated using the Shapiro-Wilk test. The p-values for STA and LTA FI residuals were 0.3706 and 0.6517, respectively; both exceeding the 0.05 threshold. Hence, null hypothesis of normality cannot be rejected. This suggests that residuals approximately follow a normal distribution,

supporting the use of the residual variance in confidence interval estimation and probability-based risk evaluation.

All selected models satisfied the multicollinearity constraint (VIF < 5), confirming that input variables are not highly correlated. Each independent variable contributes its own level of uncertainty (e.g., variability in $\Delta|G^*|$, S-value, and ΔT_c), which can be propagated to the dependent variable (FI). This may be used to estimate uncertainty bounds and quantify associated risks.

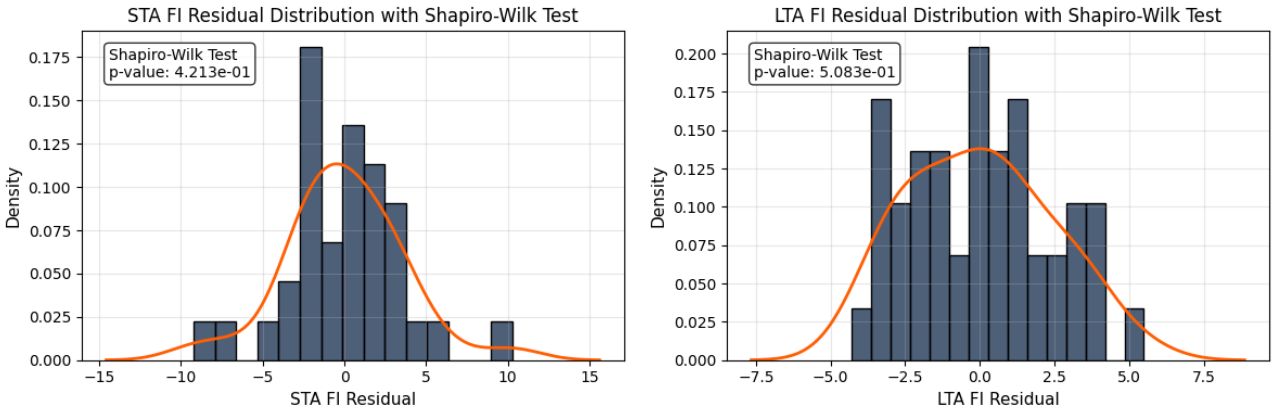

A. STA FI Residual Distribution B. LTA FI Residual Distribution

Figure 62. Graph. FI residual distribution with Shapiro-Wilk test.

FI Prediction Uncertainty and Risk Estimation

To improve the FI prediction reliability of HMA cracking potential, a quantitative uncertainty estimation and risk-based decision framework was developed. This framework details the method used to compute confidence intervals for predicted FI and the associated estimation and interpretation of potential cracking risk (i.e., FI < 8).

Step 1—FI Prediction Using Regression Models: Predicted values of FI (STA and LTA) are obtained by inputting relevant binder rheological and mix design parameters (e.g., S-value, $\Delta|G^*|_{peak\ \tau}$, ABR content, Ngyr) into the established multiple linear regression equations (Figure 56–Figure 60).

Step 2—Error Propagation and Total Prediction Uncertainty: To account for the full scope of uncertainty in FI prediction, both model residual variance and variability in input parameters are considered. The total prediction uncertainty (σy) is estimated using first-order Taylor expansion for error propagation, as follows in Figure 63:

$$\sigma_y = \sqrt{\sum_{i=1}^{p}\left(\beta_i^2 \cdot \sigma_{x_i}^2\right) + \sigma_{residual}^2}$$

Figure 63. Equation. Total prediction uncertainty.

where β_i are regression coefficients, σ_{xi} are standard deviations of input variables, and $\sigma^2_{residual}$ is variance of the regression residuals. In this study, the total uncertainty in predicting STA and LTA FI with $\Delta|G^*|_{peak\,\tau}$ is 3.656 and 2.451, respectively. On the other hand, the total uncertainty without $\Delta|G^*|_{peak\,\tau}$ is 3.700 for STA and 2.842 for LTA.

Step 3—One-Tailed Risk Estimation Below Threshold: Assuming prediction errors follow a normal distribution (as supported by residual analysis), the probability that the actual FI value falls below a critical threshold (e.g., FI < 5 for LTA) is calculated as follows in Figure 64:

$$P(FI < T) = \Phi(\frac{T - \hat{y}}{\sigma_y})$$

Figure 64. Equation. FI risk evaluation.

where y^ is predicted FI, σ_y is total standard deviation including input and residual error, ϕ is cumulative distribution function (CDF) of the standard normal distribution, and *T* is failure threshold (e.g., 5.0 for LTA, 8.0 for STA).

Step 4—Risk-Based Decision Framework: Table 26 and Figure 65 present the proposed three-tiered decision rule based on the calculated risk level.

Table 26. Risk-Based Decision Framework for FI Prediction

Risk	STA FI Value		LTA FI Value		Interpretation
	With $\Delta\|G^*\|_{peak\,\tau}$	Without $\Delta\|G^*\|_{peak\,\tau}$	With $\Delta\|G^*\|_{peak\,\tau}$	Without $\Delta\|G^*\|_{peak\,\tau}$	
> 50%	< 8.0	< 8.0	< 5.0	< 5.0	High Probability of FI < Threshold
10%–50%	8.0–12.7	8.0–12.7	5.0–8.1	5.0–8.6	Medium Probability of FI < Threshold
< 10%	> 12.7	> 12.7	> 8.1	> 8.6	Low Probability of FI < Threshold

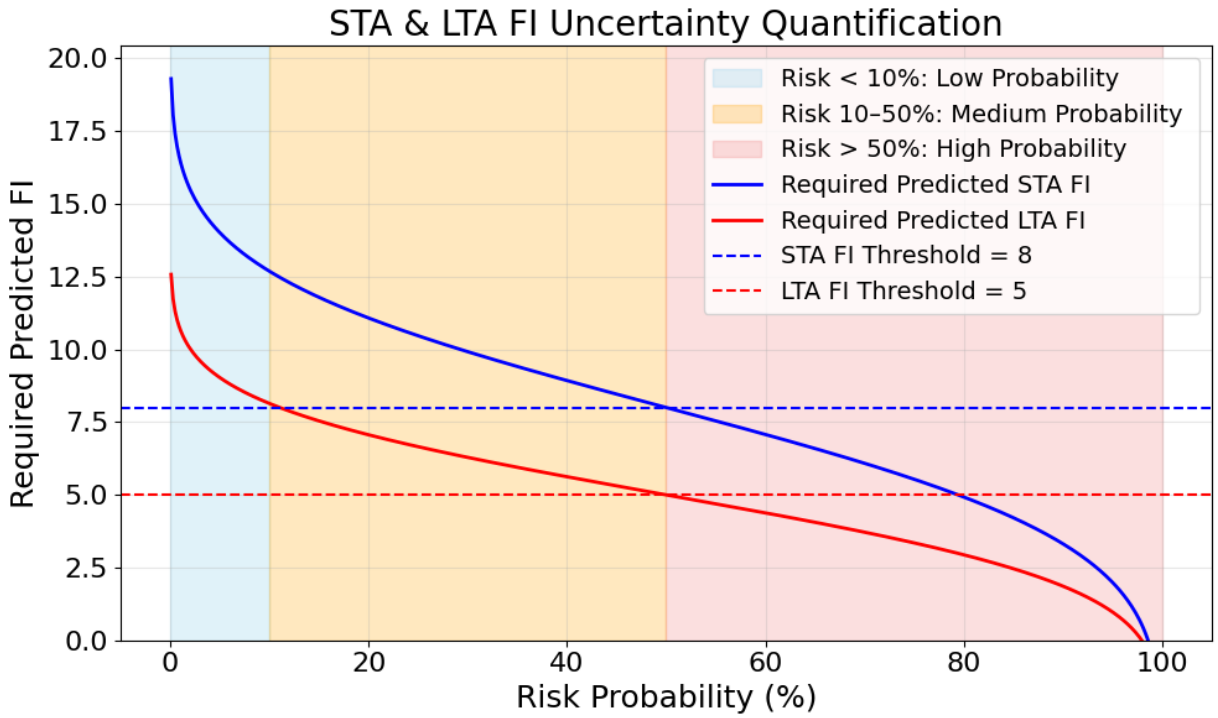

A. With $\Delta|G^*|_{peak\,\tau}$

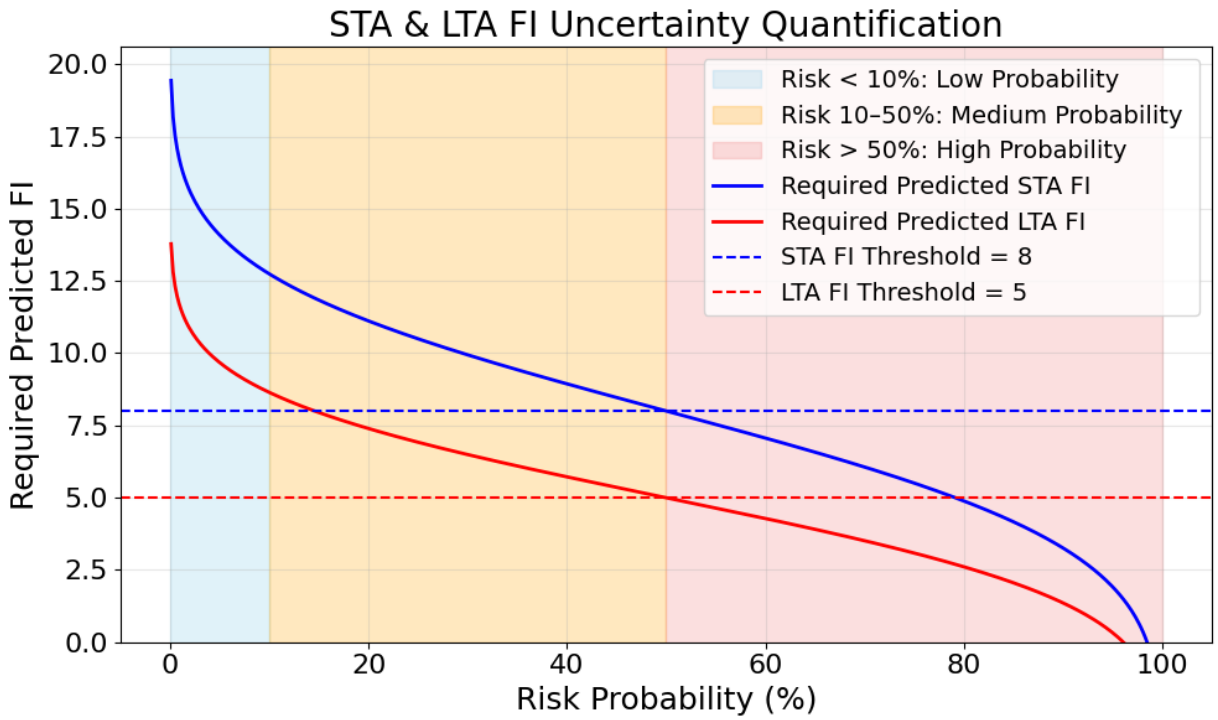

B. Without $\Delta|G^*|_{peak\,\tau}$

Figure 65. Graph. STA/LTA FI uncertainty quantification.

SUMMARY

Fracture energy (G_f), post-peak slope, and flexibility index (FI) were evaluated to understand the cracking potential of HMA with varied binder rheological parameters. The binders included SBS-modified and unmodified binders, with a wide range of softness and two levels of aging. Binder rheological parameters—such as ΔT_c, S-value, m-value, and $\Delta|G^*|_{peak\,\tau}$—were assessed for their ability to predict HMA cracking potential. Linear correlation analysis revealed that G_f is strongly associated with binder parameters compared to post-peak slope or FI. Among all tested variables, $\Delta|G^*|_{peak\,\tau}$ demonstrated the strongest and most consistent relationship with G_f under both aging conditions. For STA FI prediction, a multi-linear regression model that included ABR content, $\Delta|G^*|_{peak\,\tau}$, BC, Ngyr, S-value, and m-value, achieved high explanatory power ($R^2 = 0.770$). The LTA FI model used the same set of parameters but applied different nonlinear transformations, achieving an $R^2 = 0.835$. Leave-one-out cross-validation (LOOCV) confirmed reasonable generalization performance ($R^2 > 0.64$, MAE = 2.4–3.4), supporting the robustness of the model. Additionally, models excluding $\Delta|G^*|_{peak\,\tau}$ still achieved reasonable predictive accuracy, demonstrating flexibility for use in cases where this parameter is unavailable. Residual analyses confirmed normality assumptions, enabling estimation of prediction uncertainty using first-order error propagation. A risk-based framework was proposed to compute the probability of FI falling below a critical threshold (e.g., FI < 8 for STA). Overall, this study demonstrates that binder rheological parameters, including $\Delta|G^*|_{peak\,\tau}$, S-value, and m-value could reliably predict HMA cracking potential and inform performance-based specification.

Suggested Performance Testing Recommendations

- ΔT_c: This cracking index is sensitive to softening and polymer modification. While it rewards softening, it penalizes polymer modification as ΔT_c is usually decreased with polymer modification. Hence, the polymer-softener modification maintains the ΔT_c value close to that of the base binder. Given the importance of the base binder in controlling cracking potential of modified binder, the −5°C threshold for PAV-aged binders should be used for polymer-softener modified binders (as well as base binder if needed).
- $\Delta|G^*|_{peak\tau}$: The current threshold is 54% for softened binders. Polymer modification increases $\Delta|G^*|_{peak\tau}$ values, so 60% should be used for polymer-softener-modified binders.
- MSCR: Softeners have a marginal effect on important parameters ($R_{3.2}$, $J_{nr\,3.2}$, $J_{nr\,diff}$, and R_{diff}). Polymers, on the other hand, have a relatively major effect, so they control the blend. Given that AASHTO M 332 accounts for polymer modification, it is recommended to keep thresholds as-is for now. However, at the same high PG, polymer-softener-modified binders have better performance than polymer-modified binders. Therefore, there is a need to investigate the effect of SBS dosage and low-temperature PG on MSCR parameters, before final recommendations are suggested.
- FTIR: Although softeners may slow down polymer degradation, there is no strong evidence of that to make a recommendation. This could be because of the tests' variability and/or selected softeners used in this study were already screened as good softeners in an earlier study (Singhvi et al., 2021).

CHAPTER 7: CONCLUSIONS AND RECOMMENDATIONS

SUMMARY

This study explores the ability to use rheological binder parameters to predict the cracking potential of hot-mix asphalt (HMA), including those incorporating polymer and softener modifications. The research evaluated the rheological and thermal characteristics of modified binders and the corresponding HMA cracking potential. Two base binders were selected, classified as "good" and "borderline," and were modified with a range of softeners and styrene-butadiene-styrene (SBS) polymers, either independently or in combination. The binder blends underwent short- and long-term aging (STA and LTA) simulations using a rolling thin-film oven (RTFO) and two levels in a pressure aging vessel (PAV), respectively. Extended aging (2PAV) was utilized to better replicate field conditions.

Rheological parameters such as ΔT_c (an indicator of low-temperature cracking risk), S-value (creep stiffness at 60 s), m-value (rate of stress relaxation at 60 s), and $\Delta|G^*|_{peak\,\tau}$ (a measure of fatigue tolerance and stiffness degradation) were evaluated and correlated to HMA cracking potential for both aging conditions. The MSCR test was conducted to evaluate the stress-dependent rutting potential of binder blends, and FTIR was used to assess oxidative aging and polymer degradation.

To assess HMA performance, laboratory-produced specimens were tested using the Illinois Flexibility Index Test (I-FIT) for cracking potential and the Hamburg Wheel-Tracking Test (HWTT) for rutting potential.

Statistical analyses, primarily based on multi-linear regression, were used to develop predictive models linking binder rheological properties to HMA cracking potential. Among all binder rheological parameters, $\Delta|G^*|_{peak\,\tau}$ emerged as the most effective predictor of G_f across both aging conditions, while other variables like ABR content and gyration level contributed significantly to FI prediction accuracy.

CONCLUSIONS

- Base binder quality is critical. The inherent quality of base binder significantly influenced HMA performance with and without RAP. The use of rejuvenators and soft binders helped offset the negative effects of RAP.

- SBS and softeners exhibited synergistic effects on binder. While SBS improved elasticity and reduced rutting potential, softeners enhanced flexibility and reduced low-temperature cracking potential.

    - As evident by $\Delta|G^*|_{peak\,\tau}$ results, polymer modification leads to a higher improvement (~10.5%) in fatigue tolerance compared to softening (~1.5%).

- The polymer-softening modification sequence (choice of modifying a softened binder with polymer or softening a polymer-modified binder post-polymerization) affects the rheological performance of the binder blend.

- Polymer-softener modification led to a greater increase in performance than a simple summation of each modifier for fatigue tolerance, $\Delta|G^*|_{peak\,\tau}$, and cracking potential, FI. However, base binder characteristics remain the main influential.

- Polymer modification reduces ΔT_c values, and polymer-softener modification maintains ΔT_c of base binders. Hence, the −5°C threshold for PAV-aged binders should be maintained.

- Polymer modification increased $\Delta|G^*|_{peak\tau}$ values, so 60% should be maintained for polymer-softener-modified binders.

- The dual modification process appears to improve the R and J_{nr} parameters of the MSCR test.

- Data showed the possibility of softeners slowing the SBS degradation in the polymer-softener-modified binder blend.

- The integration of binder rheological properties offers a promising framework for predicting HMA cracking potential, ultimately aiding in the development of more durable and sustainable asphalt pavements. Leave-one-out cross-validation (LOOCV) confirmed reasonable generalization performance, supporting the robustness of the model.

    - For STA FI prediction, a multi-linear regression model that included ABR content, $\Delta|G^*|_{peak\tau}$, BC, S-value, and m-value achieved high explanatory power ($R^2 = 0.770$).

    - For LTA FI prediction, the same set of variables was used with different nonlinear transformations, resulting in an improved model fit ($R^2 = 0.835$).

    - For practical implementation, models excluding $\Delta|G^*|_{peak\,\tau}$ were developed. The models achieved reasonable predictive accuracy, with STA FI yielding $R^2 = 0.759$ and LTA FI yielding $R^2 = 0.770$, demonstrating flexibility for selecting binders when $\Delta|G^*|_{peak\,\tau}$ is unavailable.

- Residual analyses confirmed normality assumptions, enabling estimation of prediction uncertainty using first-order error propagation. A risk-based framework was proposed to compute the probability of FI falling below a critical threshold (e.g., FI < 8 for STA).

RECOMMENDATIONS

- Future work by asphalt binder manufacturers may focus on optimizing formulations by balancing SBS polymer and softener type and content to achieve optimum compatibility and

binder performance. This should be followed by considering additional mixes to verify mixture performance.

- Production techniques should minimize thermal degradation effects when using softeners. Research should explore alternative curing temperatures and times to maintain softener functionality during the modification process. High-volatility softeners, such as softener N, may be avoided when prolonged high-temperature exposure is considered. Alternatively, softening of post-polymer addition should be investigated to incorporate thermally sensitive modifiers without compromising binder integrity.

- Rheological parameters, such as $\Delta|G^*|_{peak\,\tau}$ and ΔT_c (or its surrogate, S(at m=0.3), m(S=300)), may be considered for integration into standard evaluation practices. The latter metric offers robust and predictive measure of thermal cracking potential, enabling consistent selection of modified binders. Statistical analyses, utilizing field performance data, may be considered for threshold validation.

- Field trials should be conducted to validate laboratory findings and predictive models to confirm their practical performance benefits.

- Future work should assess the economic and environmental impacts of dual-modified binders. The work should focus on their potential to reduce life cycle cost and emissions while enhancing pavement service life.

REFERENCES

AASHTO. (2013). *Standard method of test for effect of heat and air on a moving film of asphalt binder (rolling thin-film oven test)*. American Association of State Highway and Transportation Officials, AASHTO T240. Washington, DC.

AASHTO. (2014a). *Standard method of test for Hamburg wheel-track testing of compacted hot-mix asphalt (HMA)*. American Association of State Highway and Transportation Officials, AASHTO T324. Washington, DC.

AASHTO. (2019). *Standard test method for determining the flexural creep stiffness of asphalt binder using the bending beam rheometer (BBR)*. American Association of State Highway and Transportation Officials, AASHTO T313. Washington, DC.

AASHTO. (2022a). *Standard method of test for elastic recovery test of asphalt materials by means of a ductilometer.* American Association of State Highway and Transportation Officials, AASHTO T 301. Washington, DC.

AASHTO. (2022b). *Determining the fracture potential of asphalt mixtures using the Illinois flexibility index test (I-FIT)*. American Association of State Highway and Transportation Officials, AASHTO T 393. Washington, DC.

AASHTO. (2023). *Standard specification for performance-graded asphalt binder*. American Association of State Highway and Transportation Officials, AASHTO M320. Washington, DC.

AASHTO. (2024). *Standard method of test for estimating fatigue resistance of asphalt binders using the linear amplitude sweep*. American Association of State Highway and Transportation Officials, AASHTO T391. Washington, DC.

AASHTO. (2025). *Standard method of test for multiple stress creep recovery (MSCR) test of asphalt binder using a dynamic shear rheometer (DSR)*. American Association of State Highway and Transportation Officials, AASHTO T 350. Washington, DC.

Abdelrahman, M., Katti, D. R., Ghavibazoo, A., Upadhyay, H. B., & Katti, K. S. (2014). Engineering physical properties of asphalt binders through nanoclay–asphalt interactions. *Journal of Materials in Civil Engineering*, *26*(12), 04014099. https://doi.org/10.1061/(ASCE)MT.1943-5533.0001017

Aguirre, M. A., Hassan, M. M., Shirzad, S., Daly, W. H., & Mohammad, L. N. (2016). Micro-encapsulation of asphalt rejuvenators using melamine-formaldehyde. *Construction and Building Materials*, *114*, 29–39. https://doi.org/10.1016/j.conbuildmat.2016.03.157

Al-Abdul Wahhab, H. I, M. A. Dalhat, & M. A. Habib (2017). Storage stability and high-temperature performance of asphalt binder modified with recycled plastic. *Road Materials and Pavement Design*, *18*(5), 1117–1134. https://doi.org/10.1080/14680629.2016.1207554

Al-Hdabi, A. (2016). Laboratory investigation on the properties of asphalt concrete mixture with rice husk ash as filler. *Construction and Building Materials*, *126*, 544–551. https://doi.org/10.1016/j.conbuildmat.2016.09.070

Allen, R. G., Little, D. N., Bhasin, A., & Glover, C. J. (2014). The effects of chemical composition on asphalt microstructure and their association to pavement performance. *International Journal of*

Pavement Engineering, *15*(1), 9–22. https://doi.org/10.1080/10298436.2013.836192

Al-Qadi, I. L., Elseifi, M., & Carpenter, S. H. (2007). *Reclaimed asphalt pavement—A literature review* (Report No. FHWA-ICT-07-001). Illinois Center for Transportation.

Al-Qadi, I. L., Ozer, H., Lambros, J., El Khatib, A., Singhvi, P., Khan, T., Rivera-Perez, J., & Doll, B. (2015). *Testing protocols to ensure performance of high asphalt binder replacement mixes using RAP and RAS* (Report No. FHWA-ICT-15-017). https://www.ideals.illinois.edu/handle/2142/88680

Al-Qadi, I. L., Ozer, H., Zhu, Z., Singhvi, P., Ali, U. M., Sawalha, M., Luque, A. F. E., Mainieri, J. J. G., & Zehr, T. G. (2019). *Development of long-term aging protocol for implementation of the Illinois flexibility index test (I-FIT)* (Report No. FHWA-ICT-19-009). https://doi.org/10.36501/0197-9191/19-012

Anderson, D. A., Chris, D. W., Bahia, H. U., Dongre, R., Sharma, M. G., & Antle, C. E. (1994). *Binder characterization and evaluation volume 3: Physical characterization*.

Anderson, D. A., Le Hir, Y. M., Marasteanu, M. O., Planche, J.-P., Martin, D., & Gauthier, G. (2001). Evaluation of fatigue criteria for asphalt binders. *Transportation Research Record*, *1766*(1), 48–56. https://doi.org/10.3141/1766-07

Anderson, R. M., King, G. N., Hanson, D. I., & Blankenship, P. B. (2011). Evaluation of the relationship between asphalt binder properties and non-load related cracking. *Journal of the Association of Asphalt Paving Technologists*, 80, 615–664.

Araujo, M. de F. A. de S., Lins, V. de F. C., Pasa, V. M. D., & Fonseca, C. G. (2012). Infrared spectroscopy study of photodegradation of polymer modified asphalt binder. *Journal of Applied Polymer Science*, *125*(4), 3275–3281. https://doi.org/10.1002/app.36520

Asphalt Institute (AI). (2019). Use of the Delta Tc Parameter to Characterize Asphalt Binder Behavior IS-240. Asphalt Institute. Retrieved June 24, 2020, http://www.asphaltinstitute.org/engineering /delta-tc-technical-document/

ASTM. (2020). *Standard Practice for determining the separation tendency of polymer from polymer modified asphalt*. ASTM International.

Bahia, H. U., Hanson, D. I., Zeng, M., Zhai, H., Khatri, M. A., & Anderson, R. M. (2001). *Characterization of modified asphalt binders in Superpave mix design* (NCHRP Report 459). Article Project 9-10 FY ’96. https://trid.trb.org/view/692511

Bahia, H. U., Perdomo, D., & Turner, P. (1997). Applicability of Superpave binder testing protocols to modified binders. *Transportation Research Record*, *1586*(1), 16–23. https://doi.org/10.3141/1586-03

Bahia, H. U., & Anderson, D. A. (1995). The Pressure Aging Vessel (PAV): A Test to Simulate Rheological Changes Due to Field Aging. ASTM Special Technical Publication 1241, Hardin, J.C., ed. American Society for Testing and Materials.

Barry, M. K. (2016). An analysis of impact factors on the Illinois flexibility index test. Master’s thesis, University of Illinois Urbana-Champaign. https://hdl.handle.net/2142/95565

Batioja-Alvarez, D., Lee, J., & Haddock, J. E. (2019). Understanding the Illinois flexibility index test (I-

FIT) using Indiana asphalt mixtures. *Transportation Research Record*, *2673*(6), 337–346. https://doi.org/10.1177/0361198119841282

Baumgardner, G. (2021). *Delta Tc Binder Specification Parameter* [tech brief] (FHWA-HIF-21-042). https://rosap.ntl.bts.gov/view/dot/58313

Behnood, A. (2019). Application of rejuvenators to improve the rheological and mechanical properties of asphalt binders and mixtures: A review. *Journal of Cleaner Production*, *231*, 171–182. https://doi.org/10.1016/j.jclepro.2019.05.209

Behnood, A., & Modiri Gharehveran, M. (2019). Morphology, rheology, and physical properties of polymer-modified asphalt binders. *European Polymer Journal*, *112*, 766–791. https://doi.org/10.1016/j.eurpolymj.2018.10.049

Bennert, T., Shamborovskyy, D., & Maher, A. (2014). Evaluation of bio-oil rejuvenators in hot mix asphalt. *Construction and Building Materials*, *54*, 220–226.

Blankenship, P., Anderson, R. M., King, G. N., & Hanson, D. I. (2010). Airfield asphalt pavement technology program (AAPTP). 163.

Bonicelli, A., Calvi, P., Martinez-Arguelles, G., Fuentes, L., & Giustozzi, F. (2017). Experimental study on the use of rejuvenators and plastomeric polymers for improving durability of high RAP content asphalt mixtures. *Construction and Building Materials*, *155*, 37–44. https://doi.org/10.1016/j.conbuildmat.2017.08.013

Bonnetti, K. S., Nam, K., & Bahia, H. U. (2002). Measuring and defining fatigue behavior of asphalt binders. *Transportation Research Record*, *1810*(1), 33–43. https://doi.org/10.3141/1810-05

Bowers, B. F., Huang, B., Shu, X., & Miller, B. C. (2014). Investigation of reclaimed asphalt pavement blending efficiency through GPC and FTIR. *Construction and Building Materials*, *50*, 517–523. https://doi.org/10.1016/j.conbuildmat.2013.10.003

Brasileiro, L., Moreno-Navarro, F., Tauste-Martínez, R., Matos, J., & Rubio-Gámez, M. del C. (2019). Reclaimed polymers as asphalt binder modifiers for more sustainable roads: A review. *Sustainability*, *11*(3), Article 3. https://doi.org/10.3390/su11030646

Brûlé, B. (1996). Polymer-modified asphalt cements used in the road construction industry: Basic principles. *Transportation Research Record*, *1535*(1), 48–53. https://doi.org/10.1177/0361198196153500107

Cao, W., & Wang, C. (2018). A new comprehensive analysis framework for fatigue characterization of asphalt binder using the linear amplitude sweep test. *Construction and Building Materials*, *171*, 1–12. https://doi.org/10.1016/j.conbuildmat.2018.03.125

Cavalli, M. C., Zaumanis, M., Mazza, E., Partl, M. N., & Poulikakos, L. D. (2018). Aging effect on rheology and cracking behaviour of reclaimed binder with bio-based rejuvenators. *Journal of Cleaner Production*, 189, 88–97.

Chen, J. S., Liao, M. C, & Tsai, H. H. (2002). Evaluation of optimization of the engineering properties of polymer-modified asphalt. *Practical Failure Analysis*, 2(3), 75–83.

Chen, J.-S., & Tsai, C.-J. (1999). How good are linear viscoelastic properties of asphalt binder to

predict rutting and fatigue cracking? *Journal of Materials Engineering and Performance*, *8*(4), 443–449. https://doi.org/10.1361/105994999770346747

Chen, M., Geng, J., Xia, C., He, L., & Liu, Z. (2021). A review of phase structure of SBS modified asphalt: Affecting factors, analytical methods, phase models and improvements. *Construction and Building Materials*, *294*, 123610. https://doi.org/10.1016/j.conbuildmat.2021.123610

Chen, M., Leng, B., Wu, S., & Sang, Y. (2014a). Physical, chemical and rheological properties of waste edible vegetable oil rejuvenated asphalt binders. *Construction and Building Materials*, *66*, 286–298. https://doi.org/10.1016/j.conbuildmat.2014.05.033

Chen, M., Xiao, F., Putman, B., Leng, B., & Wu, S. (2014b). High temperature properties of rejuvenating recovered binder with rejuvenator, waste cooking and cotton seed oils. *Construction and Building Materials*, *59*, 10–16. https://doi.org/10.1016/j.conbuildmat.2014.02.032

Christensen, D., Mensching, D., Rowe, G., Anderson, R. M., Hanz, A., Reinke, G., & Anderson, D. (2019). Past, present, and future of asphalt binder rheological parameters: Synopsis of 2017 Technical Session 307 at the 96th Annual Meeting of the Transportation Research Board. Transportation Research Circular, E-C241. https://trid.trb.org/view/1601364

D'Angelo, J. A. (2009). The relationship of the MSCR test to rutting. *Road Materials and Pavement Design*, 10(sup1), 61–80. https://doi.org/10.1080/14680629.2009.9690236

D'Angelo, J., & Dongré, R. (2009). Practical use of multiple stress creep and recovery test: Characterization of Styrene–Butadiene–Styrene dispersion and other additives in polymer-modified asphalt binders. *Transportation Research Record*, *2126*(1), 73–82. https://doi.org/10.3141/2126-09

Domingos, M. D. I., & Faxina, A. L. (2016). Susceptibility of asphalt binders to rutting: Literature review. *Journal of Materials in Civil Engineering*, *28*(2), 04015134. https://doi.org/10.1061/(ASCE)MT.1943-5533.0001364

DuBois, E., Mehta, Y., & Nolan, A. (2014). Correlation between multiple stress creep recovery (MSCR) results and polymer modification of binder. *Construction and Building Materials*, *65*, 184–190.

Elwardany, M. D., Rad, F. Y., Castorena, C. A. S. S. I. E., & Kim, Y. R. (2018). Climate-, depth-, and time-based laboratory aging procedure for asphalt mixtures. *Journal of the Association of Asphalt Paving Technologists*, *87*, 467–511.

Espinoza-Luque, A. F., Al-Qadi, I. L., & Ozer, H. (2018). Optimizing rejuvenator content in asphalt concrete to enhance its durability. *Construction and Building Materials*, *179*, 642–648. https://doi.org/10.1016/j.conbuildmat.2018.05.256

Fatmehsari, H. H., Nsengiyumva, G. M., Kim, Y-R, Kommidi, S. R., & Amelian, S. (2019). *Research on High-RAP Asphalt Mixtures with Rejuvenators - Phase II* (NDOT Research Report SPR-(18) M070).

García Mainieri, J. J., Singhvi, P., Ozer, H., Sharma, B. K., & Al-Qadi, I. L. (2021). Fatigue tolerance of aged asphalt binders modified with softeners. *Transportation Research Record*, *2675*(11), 1229–1244. https://doi.org/10.1177/03611981211025510

García-Travé, G., Tauste, R., Moreno-Navarro, F., Sol-Sánchez, M., & Rubio-Gámez, M. C. (2016). Use

of reclaimed geomembranes for modification of mechanical performance of bituminous binders. *Journal of Materials in Civil Engineering*, *28*(7), 04016021. https://doi.org/10.1061/(ASCE)MT.1943-5533.0001507

Glover, C. J., Davison, R. R., Domke, C. H., Ruan, Y., Juristyarini, P., Knorr, D. B., & Jung, S. H. (2005). *Development of a new method for assessing asphalt binder durability with field validation* (Report No. FHWA/TX-05/1872-2). Texas Transportation Institute. https://trid.trb.org/view/761981

González-Estrada, E., & Cosmes, W. (2019). Shapiro–Wilk test for skew normal distributions based on data transformations. *Journal of Statistical Computation and Simulation*, *89*(17), 3258–3272. https://doi.org/10.1080/00949655.2019.1658763

Guo, M., Bhasin, A., & Tan, Y. (2017). Effect of mineral fillers adsorption on rheological and chemical properties of asphalt binder. *Construction and Building Materials*, *141*, 152–159. https://doi.org/10.1016/j.conbuildmat.2017.02.051

Habbouche, J., Hajj, E. Y., Sebaaly, P. E., & Piratheepan, M. (2020). A critical review of high polymer-modified asphalt binders and mixtures. *International Journal of Pavement Engineering*, *21*(6), 686–702. https://doi.org/10.1080/10298436.2018.1503273

Hajj, R., & Bhasin, A. (2018). The search for a measure of fatigue cracking in asphalt binders – a review of different approaches. *International Journal of Pavement Engineering*, *19*(3), 205–219. https://doi.org/10.1080/10298436.2017.1279490

Han, M., Li, J., Muhammad, Y., Hou, D., Zhang, F., Yin, Y., & Duan, S. (2018). Effect of polystyrene grafted graphene nanoplatelets on the physical and chemical properties of asphalt binder. *Construction and Building Materials*, *174*, 108–119. https://doi.org/10.1016/j.conbuildmat.2018.04.082

Harman, T., Youtcheff, J., & Bukowski, J. (2011). *The multiple stress creep recovery (MSCR) procedure* (Report No. FHWA-HIF-11-038). Federal Highway Administration.

Harrigan, E., Leahy, R., & Youtcheff, J. (1994). *Superpave manual of specifications, test methods and practices* (No. SHRP-A-379). Strategic Highway Research Program.

Hesp, S. A. M., Soleimani, A., Subramani, S., Phillips, T., Smith, D., Marks, P., & Tam, K. K. (2009). Asphalt pavement cracking: Analysis of extraordinary life cycle variability in eastern and northeastern Ontario. *International Journal of Pavement Engineering*, *10*(3), 209–227. https://doi.org/10.1080/10298430802343169

Hicks, R. G. (1991). *Moisture damage in asphalt concrete*. Transportation Research Board.

Hintz, C., & Bahia, H. (2013). Simplification of linear amplitude sweep test and specification parameter. *Transportation Research Record*, *2370*(1), 10–16. https://doi.org/10.3141/2370-02

Hintz, C., Velasquez, R., Johnson, C., & Bahia, H. (2011). Modification and validation of linear amplitude sweep test for binder fatigue specification. *Transportation Research Record*, *2207*(1), 99–106. https://doi.org/10.3141/2207-13

Hossain, Z., Ghosh, D., Zaman, M., & Hobson, K. (2016). Use of the multiple stress creep recovery (MSCR) test method to characterize polymer-modified asphalt binders. *Journal of Testing and*

Evaluation, *44*(1), 507–520.

Hou, X., Lv, S., Chen, Z., & Xiao, F. (2018). Applications of Fourier transform infrared spectroscopy technologies on asphalt materials. *Measurement*, *121*, 304–316. https://doi.org/10.1016/j.measurement.2018.03.001

Hu, X.-D., & Walubita L. F. (2015). Influence of asphalt-binder source on CAM mix rutting and cracking performance: A laboratory case study. *International Journal of Pavement Research and Technology*, *8*(6), 419–425. https://doi.org/10.6135/ijprt.org.tw/2015.8(6).419

IDOT. (2024). *Manual of Test Procedures for Materials*. Illinois Department of Transportation, Central Bureau of Materials. Springfield, Illinois.

Im, S., Karki, P., & Zhou, F. (2016). Development of new mix design method for asphalt mixtures containing RAP and rejuvenators. *Construction and Building Materials*, *115*, 727–734. https://doi.org/10.1016/j.conbuildmat.2016.04.081

Jahangir, R., Little, D., & Bhasin, A. (2015). Evolution of asphalt binder microstructure due to tensile loading determined using AFM and image analysis techniques. *International Journal of Pavement Engineering*, *16*(4), 337–349. https://doi.org/10.1080/10298436.2014.942863

Jeong, J., Shane Underwood, B., & Richard Kim, Y. (2022). Cracking performance predictions using index-volumetrics relationships with direct tension cyclic fatigue test and Illinois Flexibility Index Test (I-FIT). *Construction and Building Materials*, *315*, 125631. https://doi.org/10.1016/j.conbuildmat.2021.125631

Kim, H. H., Mazumder, M., & Lee, S.-J. (2017). Micromorphology and rheology of warm binders depending on aging. *Journal of Materials in Civil Engineering*, *29*(11), 04017226. https://doi.org/10.1061/(ASCE)MT.1943-5533.0002082

Kim, T. K. (2015). T test as a parametric statistic. *Korean Journal of Anesthesiology*, *68*(6), 540–546.

Kriz, P., Noel, J., Quddus, M., & Maria, S. (2019). Rheological properties of phase-incompatible bituminous binders. Proceedings of the 56th Peterson Asphalt Research Conference, Laramie, Wyoming, United States.

Kumar, A., Choudhary, R. & Kumar., A. (2021). Characterization of thermal storage stability of waste plastic pyrolytic char modified asphalt binders with sulfur. *PLOS ONE* 16(3), e0248465. https://doi.org/10.1371/journal.pone.0248465

Kumar, Y., Singh, S. K., Oberoi, D., Kumar, P., Mohanty, P., & Ravindranath, S. S. (2020). Effect of molecular structure and concentration of styrene-butadiene polymer on upper service temperature rheological properties of modified binders. *Construction and Building Materials*, *249*, 118790. https://doi.org/10.1016/j.conbuildmat.2020.118790

Kütük-Sert, T., & Kütük, S. (2013). Physical and marshall properties of Borogypsum used as filler aggregate in asphalt concrete. *Journal of Materials in Civil Engineering*, *25*(2), 266–273. https://doi.org/10.1061/(ASCE)MT.1943-5533.0000580

Lesueur, D., Elwardany, M. D., Planche, J.-P., Christensen, D., & King, G. N. (2021). Impact of the asphalt binder rheological behavior on the value of the ΔTc parameter. *Construction and Building*

Materials, *293*, 123464. https://doi.org/10.1016/j.conbuildmat.2021.123464

Lewandowski, L. H. (1994). Polymer modification of paving asphalt binders. *Rubber Chemistry and Technology*, *67*(3), 447–480

Li, X., Gibson, N., Andriescu, A., & S. Arnold, T. (2017). Performance evaluation of REOB-modified asphalt binders and mixtures. *Road Materials and Pavement Design*, 18(sup1), 128–153. https://doi.org/10.1080/14680629.2016.1266754

Lin, J., Hong, J., Huang, C., Liu, J., & Wu, S. (2014). Effectiveness of rejuvenator seal materials on performance of asphalt pavement. *Construction and Building Materials*, *55*, 63–68. https://doi.org/10.1016/j.conbuildmat.2014.01.018

Lin, P., Huang, W., Li, Y., Tang, N., & Xiao, F. (2017). Investigation of influence factors on low temperature properties of SBS modified asphalt. *Construction and Building Materials*, *154*, 609–622.

Lin, P., Huang, W., Liu, X., Apostolids, P., Wang, H., & Yan, C. (2020). Laboratory evaluation of the effects of long-term aging on high-content polymer-modified asphalt binder. *Journal of Materials in Civil Engineering*, *32*(7), 04020157.

Ling, C., Swiertz, D., Mandal, T., Teymourpour, P., & Bahia, H. (2017). Sensitivity of the Illinois flexibility index test to mixture design factors. *Transportation Research Record*, *2631*(1), 153–159. https://doi.org/10.3141/2631-17

Liu, H., Zeiada, W., Al-Khateeb, G. G., Shanableh, A., & Samarai, M. (2021). Use of the multiple stress creep recovery (MSCR) test to characterize the rutting potential of asphalt binders: A literature review. *Construction and Building Materials*, *269*, 121320. https://doi.org/10.1016/j.conbuildmat.2020.121320

Liu, Q., Wang, H., Yu, H., & Apostolidis, P. (2018). Investigation of the rejuvenation effect of different vegetable oils on aged bitumen. *Construction and Building Materials*, *199*, 449–456.

Marasteanu, M. O., Li, X., Clyne, T. R., Voller, V., Timm, D. H., & Newcomb, D. (2004). Low temperature cracking of asphalt concrete pavement. http://conservancy.umn.edu/handle/11299/792

Marsac, P., Piérard, N., Porot, L., Van den bergh, W., Grenfell, J., Mouillet, V., Pouget, S., Besamusca, J., Farcas, F., Gabet, T., & Hugener, M. (2014). Potential and limits of FTIR methods for reclaimed asphalt characterisation. *Materials and Structures*, *47*(8), 1273–1286. https://doi.org/10.1617/s11527-014-0248-0

Masson, J.-F. (2008). Brief review of the chemistry of polyphosphoric acid (PPA) and bitumen. *Energy & Fuels*, *22*(4), 2637–2640. https://doi.org/10.1021/ef800120x

Mazumder, M., Ahmed, R., Wajahat Ali, A., & Lee, S.-J. (2018a). SEM and ESEM techniques used for analysis of asphalt binder and mixture: A state of the art review. *Construction and Building Materials*, *186*, 313–329. https://doi.org/10.1016/j.conbuildmat.2018.07.126

McGennis, R. B., Anderson, R. M., Kennedy, T. W., & Solaimanian, M. (1995). *Background of Superpave asphalt mixture design and analysis* (Report No. FHWA-SA-95-003).

https://rosap.ntl.bts.gov/view/dot/42577

Mikhailenko, P., Kadhim, H., Baaj, H., & Tighe, S. (2017). Observation of asphalt binder microstructure with ESEM. *Journal of Microscopy*, *267*(3), 347–355. https://doi.org/10.1111/jmi.12574

Miliutenko, S., Björklund, A., & Carlsson, A. (2013). Opportunities for environmentally improved asphalt recycling: The example of Sweden. *Journal of Cleaner Production*, *43*, 156–165. https://doi.org/10.1016/j.jclepro.2012.12.040

Mogawer, W. S., Booshehrian, A., Vahidi, S., & Austerman, A. J. (2013). Evaluating the effect of rejuvenators on the degree of blending and performance of high RAP, RAS, and RAP/RAS mixtures. *Road Materials and Pavement Design*, 14(sup2), 193–213. https://doi.org/10.1080/14680629.2013.812836

Mogawer, W., Austerman, A., Kutay, M. E., & Zhou, F. (2011). Evaluation of binder elastic recovery on HMA fatigue cracking using continuum damage and overlay test based analyses. *Road Materials and Pavement Design*, *12*(2), 345–376. https://doi.org/10.1080/14680629.2011.9695249

Mohammad, L. N., Abadie, C., Gokmen, R., & Puppala, A. J. (2000). Mechanistic evaluation of hydrated lime in hot-mix asphalt mixtures. *Transportation Research Record*, *1723*(1), 26–36. https://doi.org/10.3141/1723-04

Nega, A., Nikraz, H., Leek, C., & Ghadimi, B. (2013). Pavement materials characterization of hot-mix asphalt mixes in Western Australia. *Advanced Materials Research*, *723*, 434–443. https://doi.org/10.4028/www.scientific.net/AMR.723.434

Newcomb, D. (2021). Test Methods to Quantify Cracking Resistance of Asphalt Binders and Mixtures.

Nguyen, L. N., Truong, V. Q., Dao, D. V., Nguyen, M. H., & Tran, T. (2024). Effects of rejuvenators and aging conditions on the properties of blended bitumen and the cracking behavior of hot asphalt mixtures with a high RAP content. *Proceedings of the Institution of Mechanical Engineers, Part L: Journal of Materials: Design and Applications*, *238*(7) 1368–1390.

Nivitha, M. R., Devika, R., Murali Krishnan, J., & Roy, N. (2022). Influence of bitumen type and polymer dosage on the relaxation spectrum of styrene-butadiene-styrene (SBS)/styrene-butadiene (SB) modified bitumen. *Mechanics of Time-Dependent Materials*. https://doi.org/10.1007/s11043-021-09531-y

Notani, M. A., Moghadas Nejad, F., Khodaii, A., & Hajikarimi, P. (2019). Evaluating fatigue resistance of toner-modified asphalt binders using the linear amplitude sweep test. *Road Materials and Pavement Design*, *20*(8), 1927–1940. https://doi.org/10.1080/14680629.2018.1474792

Oldham, D. J., Rajib, A. I., Onochie, A., & Fini, E. H. (2019). Durability of bio-modified recycled asphalt shingles exposed to oxidation aging and extended sub-zero conditioning. *Construction and Building Materials*, *208*, 543–553. https://doi.org/10.1016/j.conbuildmat.2019.03.017

Pipintakos, G., Škultecké, J., Vaitkus, A., Šernas, O., Soenen, H., & Van den Bergh, W. (2025). Optimising bitumen modification: how styrene–butadiene–styrene (SBS) characteristics and content affect bitumen behaviour. *Road Materials and Pavement Design*, *26*(sup1), 443–463.

Rahbar-Rastegar, R., Sias Daniel, J., & Reinke, G. (2017). Comparison of asphalt binder and mixture

cracking parameters. *Road Materials and Pavement Design*, 18(sup4), 211–233. https://doi.org/10.1080/14680629.2017.1389071

Reinke, G., Hanz, A., Anderson, R. M., Ryan, M., Engber, S., & Herlitzka, D. (2016). Impact of re-refined engine oil bottoms on binder properties and mix performance on two pavements in Minnesota. In Proceedings of the E&E Congress.

Rivera-Perez, J., Ozer, H., & Al-Qadi, I. L. (2018). Impact of specimen configuration and characteristics on Illinois flexibility index. *Transportation Research Record*, *2672*(28), 383–393. https://doi.org/10.1177/0361198118792114

Rohman, A., & Che Man, Y. B. (2013). Application of FTIR spectroscopy for monitoring the stabilities of selected vegetable oils during thermal oxidation. *International Journal of Food Properties*, *16*(7), 1594-1603.

Sabouri, M., Mirzaiyan, D., & Moniri, A. (2018). Effectiveness of linear amplitude sweep (LAS) asphalt binder test in predicting asphalt mixtures fatigue performance. *Construction and Building Materials*, *171*, 281–290. https://doi.org/10.1016/j.conbuildmat.2018.03.146

Salari, Z., Vakhshouri, B., & Nejadi, S. (2018). Analytical review of the mix design of fiber reinforced high strength self-compacting concrete. *Journal of Building Engineering*, *20*, 264–276. https://doi.org/10.1016/j.jobe.2018.07.025

Sengoz, B., Topal, A., & Isikyakar, G. (2009). Morphology and image analysis of polymer modified bitumens. *Construction and Building Materials*, *23*(5), 1986–1992. https://doi.org/10.1016/j.conbuildmat.2008.08.020

Sharma, B. K., Ma, J., Kunwar, B., Singhvi, P., Ozer, H., & Rajagopalan, N. (2017). *Modeling the performance properties of RAS and RAP blended asphalt mixes using chemical compositional information* (Report No. FHWA-ICT-17-001). Illinois Center for Transportation. https://rosap.ntl.bts.gov/view/dot/32024

Shi, L., Liu, Z., Li, J., & Qin, Z. (2017, April). Analysis of edible vegetable oils by infrared absorption spectrometry. In *2017 2nd International Conference on Electrical, Automation and Mechanical Engineering (EAME 2017)* (pp. 286–289). Atlantis Press.

Sigmaaldrich. (n.d.) *IR spectrum table & chart* https://web.archive.org/web/20231118063118/https://www.sigmaaldrich.com/US/en/technical-documents/technical-article/analytical-chemistry/photometry-and-reflectometry/ir-spectrum-table

Silva, H. M. R. D., Oliveira, J. R. M., & Jesus, C. M. G. (2012). Are totally recycled hot mix asphalts a sustainable alternative for road paving? *Resources, Conservation and Recycling*, *60*, 38–48. https://doi.org/10.1016/j.resconrec.2011.11.013

Sindhu, R., Binod, P., & Pandey, A. (2015). Chapter 17—Microbial Poly-3-Hydroxybutyrate and Related Copolymers. In A. Pandey, R. Höfer, M. Taherzadeh, K. M. Nampoothiri, & C. Larroche (Eds.), *Industrial Biorefineries & White Biotechnology* (pp. 575–605). Elsevier. https://doi.org/10.1016/B978-0-444-63453-5.00019-7

Singhvi, P., García Mainieri, J. J., Ozer, H., & Sharma, B. (2021). *Rheology-chemical based procedure to evaluate additives/modifiers used in asphalt binders for performance enhancements: Phase 2*.

(Report No. FHWA-ICT-21-015). Illinois Center for Transportation. https://doi.org/10.36501/0197-9191/21-020

Singhvi, P., García Mainieri, J. J., Ozer, H., Sharma, B. K., & Al-Qadi, I. L. (2020). Effect of chemical composition of bio- and petroleum-based modifiers on asphalt binder rheology. *Applied Sciences*, *10*(9), 3249. https://doi.org/10.3390/app10093249

Sulaiman, A., Mohamed Ali, U., & Al-Qadi, I. (2023). *Evaluation of the asphalt mixture design framework for airfield pavements in Illinois* (Report No. FHWA-ICT-23-010). Illinois Center for Transportation. https://doi.org/10.36501/0197-9191/23-011

Sun, D., Sun, G., Du, Y., Zhu, X., Lu, T., Pang, Q., Shi, S., & Dai, Z. (2017). Evaluation of optimized bio-asphalt containing high content waste cooking oil residues. *Fuel*, *202*, 529–540. https://doi.org/10.1016/j.fuel.2017.04.069

Tabib, S., Khuskivadze, O., Marks, P., Nicol, E., Ding, H., & Hesp, S. A. (2018). Pavement performance compared with asphalt properties for five contracts in Ontario. *Construction & Building Materials*, *171*, 719–725. https://doi.org/10.1016/j.conbuildmat.2018.03.177

Tarhan, I., Ismail, A. A., & Kara, H. (2017). Quantitative determination of free fatty acids in extra virgin olive oils by multivariate methods and Fourier transform infrared spectroscopy considering different absorption modes. *International Journal of Food Properties*, *20*(sup1), S790-S797.

Tran, N., Taylor, A., & Willis, R. (2012). Effect of rejuvenator on performance properties of HMA mixtures with high RAP and RAS contents (No. 12–05). https://trid.trb.org/view/1250368

Uzun, İ., & Terzi, S. (2012). Evaluation of andesite waste as mineral filler in asphaltic concrete mixture. *Construction and Building Materials*, *31*, 284–288. https://doi.org/10.1016/j.conbuildmat.2011.12.093

Walubita, L. F., Fuentes, L., Tanvir, H., Chunduri, H. R., & Dessouky, S. (2021). Correlating the asphalt-binder BBR test data to the HMA (ML-OT) fracture properties. *Journal of Materials in Civil Engineering*, *33*(9), 04021230. https://doi.org/10.1061/(ASCE)MT.1943-5533.0003866

Wang, J., Wang, T., Hou, X., & Xiao, F. (2019). Modelling of rheological and chemical properties of asphalt binder considering SARA fraction. *Fuel*, 238, 320–330. https://doi.org/10.1016/j.fuel.2018.10.126

Wang, Y., Sun, L., & Qin, Y. (2015). Aging mechanism of SBS modified asphalt based on chemical reaction kinetics. *Construction and Building Materials*, *91*, 47–56.

Wang, Y., Yi, H., Liang, P., Chai, C., Yan, C., & Zhou, S. (2022). Investigation on preparation method of SBS-modified asphalt based on MSCR, LAS, and fluorescence microscopy. *Applied Sciences*, *12*(14), 7304.

Wasage, T. L. J., Stastna, J., & Zanzotto, L. (2011). Rheological analysis of multi-stress creep recovery (MSCR) test. *International Journal of Pavement Engineering*, *12*(6), 561–568. https://doi.org/10.1080/10298436.2011.573557

Xie, W., Castorena, C., Wang, C., & Richard Kim, Y. (2017). A framework to characterize the healing potential of asphalt binder using the linear amplitude sweep test. *Construction and Building*

Materials, *154*, 771–779. https://doi.org/10.1016/j.conbuildmat.2017.08.021

Xie, Z., Tran, N., Julian, G., Taylor, A., & Blackburn, L. D. (2017). Performance of asphalt mixtures with high recycled contents using rejuvenators and warm-mix additive: Field and lab experiments. *Journal of Materials in Civil Engineering*, *29*(10), 04017190. https://doi.org/10.1061/(ASCE)MT.1943-5533.0002037

Xiong, R., Fang, J., Xu, A., Guan, B., & Liu, Z. (2015). Laboratory investigation on the brucite fiber reinforced asphalt binder and asphalt concrete. *Construction and Building Materials*, *83*, 44–52. https://doi.org/10.1016/j.conbuildmat.2015.02.089

Xu, G., Wang, H., & Zhu, H. (2017). Rheological properties and anti-aging performance of asphalt binder modified with wood lignin. *Construction and Building Materials*, *151*, 801–808. https://doi.org/10.1016/j.conbuildmat.2017.06.151

Xu, O., Xiao, F., Han, S., Amirkhanian, S. N., & Wang, Z. (2016). High temperature rheological properties of crumb rubber modified asphalt binders with various modifiers. *Construction and Building Materials*, *112*, 49–58. https://doi.org/10.1016/j.conbuildmat.2016.02.069

Xu, S., Tabaković, A., Liu, X., & Schlangen, E. (2018). Calcium alginate capsules encapsulating rejuvenator as healing system for asphalt mastic. *Construction and Building Materials*, *169*, 379–387. https://doi.org/10.1016/j.conbuildmat.2018.01.046

Xu, T., & Huang, X. (2010). Study on combustion mechanism of asphalt binder by using TG–FTIR technique. *Fuel*, *89*(9), 2185–2190. https://doi.org/10.1016/j.fuel.2010.01.012

Yan, C., Huang, W., Xiao, F., Wang, L., & Li, Y. (2018). Proposing a new infrared index quantifying the aging extent of SBS-modified asphalt. *Road Materials and Pavement Design*, *19*(6), 1406–1421.

Yan, C., Yuan, L., Yu, X., Ji, S., & Zhou, Z. (2022). Characterizing the fatigue resistance of multiple modified asphalts using time sweep test, LAS test and elastic recovery test. *Construction and Building Materials*, *322*, 125806. https://doi.org/10.1016/j.conbuildmat.2021.125806

Yang, X., You, Z., & Mills-Beale, J. (2014). Asphalt binders blended with a high percentage of biobinders: Aging mechanism using FTIR and rheology. *Journal of Materials in Civil Engineering*, 27. https://doi.org/10.1061/(ASCE)MT.1943-5533.0001117

Yao, H., Dai, Q., & You, Z. (2015). Fourier transform infrared spectroscopy characterization of aging-related properties of original and nano-modified asphalt binders. *Construction and Building Materials*, *101*, 1078–1087. https://doi.org/10.1016/j.conbuildmat.2015.10.085

Yildirim, Y. (2007). Polymer modified asphalt binders. *Construction and Building Materials*, *21*(1), 66–72.

Yilmaz, M., Kök, B. V., & Kuloğlu, N. (2011). Effects of using asphaltite as filler on mechanical properties of hot mix asphalt. *Construction and Building Materials*, *25*(11), 4279–4286. https://doi.org/10.1016/j.conbuildmat.2011.04.072

Yut, I., & Zofka, A. (2011). Attenuated total reflection (ATR) Fourier transform infrared (FT-IR) spectroscopy of oxidized polymer-modified bitumens. *Applied Spectroscopy*, *65*(7), 765–770.

Zaumanis, M., Mallick, R. B., & Frank, R. (2015). Evaluation of different recycling agents for restoring aged asphalt binder and performance of 100% recycled asphalt. *Materials and Structures*, *48*(8),

2475–2488. https://doi.org/10.1617/s11527-014-0332-5

Zaumanis, M., Mallick, R. B., Poulikakos, L., & Frank, R. (2014). Influence of six rejuvenators on the performance properties of reclaimed asphalt pavement (RAP) binder and 100% recycled asphalt mixtures. *Construction and Building Materials*, *71*, 538–550. https://doi.org/10.1016/j.conbuildmat.2014.08.073

Zeiada, W., Liu, H., Ezzat, H., Al-Khateeb, G. G., Shane Underwood, B., Shanableh, A., & Samarai, M. (2022). Review of the Superpave performance grading system and recent developments in the performance-based test methods for asphalt binder characterization. *Construction and Building Materials*, *319*, 126063. https://doi.org/10.1016/j.conbuildmat.2021.126063

Zhang, J., Simate, G. S., Lee, S. I., Hu, S., & Walubita, L. F. (2016b). Relating asphalt binder elastic recovery properties to HMA crack modeling and fatigue life prediction. *Construction and Building Materials*, 111, 644–651. https://doi.org/10.1016/j.conbuildmat.2016.02.175

Zhang, J., Walubita, L. F., Faruk, A. N. M., Karki, P., & Simate, G. S. (2015). Use of the MSCR test to characterize the asphalt binder properties relative to HMA rutting performance – A laboratory study. *Construction and Building Materials*, *94*, 218–227. https://doi.org/10.1016/j.conbuildmat.2015.06.044

Zhang, L., Xing, C., Gao, F., Li, T., & Tan, Y. (2016a). Using DSR and MSCR tests to characterize high temperature performance of different rubber modified asphalt. *Construction and Building Materials*, *127*, 466–474. https://doi.org/10.1016/j.conbuildmat.2016.10.010

Zhang, R., You, Z., Wang, H., Chen, X., Si, C., & Peng, C. (2018). Using bio-based rejuvenator derived from waste wood to recycle old asphalt. *Construction and Building Materials*, *189*, 568–575. https://doi.org/10.1016/j.conbuildmat.2018.08.201

Zhao, S., Huang, B., Shu, X., & Woods, M. E. (2016). Quantitative evaluation of blending and diffusion in high RAP and RAS mixtures. *Materials & Design*, *89*, 1161–1170. https://doi.org/10.1016/j.matdes.2015.10.086

Zhou, F., Mogawer, W., Li, H., Andriescu, A., & Copeland, A. (2013). Evaluation of fatigue tests for characterizing asphalt binders. *Journal of Materials in Civil Engineering*, *25*(5), 610–617. https://doi.org/10.1061/(ASCE)MT.1943-5533.0000625

Zhou, F., Newcomb, D., Gurganus, C., Banihashemrad, S., Park, E. S., Sakhaeifar, M., & Lytton, R. L. (2016). Experimental design for field validation of laboratory tests to assess cracking resistance of asphalt mixtures.

Zhou, Z., Gu, X., Dong, Q., Ni, F., & Jiang, Y. (2019). Rutting and fatigue cracking performance of SBS-RAP blended binders with a rejuvenator. *Construction and Building Materials*, *203*, 294–303. https://doi.org/10.1016/j.conbuildmat.2019.01.119

Zhou, Z., Gu, X., Dong, Q., Ni, F., & Jiang, Y. (2020). Low- and intermediate-temperature behaviour of polymer-modified asphalt binders, mastics, fine aggregate matrices, and mixtures with reclaimed asphalt pavement material

Zhu, Z., Singhvi, P., Ali, U. M., Ozer, H., & Al-Qadi, I. L. (2020). Quantification of the effect of binder source on flexibility of long-term aged asphalt concrete. *Transportation Research Record*, *2674*(9), 605–616. https://doi.org/10.1177/0361198120930717


Illinois Department
of Transportation


ILLINOIS